Aus dem Fachbereich Medizin
der Johann Wolfgang Goethe-Universität
Frankfurt am Main

aus dem
Zentrum der Pharmakologie
Institut für Klinische Pharmakologie
Direktor: Prof. Dr. Dr. Gerd Geißlinger

Betreut am
Institut für Pharmakologie und Klinische Pharmazie

Specific functions of Slack potassium channels in sensory neurons and spinal dorsal horn neurons in pain processing

Dissertation
zur Erlangung des Doktorgrades der Medizin
des Fachbereichs Medizin
der Johann Wolfgang Goethe-Universität
Frankfurt am Main

vorgelegt von
Fangyuan Zhou
aus Henan, Volksrepublik China

Frankfurt am Main, 2022

Dekan:	Prof. Dr. Stefan Zeuzem
Referent:	Prof. Dr. Dr. Achim Schmidtko
Korreferent:	Prof. Dr. Dr. Gerd Geißlinger
Tag der mündlichen Prüfung:	31.05.2023

Schriftliche Erklärung

Ich erkläre ehrenwörtlich, dass ich die dem Fachbereich Medizin der Johann Wolfgang Goethe-Universität Frankfurt am Main zur Promotionsprüfung eingereichte Dissertation mit dem Titel

Specific functions of Slack potassium channels in sensory neurons and spinal dorsal horn neurons in pain processing

im Institut für Pharmakologie und Klinische Pharmazie
unter Betreuung und Anleitung von Prof. Dr. Dr. Achim Schmidtko ohne sonstige Hilfe selbst durchgeführt und bei der Abfassung der Arbeit keine anderen als die in der Dissertation angeführten Hilfsmittel benutzt habe. Darüber hinaus versichere ich, nicht die Hilfe einer kommerziellen Promotionsvermittlung in Anspruch genommen zu haben.

Die vorliegende Arbeit wurde bisher nicht als Dissertation eingereicht.

Vorliegende Ergebnisse der Arbeit wurden in folgendem Publikationsorgan veröffentlicht:
Zhou F, Metzner K, Engel P, Balzulat A, Sisignano M, Ruth P, Lukowski, R, Schmidtko A, Lu R. Slack potassium channels modulate TRPA1-mediated nociception in sensory neurons. Cells;11(10):1693; 2022.

Wuhan, China. 02.06.2023 — Fangyuan Zhou

(Ort, Datum) (Unterschrift)

Table of Contents

1. Introduction

1.1 Pain processing

Pain is an unpleasant sensory and emotional experience associated with actual or potential tissue damage, or described in terms of such damage [1]. The sensation of pain protects the body from damaging events and is thus an essential aspect of an organism's survival and well-being [2]. Individuals who suffer from a congenital deficiency in detecting painful stimuli, such as a sharp object, the heat of an open flame, or even discomfort associated with internal injuries, cannot respond appropriately against these conditions, hence many of these conditions can be life-threatening [3]. Pain does not always serve as a protective function. Individuals who suffer from trauma, infection, metabolic or autoimmune disorders, postherpetic neuralgia or cancer typically report an increased sensitivity to thermal or mechanical stimuli, which can last for months or even years [4, 5]. Chronic pain is defined as pain that persists or recurs for more than three months [6]. Based on the International Association for the Study of Pain (IASP) Classification of Chronic Pain for the International Classification of Diseases-11th edition (ICD-11), chronic pain can be the sole or a leading symptom in conditions such as fibromyalgia or nonspecific low-back pain, and has been defined as the subgroup "chronic primary pain" [1, 6]. "Chronic secondary pain" can be attributed to 6 other subgroups: chronic cancer-related pain, chronic neuropathic pain, chronic secondary visceral pain, chronic post-traumatic and post-surgical pain, chronic secondary headache and orofacial pain, and chronic secondary musculoskeletal pain; these are conditions where the pain is secondary to the underlying disease [6]. Epidemiological surveys put estimates of the overall prevalence of pain across 52 countries to be 27.5%, with significant variation across the countries (ranging from 9.9% to 50.3%) [7]. It has a considerable impact on patients' quality of life and induces a high economic burden on the individual and society [8, 9]. The complexity of chronic pain mechanisms poses a major therapeutic challenge [1, 2, 10-12].

The somatosensory information begins in the periphery nervous system, where the peripheral terminals of the primary afferent fibers respond to a myriad of stimuli from the skin, muscle, joints and viscera. The information is detected by the periphery sensory neurons of the trigeminal ganglia and the dorsal root ganglia (DRG). This experience is

then transmitted into the dorsal horn of the spinal cord where the central ends of these fibers terminate and trigger the release of neurotransmitters and, thus, activate second-order neurons that project into the brain, or into its trigeminal homologue in the brainstem (see Figure I). Primary sensory neurons are pseudounipolar, projecting axons that bifurcate into two branches: one branch, termed the *distal process*, terminates in the peripheral tissues, while the other branch, referred to as the *proximal process*, synapses with second-order spinal cord neurons or the sensory nuclei of the brain stem [13].

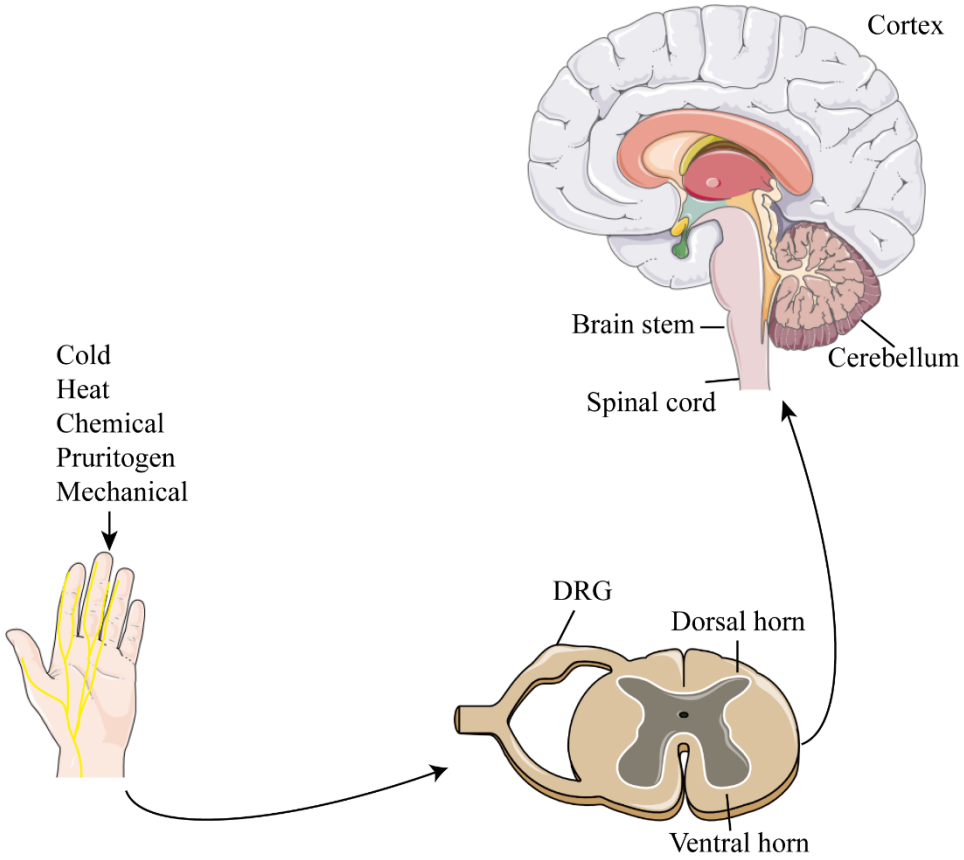

Figure I. Diagram of somatosensory circuits. This figure was adapted from Peirs and Seal, 2017 [14].

Traditionally, sensory neurons have been distinguished into four main class types by their degree of myelination and conduction velocity: heavily and moderately myelinated Aα/Aβ fibers; thinly myelinated Aδ fibers; and unmyelinated C fibers. The differences in the degree of myelination and conduction velocity have profound effects on their association with their discrete functions. For instance, the detection of a light touch and the relay of proprioceptive information principally give rise to the activation of heavily and moderately myelinated Aα/Aβ fibers [15]. Thinly myelinated Aδ fibers are

considered as the main afferents that detect a variety of innocuous (non-harmful) and noxious stimuli, while the unmyelinated C fibers, even though some of them are also involved in relaying innocuous light touch stimuli, are largely associated with the detection of nociceptive information [13, 16]. Previous studies have used neurochemical features to categorize the C-fiber primary sensory neurons into peptidergic and non-peptidergic neurons. The peptidergic neurons comprise the C- or Aδ fibers, while the non-peptidergic neurons are all C-fibers [17, 18]. Peptidergic neurons are defined by containing neuropeptides such as calcitonin gene-related peptide (CGRP) and substance P, somatostatin and the nerve growth factor (NGF) receptor─ tyrosine kinase receptor TrkA (Ntrk1). While non-peptidergic C-fiber neurons do not express these neuropeptides, they do contain the glial-derived neurotrophic factor (GDNF) Ret. In addition, the majority of non-peptidergic C-fiber neurons bind the plant lectin isolectin-B4 (IB4) from *Griffonia simplicifolia* and express the Mas-related G protein-coupled receptor (Mrgpr) family [19-24]. A more recent classification of the primary afferents using single-cell RNA sequencing has identified 11 neuronal types: one unmyelinated peptidergic C-fiber neuron population (termed PEP1), one lightly myelinated Aδ-nociceptor type (termed PEP2), five A-fiber neurons expressing neurofilament heavy chain (Nefh) (termed NF1, NF2, NF3, NF4 and NF5), three non-peptidergic C-fiber neurons (termed NP1,NP2 and NP3) and one neuron type expressing Vesicular Glutamate Transporter 3 (VGLUT3) and tyrosine hydroxylase (TH), referred to as the TH type [25].

The spinal cord comprises two main types of neuronal populations: projection neurons and spinal interneurons (SpINs) [26]. Spinal projection neurons (which are primarily located in the superficial layer (lamina I) of the spinal dorsal horn, with some scattered throughout the deep layers (laminae III–VIII and X) and the lateral spinal nucleus (LSN)), are those neurons where the cell body lies within the spinal cord but which have projections either to other parts of central nervous system (CNS) or to the periphery [26, 27], while the SpINs are cells located within the spinal cord that project to other cells within the spinal cord [28]. The vast majority of neurons in laminae I–III of the dorsal horn are interneurons that play a major role in the neuronal circuits that process sensory inputs, including those perceived as pain [29, 30]. Based on their neurotransmitter content, SpINs can be classified further into two broad functional populations: excitatory (75%) and inhibitory (25%) neurons in mice [14, 30]. The excitatory interneurons are marked by the transient expression of glutamate, while the inhibitory interneurons are defined by

releasing GABA and/or glycine [29-33]. Primary afferent nerve fibers containing peripheral information project to six distinct Rexed laminae of the spinal cord dorsal horn [14]. Most of the C and Aδ nociceptors project into the superficial laminae I and II of the dorsal horn, where mechanical and thermal nociception are largely processed, although deeper dorsal horn neurons also receive nociceptive input via a polysynaptic pathway mediated by relay excitatory interneurons [3]. Meanwhile, neurons within deeper laminae (III to V) are mainly sensitive to innocuous stimulation via the Aδ- and Aβ-fibers [3]. Current evidence points to at least five distinct populations of either excitatory or inhibitory interneurons that are involved in neuropathic pain: somatostatin-, VGLUT3-, calretinin-, protein kinase C-γ (PKC-γ) and neuropeptide Y (NPY)-expressing neurons [34-38]. However, it remains undetermined as to how these interneurons are coordinated in nociceptive perception in the spinal cord-brain axis.

1.2 Pain classification

Pain can be classified according to the body location, the duration of pain, severity, frequency, etiology, pathophysiology, and so on. For instance, pain can be described as acute or chronic, depending on the length of time that the patient experiences it. Based on the ICD-11, acute pain has a duration of less than three months, while chronic pain persists or recurs for longer than three months. In addition, pain can be adaptive, reparative and maladaptive in response to conditions such as tissue damage, inflammation or injury of the nervous system [39]. Multiple molecular and cellular mechanisms, different clinical symptoms and pain treatments can operate alone or in combination within the peripheral and central nervous systems to produce the different forms of pain: nociceptive pain, inflammatory pain and neuropathic pain [39]. Admittedly, inflammatory and neuropathic pain may share some common mechanisms, however, they are generally considered as separate categories, both in terms of etiology and treatment.

Nociceptive pain is “pain that arises from actual threatened damage to non-neural tissue and is due to the activation of nociceptors” (IASP Terminology). It is usually caused by tissue-damaging stimuli and serves as a protective function. Thus, nociceptive pain can often be acute pain [40]. Noxious heat or cold stimuli, noxious mechanical insults and chemical irritants are detected by the relevant thermal, mechanical or chemical nociceptors and conveyed to the central nervous system [3, 41-43]. Without the ability to sense acute pain, the individual would be unable to react to harmful stimuli.

Inflammatory pain is the perception of and affective response to noxious stimuli that occur during an inflammatory or immune response [44]. Once tissue damage has occurred, many inflammatory mediators (such as cytokines) are released from the injured sites and the infiltrating immune cells can reduce the threshold for nociceptive neurons to fire action potentials, thereby inducing pain sensitization (hyperalgesia), the perception of non-noxious stimuli as painful (allodynia) or even persistent pain [45, 46]. Generally, inflammatory pain is the biological consequence of the interaction between neurons and immune cells; this is specifically initiated through the activation of nociceptive sensory neurons by hot or cold thermal stimulation, by mechanical stimulation or by inflammatory mediators [47, 48].

Neuropathic pain is a term that describes the abnormal function in the somatosensory system; this is in contrast to nociceptive pain that depicts pain occurring with a normal function (IASP Terminology). As it is widely accepted that neuropathic pain is caused by a lesion or disease of the somatosensory nervous system [49], it often results from traumatic nerve, spinal cord or brain injury (including stroke) and is usually associated with postherpetic neuralgia, trigeminal neuralgia, painful radiculopathy, diabetic neuropathy, HIV infection, leprosy, amputation, multiple sclerosis, cancer and/or the toxic effects of chemotherapeutic agents [11, 50]. The affected individuals typically suffer a combination of sensory abnormalities including spontaneous pain, hypersensitivity to stimuli, dysesthesias and paresthesias [8]. The symptoms persist and those affected may also tend to develop sleep disturbances, anxiety and depression [9].

Nociplastic pain was first proposed in 2016 as a semantic term to describe a specific chronic pain states that mechanistically distinct from nociceptive pain or neuropathic pain [51, 52]. Based on the IASP Terminology and the ICD-11, nociplastic pain refers to a physiologically based category that is particularly applicable to chronic primary pain conditions, which is mechanistically and clinically distinct from the other pain categories [51, 53]. Nociplastic pain can be defined as pain arising from the altered function of pain-related sensory pathways in the periphery and CNS, causing increased sensitivity [52]. This type of pain can occur in isolation or as a comorbidity in individuals with chronic pain conditions such as fibromyalgia or tension-type headache, or as part of a mixed-pain state in combination with ongoing nociceptive or neuropathic pain [52, 54].

1.3 Ion channels in pain sensation

The expression and function of ion channels define the resting membrane potential, action potential initiation, depolarization and repolarization and also the refractory period between the action potentials in primary afferent neurons [3, 55]. When a noxious stimulus occurs, nonselective cation channels such as the transient receptor potential (TRP) channels and voltage-gated sodium (Na^+) channels present in the free endings of the dorsal root ganglion neurons can be activated [55]. This allows the afferent neurons to initiate action potentials that propagate along the axons to synaptic sites in the spinal cord dorsal horn via the activity of voltage-gated Na^+ and potassium (K^+) channels [55-58]. Subsequently the depolarization-induced opening of voltage-gated calcium (Ca^{2+}) channels results in the release of neurotransmitters such as glutamate and substance P that activate spinal interneurons and the neurons that project into the brain [55].

1.3.1 K^+ channels in pain sensation

K^+ channels play a crucial role in the regulation of the resting membrane potential and action potential repolarization, controlling the neuronal activity and signal propagation throughout the nervous system. K^+ channels constitute a highly diverse family of ion channels encoded by approximately 80 genes in mammals [59, 60]. Based on their structural and physiological characteristics, K^+ channels can be organized into voltage-gated K^+ channels (K_v), Ca^{2+}-activated K^+ channels (K_{Ca}), Na^+-activated K^+ channels (K_{Na}), two-pore potassium channels (K_{2p}) and inward rectifiers (K_{ir}) [60-62]. It is well established that K_v channels limit the neuronal firing frequency and spike duration, thus, the reduction of Kv channels leads to an increase in spike frequency, threshold and duration that results in the hyperexcitability of the membrane [63]. In contrast, K_{2p} channels play an important role in the maintenance of a hyperpolarized resting membrane potential and can regulate the excitability of the primary afferent fiber [64], thus, these channels can modulate the pain signaling. Unlike other types of K^+ channels, K_{ir} channels are widely expressed in supporting cells such as the satellite glial cells [65, 66]. Through the conduction of atypical inward K^+ currents at depolarized membrane potentials, K_{ir} channels prevent the action potential from 'short-circuiting' and uncontrolled excitability changes [67]. Another well-established type of K^+ channel is the K_{Ca} channel which can

hyperpolarize the membrane and limit the Ca^{2+} influx and excitability during neuron firing, thus regulating the synaptic transmission in the nerve terminals [59].

Furthermore, K_{Na} channels have been found to be involved in after-hyperpolarization and firing rate adaptation [68]. So far, two K_{Na} subtypes have been identified: $K_{Na}1.1$ (also known as Slack (sequence like a Ca^{2+}-activated K^+ channel), Slo2.2 or *Kcnt1*) and $K_{Na}1.2$ (also known as Slick (sequence like an intermediate conductance K^+ channel), Slo2.1 or *Kcnt2*) channels. Both of these channels are highly expressed in neurons [69-76]. Previous researches have revealed that Slack dysfunction in the brain causes intellectual disability and childhood epilepsy [77-79], whereas Slack expressed in non-peptidergic C-fiber neurons is responsible for peripheral nerve injury-induced neuropathic pain, and acute histamine- and chloroquine-induced itch [80]. Slick has been found in Aδ-fibers and dorsal horn interneurons; it can play an inhibitory function in heat-induced pain sensation but also facilitates somatostatin-induced itch [81]. Häring et al. found that Slack is widely expressed in the GABAergic and glutamatergic neurons types, while Slick mainly defines the GABA2, GABA3, GABA8, GABA9, Glut6 and Glut7 neurons types in the spinal dorsal horn [82]. Therefore, based on the distribution pattern in pain-relevant primary afferent and spinal dorsal horn neurons, we hypothesized that Slack may possess several functions in pain processing.

1.3.2 TRP channels in pain sensation

The transient receptor potential (TRP) cation channels were first discovered in the eye cells of Drosophila fruit flies in 1961 [83]. The TRP channels from different subunits share general structural features. They are composed of six putative transmembrane domains (S1–S6), intracellular amino and carboxyl termini (N and C termini), and a pore-forming loop between S5 and S6 with a selectivity filter that renders most of these proteins as non-selective cation channels with high Ca^{2+} permeability [84, 85]. Studies over the past decades have recognized that the mammalian TRP channel superfamily consists of 28 channels; these can be divided according to their amino sequence homology into seven subgroups: TRPA (ankyrin), TRPC (canonical), TRPM (melastatin), TRPV (vanilloid), TRPML (mucolipin), TRPP (polycystin) and TRPN (NOMP-C) [86-88]. Various TRP ion channels are present in nociceptors and these allow the organisms to transduce environmental signals that contribute to their responses to diverse types of external stimuli [89]. Pungent irritants from certain natural plants (such as allicin in garlic)

or toxic molecules from animals (such as funnel web spider venom) have served as useful pharmacological tools for identifying molecules and mechanisms gating these channels and producing irritation and pain through binding specific strong covalent bonds [90-93]. TRPV1 is well known as the capsaicin receptor or vanilloid receptor 1 [94]; it is a heat-activated cation channel and is modulated by a range of inflammatory agents, such as extracellular protons and bioactive lipids, which contribute to pain hypersensitivity [93-95]. TRPM8 functions as a cold thermosensor that is activated by temperatures below 26 °C, menthol, eucalyptol and icilin [96]. TRPA1 is a noxious signal sensor that can be activated by a wide spectrum of noxious stimuli such as thermal, pungent compounds and reactive chemical species or by endogenous signals related to cell damage [88, 97-100].

Extensive evidence has revealed that TRPA1 is absent from heavily myelinated DRG neurons [101, 102] and is mainly expressed in non-peptidergic C fibers [103, 104]. Several investigations have revealed that TRPA1 can mediate pain evoked by mechanical stimuli in the peripheral neuropathy, while blocking of TRPA1 can reduce mechanical hypersensitivity of peripheral diabetic neuropathy or spinal nerve injury-induced pain [105-109]. TRPA1-mediated pain hypersensitivity is involved in a variety of mechanisms; it can be activated by G-protein-coupled or growth factor receptors via stimulating phospholipase C signaling pathways [97, 101, 110] and also by electrophiles through the covalent modification of cysteine residues within the channel's cytoplasmic amino terminus [88, 111-113]. In another study, genetic deletion and pharmacological blockade (HC-030031 and A-967079, respectively) of TRPA1 abrogated the painlike behaviors in mice; this was elicited by the constriction of the infraorbital nerve mouse model and was associated with the reduced oxidative stress by-products released from the monocytes and macrophages recruited at the injury site [114]. A subsequent study reported that TRPA1 channels expressed in Schwann cells but not in nociceptors were activated by the NADPH oxidase 2 (NOX2)-dependent oxidative burst which in turn can activate the TRPA1-NOX1 pathway in Schwann cells, resulting in the release of H_2O_2 that ultimately activates TRPA1 in nociceptors [115]. TRPA1 also plays an important role in inflammation. Trevisan et al. found that H_2O_2-induced activation of TRPA1 mediates the inflammatory response in an acute gout attack rodent model [116]. In addition, the absence of TRPA1 yielded reduced inflammation in cultured ocular fibroblasts and fibrosis/scarring in the corneal stroma during wound healing in TRPA1 knockouts [117]. It has also been shown that the TRPA1 antagonist HC-030031 produces antinociceptive and anti-inflammatory

effects in a rat thermal injury model [118]. Furthermore, TRPA1 displays bimodal modulation by calcium [119-123]. A recent research characterized a calcium-binding pocket accounting for all aspects of calcium-dependent TRPA1-dependent potentiation, desensitization and activation [123]. Once TRPA1 is activated, it mediates the transmembrane flux of small cations (e.g., Ca^{2+}, Mg^{2+}, Na^{+}, K^{+}, etc.), thus contributing to the regulation of membrane depolarization, action potential generation and neurotransmitter release [124, 125]. Various interactors of TRPA1 in primary afferent neurons have been identified, including TRPV1 [126], T-type Ca^{2+} channels [127] and voltage-gated K^{+} channels [128]. Due to its restricted expression pattern and unique function in the sensing of various irritants, it has long been proposed that the blockade of TRPA1 could be a therapeutic strategy to treat pain and other diseases [129-132]. Recent single-cell RNA-sequencing studies suggest that in primary afferent neurons there is a substantial expressional overlap of TRPA1 and Slack [25, 133]. Nevertheless, how TRPA1 functionally interacts with Slack remains poorly understood.

1.4 Aim of this work

There is increasing evidence that Slack is involved in the processing of pain. To further investigate the role of Slack in peripheral sensory neurons and spinal dorsal horn neurons, we generated mice lacking Slack globally (Slack$^{-/-}$), conditionally in sensory neurons (SNS-Slack$^{-/-}$), or conditionally in spinal dorsal horn neurons (Lbx1-Slack$^{-/-}$).

The first aim was to test the hypothesis that Slack might be a modulator of TRPA1-mediated activation of sensory neurons. We therefore assessed the extent of co-localization of TRPA1 with Slack in DRG neurons. In the allyl isothiocyanate (AITC)-induced pain model, we then investigated the pain behavior of Slack$^{-/-}$, SNS-Slack$^{-/-}$, Lbx1-Slack$^{-/-}$ mice and littermate controls. In calcium imaging experiments we analyzed the Ca^{2+} influx in DRGs neurons of Slack$^{-/-}$ and WT mice after stimulation with AITC. Furthermore, we investigated the effects of activation of TRPA1 channels on Slack-dependent potassium currents in DRG neurons using patch-clamp recordings.

The second aim of this work was to explore the function of Slack expressed in spinal cord neurons in pain processing. Using Lbx1-Slack$^{-/-}$ mice, we investigated the basal pain sensitivity, Complete Freund's Adjuvant (CFA)-induced inflammatory pain behavior and spared nerve injury (SNI)-induced neuropathic pain behavior. Finally, we

administered the Slack opener loxapine to explore whether Slack activation can ameliorate SNI-induced neuropathic pain behavior.

2. Materials and Methods

2.1 Experimental Animals

Knockout mouse lines lacking Slack globally (Slack$^{-/-}$) or conditionally in sensory neurons (SNS-Slack$^{-/-}$) or in spinal dorsal horn neurons (Lbx1-Slack$^{-/-}$) were used in this thesis. Generation of Slack$^{-/-}$ and SNS-Slack$^{-/-}$ mice has been described previously [134, 135].

To generate Lbx1-Slack$^{-/-}$ mice, 6–12 weeks old male Lbx1^{Cre} mice and female floxed Slack mice were cross-bred. In the Lbx1^{cre} strain, Cre is mainly restricted to spinal cord dorsal horn neurons [136, 137]. The resulting homozygous Lbx1-Slack$^{-/-}$ and littermate floxed mice (referred to as control) were used in experiments.

Experiments were performed in 6–12-week-old mice of either sex. Animals were housed on a 12 hours' light/dark cycle with access to food and water ad libitum. All experiments adhered to the guidelines of the International Association for the Study of Pain and to the ARRIVE (Animal Research: Reporting on *In Vivo* Experiments) guidelines and were approved by our local Ethics Committee for Animal Research (Regierungspräsidium Darmstadt).

2.2 Genotyping

The genotyping of the mouse lines was carried out with ear biopsies. For DNA extraction, ear biopsies were lysed in 50 µl of lysis buffer (lysis buffer for genotyping) containing 0.7 µl Proteinase-K for 4 hours or overnight at 55 °C. To inactivate Proteinase-K, the samples were incubated at 90 ° C for 20 minutes and centrifuged at 13,000 g for 5 minutes. The supernatant containing the DNA was used for the subsequent polymerase chain reaction or stored at –20 °C.

A mixture (Table 1) containing dNTPs and the polymerase (Tag DNA polymerase 2× Master Mix RED; Ambliqon, Odense, Denmark) was used for PCR. In the polymerase chain reaction, a selected section of DNA is first flanked by specific primers and then amplified exponentially. The individual step was proceeded as follows: denaturation of the DNA double-strand, primer hybridization, and extension of the DNA oligonucleotides with deoxynucleotide triphosphates (dNTPs) catalyzed by a thermostable DNA

polymerase. The hybridization temperature was defined by the melting temperatures of the respective primers and the length of the expected PCR products determined the polymerization time. The PCR programs for polymerase chain reaction are listed in Table 2 (for Slack amplification) and Table 3 (for Cre amplification).

Slack		Cre	
Kcnt1 fwd_1	1.5 µl	CB1 fwd	1.5 µl
Kcnt1 rev_1	1.5 µl	CB1 rev	1.5 µl
Kcnt1 rev_2	1.5 µl	Cre fwd	1.5 µl
H_2O	1.5 µl	Cre rev	1.5 µl
RED Extract	10 µl	RED Extract	10 µl
DNA	4 µl	DNA	4 µl

Table 1. Mixture for polymerase chain reaction

Step	Temp. (˚C)	Time (s)	Cycle
Denaturation	95	180	1
Annealing/Extension	95	30	30
	59.7	30	
	72	30	
Stop	72	300	1

Table 2. PCR program for Slack polymerase chain reaction

Step	Temp. (˚C)	Time (s)	Cycle
Denaturation	95	300	1
Annealing/Extension	95	60	40
	55	60	
	72	120	
Stop	72	300	1

Table 3. PCR program for Cre polymerase chain reaction

2. 3 Behavioral studies

Littermate mice were used in all behavioral studies. All animals were habituated to the experimental room maintained at 22 ± 2 °C and 55 ± 10% humidity at least 2

consecutive days before the testing day. On the day of the experiment, mice were allowed to acclimatize in the testing apparatus for 30 minutes prior to the experiment. All behavioral tests were performed by an observer blinded for the genotype and treatment of the animals.

2.3.1 Rotarod test

Mice were tested for overall motor coordination and balance using a Rotarod apparatus (Ugo Basile, Comerio, Italy) programmed to accelerate from 4 to 40 rpm in 300 seconds. After mice were trained on 3 consecutive days, the latency to the first fall was recorded on the experimental day [138].

2.3.2 Dynamic plantar test

The mechanonociceptive threshold was measured using a dynamic plantar aesthesiometer (Ugo Basile, Comerio, Italy). This device employs a non-flexible filament (0.5-mm diameter) with increasing force through a wire mesh floor against the plantar surface of a hindpaw from beneath, and it automatically stops and records the latency time, until the animal withdraws the paw. The force increased from 0 to 5 g over 10 seconds (0.5 g/s ramp) and was then remained at 5 g for a further 10 seconds. The latency time was calculated as the average of 6 consecutive exposures with at least 20 seconds in between [134, 135, 139, 140].

2.3.3 von Frey filament test

Calibrated von Frey filaments (Ugo Basile, Comerio, Italy) ranging from 0.20 to 19.6 mN (0.02 to 2.0 g) were applied to the plantar surface of a hindpaw. In brief, animals were individually placed in a chamber with a wire mesh floor, and allowed to habituate for 30 minutes before testing. Application of the von Frey filaments was started from the 0.6 g filament. Clear paw withdrawal, shaking, or licking during or immediately following the stimulus (up to 3 seconds since the filament was bowed) was determined as nociceptive-like response. The 50% withdrawal thresholds were determined using the up-down method and calculated using of online tool “Up-down method for von Frey experiments” (https://bioapps.shinyapps.io/von_frey_app/) [141].

2.3.4 Hot plate and cold plate test

Mice were placed on an electronically heated or cooled metal surface (Hot/Cold Plate, Ugo Basile, Comerio, Italy). In the hot plate test, the temperature causing shaking or licking of a hindpaw, or jumping was recorded as the nociceptive endpoint. Temperatures of 50, 52 and 54°C were applied with cutoff times of 40, 30, and 20 seconds, respectively. For the cold plate test, the plate was maintained at 10 or 5 °C and the total time that the animal spent lifting or shaking the forepaw within 60 seconds was measured. Only one test per animal was performed [81, 134, 139].

2.3.5 Cold Plantar assay

Mice were acclimated on a borosilicate glass plate (6.5 mm thickness, GVB, Germany) in transparent plastic enclosures for 60 minutes. Powdered dry ice was packed into a modified syringe (3 ml, B. Braun, Germany) with a cut top (1 cm diameter). The open end of the syringe was held against a flat surface while pressure was applied to the plunger to compress the dry ice, and then the dense dry ice pellet was applied to the glass surface underneath a hindpaw. The latency to move the paw vertically or horizontally away from the glass plate was measured with a stopwatch. An interval of at least 7 minutes was allowed between testing separate paws of a single mouse, and an interval of at least 15 minutes was allowed between trials on any single paw. A cutoff time of 20 seconds was used to prevent injury. Three to five measurements per paw were performed [81, 142].

2.3.6 Allyl isothiocyanate (AITC)- and Capsaicin-induced pain behavior

Mice were habituated in a Plexiglass cylinder for 30 minutes before the experiment. Allyl isothiocyanate (AITC) (10 mM in 20 µl saline containing 0.05% DMSO; Sigma Aldrich, Steinheim, Germany) or Capsaicin (5 µg in 20 µl saline containing 2% DMSO; Sigma Aldrich, Steinheim, Germany) was injected into a hindpaw. The time spent licking and biting the injected paw was recorded up to 30 minutes with a full HD camera (Panasonic, HC-V380, Germany). Immediately thereafter, mice were habituated in separate, transparent, plastic chambers (10 × 10 × 12 cm) for 30 minutes. Afterwards, AITC-induced mechanical hypersensitivity of the hindpaw was evaluated using the von Frey test.

2.3.7 Complete Freund's Adjuvant (CFA)-induced inflammatory pain behavior

Mice received 20 µl of CFA (containing 1 mg/mL heat-killed Mycobacterium tuberculosis in 85% paraffin oil and 15% mannide monooleate; Sigma-Aldrich, Steinheim, Germany) in the plantar subcutaneous space of a hindpaw [143]. Mechanical threshold was assessed using the von Frey test.

2.3.8 Spared nerve injury (SNI)-induced neuropathic pain behavior

The spared nerve injury (SNI) model was used to induce neuropathic pain. Briefly, Carprofen (Zoetis, New Jersey, USA) was injected subcutaneously 30 minutes before surgery. Under isoflurane anesthesia, Emla crème (Recipharm Karlskoga, Karlskoga, Sweden) was administrated on the skin of the surgery site and an approximately 1 cm incision in the longitudinal direction proximal to the knee was made. The subcutaneous and muscle layer were dissected bluntly and the sciatic nerve was exposed. Then the tibial and common peroneal branches of the sciatic nerve were tightly ligated and transected distally, while the sural nerve was kept intact [144, 145]. Mechanical hypersensitivity at the lateral surface of the hindpaw was measured using the von Frey filament or dynamic plantar test.

2.4 Real-time reverse transcription PCR

Mice were euthanized by carbon dioxide (CO_2) inhalation and lumbar spinal cord (L3–L5), lumbar DRGs (L3–L5), cerebellum, and the cerebral cortex were rapidly dissected and snap-frozen in liquid nitrogen and stored at –80°C until use. Total RNA from spinal cord and cortex was extracted using TRIzol reagent (Thermo Fisher Scientific, Waltham, USA) and chloroform in combination with the RNeasy Mini Kit (Qiagen, Hilden, Germany) according to the manufacturer´s recommendations. Total RNA from DRGs was isolated using the innuPREP Micro RNA Kit (AJ Innuscreen, Berlin, Germany). Isolated RNA concentration was quantified with a NanoDrop 2000 (Thermo Fisher Scientific, Waltham, USA).

The First Strand cDNA Synthesis Kit (Thermo Fisher Scientific, Waltham, USA) was used to synthesize cDNA from the previously extracted RNA. This contains reverse transcriptase (RT), an RNase inhibitor, deoxyribonucleoside triphosphate (dNTP), primers, and a reaction buffer with the salts required for the reaction. A total volume of

20 µl containing 200 ng RNA and random hexamer primer were used for cDNA synthesis according to the manufacturer's protocol (Table 4).

Quantitative real-time reverse transcription PCR (qRT-PCR) was performed on a CFX96 Touch Real-Time System (Bio-Rad, Hercules, USA) using the iTaq Universal SYBR Green SuperMix (Bio-Rad, Hercules, USA). Primer pairs for Slack, Slick, Slo1, and GAPDH (sequences are described in section 7.8) were all purchased from Biomers (Ulm, Germany). qRT-PCR of TRPV1 mRNA was performed using Taqman gene expression assays (Applied Biosystems, San Mateo, USA) for TRPV1 (Mm01246302_ml) and GAPDH (Mm99999915_gl) mRNA. The primers were used in a final concentration of 10 µM. Positive and negative control reactions were used to verify the results of the first-strand cDNA synthesis steps. A control reaction containing every reagent for the reverse transcription reaction except for the RT enzyme was used to assess for genomic DNA contamination of the RNA sample. No template negative control (NTC) containing every reagent for the reverse transcription reaction except for the RNA template was used to assess for reagent contamination. Human GAPDH control RNA (1.3 kb) and GAPDH-specific control PCR primers supplied in the kit were used for positive control RNA template.

For the qRT-PCR, the iTaq master mix (iTaq Universal SYPR Supermix, Bio-Rad, Hercules, USA) was used to optimize for SYBR Green I dye quantitative PCR on a CFX96 Touch Real-Time System. For each RT-qPCR reaction unit, 1 µl of the cDNA and 9 µl reaction mixture were used, according to the manufacturer's protocol (Table 5). Each reaction (total volume of 10 µl) was performed in duplicate or triplicate by incubating for 2 minutes at 50 °C and 10 minutes at 95 °C, followed by 40 cycles of 15 seconds at 95 °C and 60 seconds at 60 °C (Table 6). Relative expression of target gene levels was determined using the comparative $2^{-\Delta\Delta Ct}$ method. Ct value indicates the cycle number at which the signal of the PCR product crosses an arbitrary threshold set within the exponential phase of the PCR. GAPDH was used as a housekeeping gene for normalization.

RNA	0.2 µg
Nuclease-Free Water	to 10 µl
Primer random hexamer	1 µl
5× Reaction buffer	4 µl

Ribolock RNase Inhibitor	1 µl
dNTP-Mix	2 µl
M-MULV Reverse Transcriptase	2 µl
Total volume	20 µL

Table 4. Protocol for cDNA synthesis.

Component	Volume (µl)
cDNA	1 µl
iTaq-Master Mix (2×)	5 µl
Primer forward (1:10)	1 µl
Primer reverse (1:10)	1 µl
Nuclease-Free Water	2 µl
Final volume	10 µl

Table 5. Reaction mixture for RT-qPCR with iTaq Universal SYBR Green SuperMix.

Step	Temp. (˚C)	Time (s)	Cycle
UDG pre-treatment	50	120	1
Initial Denaturation	95	600	1
Denaturation	95	15	40
Annealing/Extension	60	60	

Table 6. qPCR cycling program.

2.5 Western blot

To detect Slack protein in the spinal cord, mice were euthanized by carbon dioxide (CO_2) inhalation and the lumbar spinal cord (L3–L5) was rapidly dissected, frozen in liquid nitrogen and stored at –80 °C until use. For protein extraction, the tissues were homogenized in ice-cold buffer containing 100 mM Tris-HCl and 1 mM $MgCl_2$, pH 8.0, combined with a protease inhibitor mixture (Protease Inhibitor Cocktail Tablets, Roche, Mannheim, Germany). After freezing the sample solution at –80°C for 40 minutes, lysates were homogenized again and then mixed with a six-fold volume of sucrose buffer (250 mM sucrose, 10 mM Tris-HCl, pH 7.4, supplemented with protease inhibitor mixture). Following centrifugation at 4 ° C at 1000 g for 20 minutes, the supernatant was collected and then centrifuged at 4 °C at 20,000 g for 20 minutes. At the end, the supernatant was

discarded and the resulting pellets were re-suspended in sucrose buffer. Protein concentration was calculated by using a Bradford assay.

Extracted proteins (50 µg) were 1:4 diluted in gel loading buffer (ROTI Load 1, Carl Roth, Karlsruhe, Germany) and denatured at 37°C for 30 minutes. Marker (Prestained Protein Ladders, Bio-Rad, Hercules, USA) and proteins were then loaded to 6% SDS-PAGE (Sodium Dodecyl Sulfate Poly-Acrylamide Gel Electrophoresis) in the Mini-Protean 3 electrophoresis tank (Bio-Rad, Hercules, USA) filled with 1× SDS-PAGE running buffer. A SDS-PAGE was performed to separate proteins with different size into distinct bands within the gel. After electrophoresis, proteins were blotted onto a 0.45 µm pore size nitrocellulose membrane (Amersham Biosciences, Freiburg, Germany) by electroblotting (Trans-Blot Turbo System, Bio-Rad, Hercules, USA) for 7 minutes. The membrane was then incubated with blocking buffer (Intercept Blocking Buffer; LI-COR Biosciences, Lincoln, USA) for 1 hour at room temperature.

Afterwards, membranes were incubated with mouse anti-slo2.2 (1:500; NeuroMab, Davis, USA) or mouse anti-α-tubulin (1:800, Millipore, Billerica, USA) dissolved in blocking buffer containing 0.2% Tween 20 overnight at 4°C on a shaker. The following day, the membranes were washed 3 times in Phosphate Buffered Saline with 0.1 % Tween 20 (PBS-T) and then incubated with secondary antibodies for 1 hour at room temperature. The following second antibodies were used: IRDye 800CW Goat anti-Mouse IgG_1 (1:10000; LI-COR Biosciences, Lincoln, USA) and IRDye 680LT Goat anti-Mouse IgG_1 (1:10000; LI-COR Biosciences, Lincoln, USA). After washing 3 times with PBS-T, the membrane was then visualized using an Odyssey Infrared Imaging System (LI-COR Biosciences, Lincoln, USA).

2.6 Immunohistochemistry

Mice were killed by CO_2 and immediately perfused intracardially with 0.9% saline, followed by 1% or 4% paraformaldehyde in Phosphate Buffered Saline (PBS), pH 7.4. The lumbar spinal cord and DRGs (L3–L5) were dissected and cryo-protected in 30% sucrose overnight. Tissues were embedded and frozen in tissue freezing medium (Tissue-Tek O.C.T. Compound, Sakura, Torrance, USA) on dry ice, cryostat sectioned into 14 µm (DRGs) or 20 µm (Spinal cord) sections, and stored at –80°C until use.

For immunostaining, sections were permeabilized for 5 minutes with PBS containing

0.1% Triton X-100 (PBST), and then incubated for 1 hour with blocking solution containing 10% normal goat serum (Invitrogen, Rockford, USA) and 3% bovine serum albumin (BSA; Invitrogen, Rockford, USA) in PBS. After the blocking step, sections were incubated with primary antibodies diluted in 3% BSA in PBS overnight at 4°C or for 2 hours at room temperature. The following primary antibodies were used: mouse anti-slo2.2 (1:400; NeuroMab), rabbit anti-calcitonin gene-related peptide (anti-CGRP; 1:800; Calbiochem, San Diego, USA), rabbit anti-NF200 (1:2000; Sigma Aldrich, Steinheim, Germany), rabbit anti-tyrosine hydroxylase (anti-TH; 1: 600; Millipore, Temecula, USA), rabbit anti-glutamate decarboxylase 67 (GAD67; 1:500; Chemicon, Temecula, USA), and guinea pig anti-protein kinase C isoform γ (PKC-γ; 1:800; Frontier Institute, Tokyo, Japan), rabbit anti-VGLUT3 (1:400, Synaptic Systems, Göttingen, Germany), rabbit anti-TRPV1 (1:800; Alomone, Jerusalem, Israel), and rabbit anti-VGLUT2 (1:400, Synaptic Systems, Göttingen, Germany). Sections were then washed in PBS and stained with secondary antibodies conjugated with Alexa Fluor 488 or 555 (Invitrogen, Eugene, USA) at room temperature for 2 hours. For staining with Griffonia simplicifolia isolectin B4 (IB4), sections were incubated with Alexa Fluor 488-conjugated IB4 (10 µg/ml in PBS buffer containing 1 mM $CaCl_2 \cdot 2H_2O$, 1 mM $MgCl_2$, 1 mM $MnCl_2$, and 0.2% Triton X-100, pH 7.4; Invitrogen, Eugene, USA) for 2 hours at room temperature. After staining, slides were immersed for 5 minutes in 0.06% Sudan black B (in 70% ethanol; Sigma-Aldrich, Steinheim, Germany) to reduce lipofuscin-like autofluorescence [146]. After washing for 3 times in PBS, slides were mounted with Fluoromount G (Thermo Fisher Scientific, Waltham, USA). Images were taken using an Eclipse Ni-U (Nikon, Düsseldorf, Germany) microscope equipped with a monochrome charge-coupled device camera, and were pseudocolored and superimposed. Adjustment of brightness and contrast was done with Adobe Photoshop 2020 software (Adobe Systems, San Jose, USA). Negative controls for immunohistochemistry were carried out by omitting the first and/or the second antibodies or by incubating tissues of $Slack^{-/-}$ mice. Only cells showing clear staining signals above background level, with a threshold set based on negative control staining, were included. The total number of DRG neuron somata was counted based on their autofluorescence visualized in the FITC channel.

2.7 In situ hybridization (ISH)

In situ hybridization (ISH) was performed using the QuantiGene ViewRNA ISH tissue assay (Thermo Fisher Scientific, Waltham, USA) following the manufacturer's protocol and our previous report [139]. We used hybridization probes (all designed by Thermo Fisher Scientific) for mouse Slack (Kcnt1, type 1 probe; #VB1-21049), vesicular GABA transporter (VGAT, type 6 probe; #VB6-17400), TRPA1 (type 6 probe; #VB6-18246) and vesicular glutamate transporter 2 (VGLUT2, type 6 probe; # VB6-16625). Controls included scramble type 1 (#VF1-17155) and type 6 (#VF6-18580) probe sets. Briefly, tissue sections were fixed in 4% PFA for 16–18 hours at 4°C, dehydrated through 50%, 70% and 100% ethanol, treated with protease QF for 25 minutes at 40 °C, and incubated with probe sets for 2 hours at 40 °C. In double ISH experiments, type 1 and type 6 labeled probes were simultaneously incubated. After preamplifier and amplifier hybridization, the signal was developed via reaction with fast red and blue substrate (for type 1 and 6 probes, respectively). Finally, sections were stained with DAPI (Invitrogen, Carlsbad, USA) and mounted with Fluoromount G.

Images were taken using an Eclipse Ni-U microscope equipped with a monochrome charge-coupled device camera, and were pseudocolored and superimposed. Adjustment of brightness and contrast was done using Adobe Photoshop 2020. Negative control sections for in situ hybridization were performed by incubating type 1 and type 6 scramble probes. Only cells containing DAPI-positive nuclei and showing clear staining signals above background level, with a threshold set based on scramble control hybridization, were included.

2.8 Cell Culture

All work in the cell culture was carried out under a clean workbench (Haraeus Instruments, Hanau, Germany) to ensure sterile work. Autoclaved Millipore water was used to prepare solutions for cell culture. Cell culture media were stored according to the manufacturer's instructions.

2.8.1 HEK-293 cell culture for patch clamp recordings

A human embryonic kidney 293 (HEK293) cell line and a HEK293 cell line stably expressing human Kcnt1 (referred to as HEK-Slack cells; SB Drug Discovery,

Lanarkshire, UK) were cultured in minimum essential medium with 10% fetal calf serum, supplemented with 2 mM L-glutamine and 0.6 mg/mL G-418 (all from Gibco/Thermo Fisher Scientific) at 37 °C in humidified 5% CO_2. Cells were split every 3 to 4 days and seeded 2 days before experiments. HEK-Slack cells that additionally express TRPA1 (referred to as HEK-Slack-TRPA1 cells) were generated with a pcDNA3.1$^+$ vector plasmid (NM_007332.2, GenScript, Leiden, the Netherlands) combined with a GFP-tagged reporter plasmid (pIRES2-EGFP) using Roti-Fect transfection reagent (Carl Roth, Karlsruhe, Germany) according to the manufacturer's instructions. Before transfection, the cells were passaged once or twice until they reached 60% to 70% confluency. After transfection, 70 µl of the harvested and trypsinized HEK-Slack-TRPA1 cells with a confluence of 50% were seeded on Poly-D-Lysine (200 µg/ml, Sigma-Aldrich, Steinheim, Germany) glass coverslips and incubated at 37 °C one day before the experiment.

2.8.2 Primary cell culture for patch clamp recordings

Twelve-Well Cell Culture Plates (Greiner Bio-One, Germany) were prepared before DRG dissection. Briefly, 10 mm coverslips (Thermo Fisher, Braunschweig, Germany) were put into cell culture plate and washed with 70% Ethanol. Poly-D-Lysine (200 µg/ml) was dropped to the middle of each coverslip. After drying, coverslips were washed with sterilized water.

Lumbar DRGs (L3–L5) were dissected from 6–8-week-old mice and pooled in ice cold Dulbecco´s Modified Eagel Medium (DMEM; Life Technologies, Paisley, UK). After centrifugation at 800 rpm for 3 minutes, the supernatant was discarded. Each remnant was incubated in the DMEM containing 500 U/ml Collagenase Type IV (Sigma-Aldrich, Mannheim, Germany) and 2.5 U/ml Dispase II (Sigma-Aldrich, Mannheim, Germany) at 37° C for 30 minutes. Then cells were washed twice with DMEM, mechanically dissociated by pipetting up and down, transferred to coverslips, and incubated at 37° C in a 5% CO_2 incubator for 30 minutes. Finally, cells were cultured in supplemented Neurobasal medium with 2% B27 (Life Technologies, Grand Island, USA), 1% L-glutamine (Life Technologies, Paisley, UK), 0.1% Gentamicin (Carl Roth, Karlsruhe, Germany) and 1% Penicillin-Streptomycin (Life Technologies, Paisley, UK) at 37 °C in a 5% CO_2 incubator until use.

2.8.3 Primary cell culture for Ca^{2+} Imaging

Lumbar DRGs (L3–L5) were dissected from 6-8 weeks old mice and transferred to ice cold Hanks's balanced solution (HBSS; Life Technologies, Paisley, UK). After centrifugation at 800 rpm for 3 minutes, the supernatant was removed. Then tissues were incubated at 37° C for 90 minutes with HBSS containing 500 U/ml Collagenase Type IV and 2.5 U/ml Dispase II. After washing twice with supplemented Neurobasal Medium with 10% fetal calf serum (FCS; Sigma-Aldrich, Steinheim, Germany) and once with HBSS, tissues were digested with 0.05 % Trypsin/EDTA (Life Technologies, Paisley, UK) at 37° C for 10 minutes. Following washing twice with Neurobasal Medium plus 10% fetal calf serum, the supernatant was discarded and the cell pellet was re-suspended in Neurobasal Medium containing 10% fetal calf serum. Cells were transferred to 10 mm coverslip in cell culture dish and incubated at 37°C in a 5% CO_2 incubator for 2 hours. Then the cells were cultured in Neurobasal medium containing 2% B27, 1% L-glutamine, 0.1% Gentamicin and 1% Penicillin-Streptomycin at 37 ° C and 5% CO_2 overnight.

2.9 Ca^{2+} Imaging

A coverslip with the cultured neurons was incubated for 45 minutes at 37 ˚C in the supplemented Neurobasal Medium loaded with 5 μM Calcium indicator Fura-2-AM-ester (Biotium, Fremont, USA) dissolved in DMSO. After the incubation, the coverslip was transferred onto the imaging chamber of a motorized microscope stage (Märzhäuser Wetzlar, Wetzlar, Germany), and continuously superfused with a physiological Ringer solution (145 mM NaCl, 1.25 mM $CaCl_2$, 1 mM $MgCl_2$, 5 mM KCl, 10 mM Glucose, and 10 mM HEPES; pH 7.4). Once mounted, the chamber was connected to the perfusion system (ValveLink8.2 Perfusion Controller, Automate Scientific, Berkeley, USA). Neurons were then focused under a Nikon Eclipse Ts2R inverse microscope (Nikon, Düsseldorf, Germany) equipped with a complete illumination system DG4 (Sutter Instruments, Novato, USA), a digital camera (ORCA-05G, Hamamatsu, Tokyo, Japan) and Fura-2 filters (Nikon, Düsseldorf, Germany). In our experiment, four or five fields of images from each coverslip were chosen and captured under 340 and 380 nm wavelengths. Images were taken every 2 seconds at two wavelengths. During the experimental period, the motorized microscope stage was moved automatically to a field to collect an image at 340 and 380 nm wavelengths, then to the next field rapidly until all fields were collected.

Exposure times for each wavelength were consistent. For analysis, we used NIS-Elements software (Nikon) to measure the ratio of 340:380 nm wavelength at each region of interest. A calcium response was defined as a simultaneous increase at 340 nm and a decrease at 380 nm, when the 340/380 nm ratio normalized to baseline exceeded 20% of the baseline level. For stimulation, 50 or 200 μM AITC dissolved in Ringer solution was applied by bath perfusion for 20 seconds at room temperature. At the end of each measurement, cells were stimulated for 20 seconds with 75 mM KCl to identify viable neurons for evaluation.

2.10 Patch-clamp recordings

Recording microelectrodes (< 1 μm) were fabricated by a horizontal puller (Flaming/Brown Micropipette Puller, Sutter Instrument, Novato, USA) from a Borosilicate glass capillary (0.86×1.50×80 mm without filament; Science Products, Hofheim, Germany). The input resistance of recording Microelectrodes should be around 5–8 Mega-Ohm. The resistance was measured by the patch-clamp amplifier and the software when the tip of micropipette loading with electrode solution was placed in the bath solution.

Whole-cell voltage clamp recordings were conducted with an EPC 9 amplifier combined with Patchmaster software (HEKA, Reutlingen, Germany). Briefly, the bath application system was running at 1−2 ml per minute with extracellular solution at room temperature when a coverslip was placed in. Afterwards, the micropipette was loaded with the half-full of intracellular solution. Air bubbles were removed before placing it on the pipette holder. When a targeted cell was found, the pipette was lowered into the bath solution through the micromanipulator and approached to surface of the interested cell until an obvious change in Recording Microelectrodes resistance was obtained. To form a high resistance Giga-Ohm seal, the chosen cell was gently touched with the pipette by using negative pressure (suction with a syringe). Once a Giga-Ohm seal had been formed, the voltage clamp was changed to a negative voltage close to the expected cell resting potential (–60 to –70 mV). Rupture of the membrane patch was achieved by applying suction accompanied with sudden appearance of large capacity transients at the leading and trailing edges of the pulse. For acquisition, currents were filtered at 5 kHz and sampled at 20 kHz. I_K were elicited by maintaining the cell at a holding potential of –70 mV. The test pulses were ascended in gradients of 20 mV from –120 to +120 mV in 500 milliseconds.

Offline analyses were performed using the Fitmaster software (HEKA). For patch-clamp recording with DRG neurons, the coverslip was incubated in extracellular solution containing 10 μg/mL fluorescein isothiocyanate conjugated IB4 for 10 min, and only IB4-binding DRG neurons were analyzed. For HEK-TRPA1 and HEK-Slack-TRPA1 cells recording, only cells with GFP fluoresce were analyzed. AITC stock solution (5 μL, 24 mM in 20% DMSO) was added with a pipette to the bath chamber (volume 600 μL) to reach a final concentration of 200 μM, and recordings were started 60 s thereafter. A-967079 stock solution (5 μL, 1.2 mM in 20% DMSO) was added with a pipette to the bath chamber to reach a final concentration of 10 μM, and recordings were started 180 s thereafter. All recordings were taken while the perfusion system was stopped.

2.11 Quantification and statistical analysis

For quantification of Slack mRNA-positive DRG neuron populations in in situ hybridization experiments, lumbar DRGs (L3–L5) from 3 mice were cut into serial sections. Per animal $\geqslant$ 2 sections at least 100 μm apart with at least 100 cells were counted manually. Only cells containing DAPI-positive nuclei and showing clear staining signals above background level, with a threshold set based on scramble control hybridization, were included.

For quantification of markers of DRG neuron subpopulations, serial sections of lumbar DRGs (L3–L5) from SNS-Slack$^{-/-}$ and WT mice (3–4 mice per genotype) were used. At least 2 sections per animal were counted manually. Each section was at least 100 μm apart from others with more than 100 cells counted. Only cells showing clear staining signals above background level were included. For calculation of the percentage of marker-positive DRG neurons, the total number of DRG neuron somata was counted based on their autofluorescence visualized in the FITC channel.

For quantification of Slack mRNA and protein in qRT-PCR and western blot experiments, lumbar DRGs (L3–L5) were taken from at least 3 mice per genotype.

Data are shown as mean ± SEM. Statistical evaluation was done with GraphPad Prism 8 for windows (GraphPad, San Diego, USA). Normal distribution of data was investigated using the Kolmogorov-Smirnov test. For behavioral experiments with time courses, a two-way analysis of variance (ANOVA) followed by Sidak´s multiple comparisons test was performed to measure effects across time between groups. An unpaired t test was used to compare the mean of two groups in behavioral experiments,

western blot, qRT-PCR analyses, calcium imaging experiments, and for quantification of cell populations. For patch clamp experiments, a two-way ANOVA with Holm-Sidak´s multiple comparisons were used for current voltage relationships between before and after AITC. No statistical methods were used to predetermine sample sizes, but the sample sizes are based on our previous knowledge and similar to those reported in previous publications and standard practices in the field. No animals or data points were excluded from the analyses. Numbers of experiments and statistical results are provided in the figure legends. A probability value $p < 0.05$ was considered as statistically significant.

3. Results

3.1 Slack controls AITC-induced pain behavior in mice

3.1.1 Slack$^{-/-}$ mice demonstrate increased nociceptive responses to TRPA1 activation

To assess a potential role of Slack in TRPA1-mediated pain pathways, we first compared the nociceptive behavior of WT and Slack$^{-/-}$ mice following intraplantar injection of the TRPA1 activator AITC (10 mM in 20 µl saline containing 2% DMSO) into a hindpaw. Both genotypes displayed an immediate licking and biting behavior, which is an indication of pain. Interestingly, the paw licking and biting in Slack$^{-/-}$ mice was significantly increased as compared to WT mice (Figure 1A). Moreover, the cumulative paw licking and biting time over 30 minutes was considerably higher in Slack$^{-/-}$ mice than in WT mice (Figure 1A, right), suggesting that Slack$^{-/-}$ mice experienced increased acute nociceptive pain after TRPA1 activation as compared to WT mice.

In addition to the immediate nocifensive behavior, intraplantar injection of AITC can also elicit a persistent hypersensitivity of the affected paw [130]. We therefore tested the mechanical paw sensitivity after AITC injection. As shown in Figure 1B, intraplantar AITC elicited marked mechanical hypersensitivity during the 1–72-hour period after AITC injection. Of note, the extent of mechanical hypersensitivity was significantly increased in Slack$^{-/-}$ mice as compared to WT mice (Figure 1B). qRT-PCR control experiments revealed similar TRPA1 mRNA expression in DRGs of WT and Slack$^{-/-}$ mice (Figure 1C), suggesting that there was no compensatory regulation due to the Slack knockout. Taken together, these results suggest that Slack may play an inhibitory role in the immediate and persistent behavioral responses to TRPA1 activation.

In addition to TRPA1, TRPV1 acts as a major detector of nociceptive stimuli and potentiates the inflammatory process [147]. To examine if Slack is also involved in TRPV1-mediated pain processing, we next assessed the nocifensive response of WT and Slack$^{-/-}$ mice after intraplantar injection of the TRPV1 activator capsaicin (5 µg in 20 µl saline containing 2% DMSO) into a hindpaw. Unlike the AITC-induced pain response, the capsaicin evoked licking and biting behavior was comparable between WT and

Slack$^{-/-}$ mice during the 10-minute test period (Figure 1D). We subsequently tested capsaicin-induced mechanical pain sensitivity; however, no significant differences were observed between WT and Slack$^{-/-}$ mice (Figure 1E). qRT-PCR experiments demonstrated similar TRPV1 mRNA levels in DRGs of Slack$^{-/-}$ and WT mice (Figure 1F). These results point to a limited contribution of Slack to TRPV1-mediated pain processing, whereas it specifically controls TRPA1-mediated pain processing.

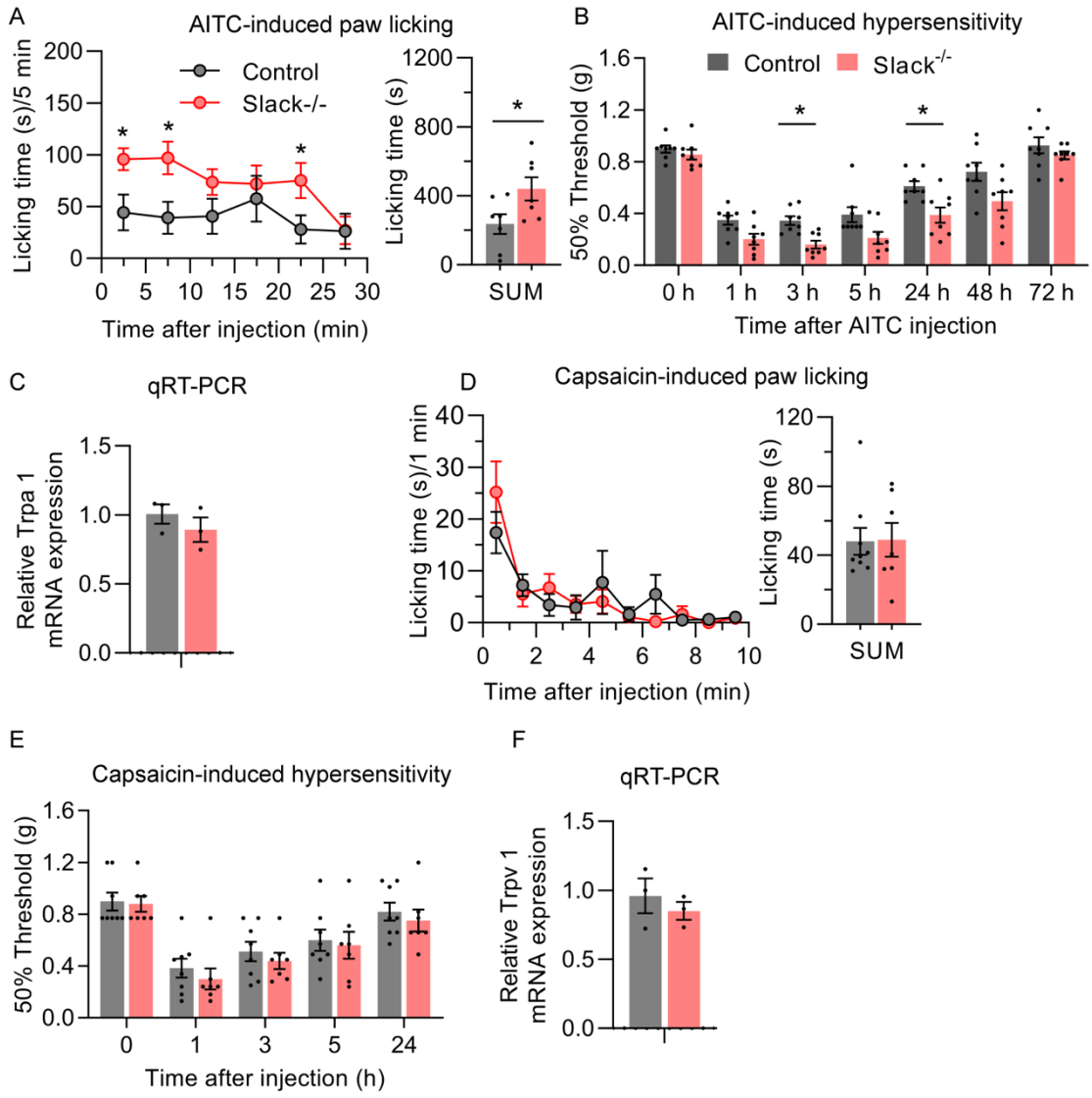

Figure 1. Slack$^{-/-}$ mice display increased AITC-evoked but normal capsaicin-evoked pain behavior. (A) Time course of paw licking and biting (left) and sum of licking and biting time over 30 minutes (right; p = 0.0394; n = 7 mice per group) after intraplantar AITC injection in wildtype (WT) and Slack$^{-/-}$ littermates. (B) Time course of mechanical hypersensitivity after intraplantar AITC injection. Two-way analysis of variance (ANOVA), effect of genotype (p = 0.0007) with Sidak´s multiple comparisons test (p values represent comparisons between

genotypes for each time point: 3 h, p = 0.0421; 24 h, p = 0.0076; 48 h, p = 0.0064; n = 8 mice per group). Note that both licking/biting behavior and mechanical hypersensitivity are significantly increased in Slack$^{-/-}$ mice after AITC injection. (C) Quantitative RT-PCR in DRGs of WT and Slack$^{-/-}$ mice reveals that the transient receptor potential (TRP) ankyrin 1 (TRPA1) mRNA expression is not compensatory regulated in the absence of Slack (p = 0.3727; n = 3 mice per group). (D) Time course of paw licking and biting (left) and sum of licking and biting time over 10 minutes (right; p = 0.9621; n = 7-8 mice per group) after intraplantar capsaicin injection. (E) Time course of mechanical hypersensitivity after intraplantar capsaicin injection. Two-way ANOVA, effect of genotype (p = 0.5893; n = 7-8 mice per group). Note that the capsaicin-induced pain behavior is unaltered in Slack$^{-/-}$ mice. (F) Quantitative RT-PCR in DRGs of WT and Slack$^{-/-}$ mice reveals that TRP vanilloid 1 (TRPV1) mRNA expression is not compensatory regulated in the absence of Slack (p = 0.4874; n = 3 mice per group).

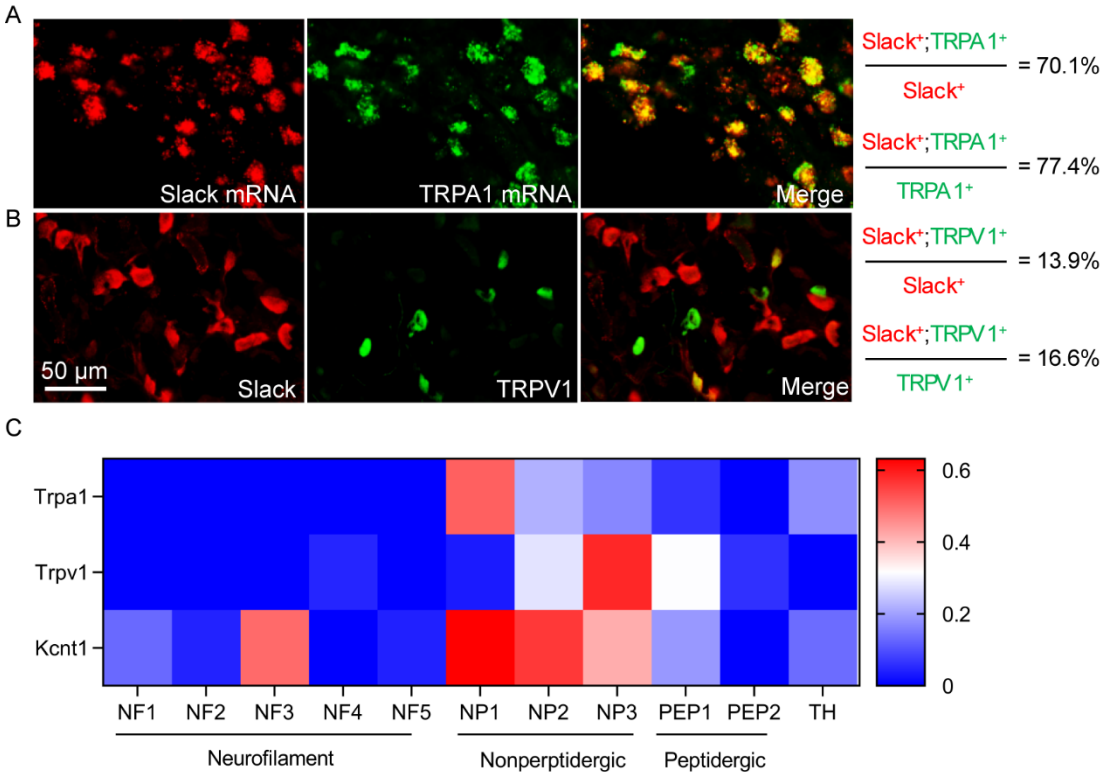

Figure 2. (A) Double in situ hybridization of Slack mRNA and TRPA1 mRNA in DRGs. n = 7-12 sections from 3 mice per group; Scale bar, 50 µm. (B) Double-labeling immunostaining of Slack and TRPV1 in DRGs. n = 7-12 sections from 3 mice per group; Scale bar: 50 µm. Quantitative summary of co-expression in A and B is shown on the right. (C) Expression of TRPA1, TRPV1, and Slack (gene Kcnt1) across sensory neuron subsets from published scRNA-seq data [148].

To assess the cellular distribution of TRPA1 and Slack in the DRG neurons, we performed double-labeling *in situ* hybridization of Slack mRNA with TRPA1 mRNA. We found 70.1 ± 0.3% of Slack-positive (Slack^{+}) sensory neurons expressed TRPA1, whereas 77.4 ± 3.7% TRPA1-positive (TRPA1^{+}) sensory neurons expressed Slack (Figure 2A). Further immunostainings using a previously validated Slack monoclonal antibody [134, 135] revealed that 13.9 ± 1.6% of Slack^{+} cells were positive for TRPV1,

and 16.6 ± 2.3% of the TRPV1$^+$ cells were positive for Slack (Figure 2B). In accordance with these findings, in a published single-cell RNA-sequencing dataset of mouse DRG neurons [25], the expression of TRPA1 was highest in the NP1 cell population that also showed high *Kcnt1* (Slack) expression, whereas expression of TRPV1 was highest in the NP3 cell population with only moderate Slack expression (Figure 2C). Hence, the observation that Slack in sensory neurons is highly co-expressed with TRPA1 but has only a minor co-expression with TRPV1 supports our behavioral findings described above. Collectively, these results indicate that Slack specifically regulates TRPA1-mediated pain processing.

3.1.2 AITC-induced pain behavior is increased in sensory neuron-specific Slack mutants

Based on our findings described in section 3.1.1 that depletion of Slack globally resulted in increased responses to AITC and that our *in situ* hybridization experiments revealed a high co-expression of Slack and TRPA1 in sensory neurons [25, 133], we hypothesized that there is a specific contribution of Slack in sensory neurons to AITC-induced pain processing *in vivo*. To test this hypothesis, we generated SNS-Slack$^{-/-}$ mice which specifically lack Slack in sensory neurons. Genotyping was performed by PCR using specific primers (primers sequences are described in section 7.8) (Figure 3A). qRT-PCR analysis indicated that the Slack mRNA levels were not altered in the spinal cord, cerebellum and cortex, but they were significantly reduced in the DRGs of SNS-Slack$^{-/-}$ mice (Figure 3B). Furthermore, the overall frequencies of the DRG neuron populations positive for NF200, IB4 or CGRP were similar between the SNS-Slack$^{-/-}$ and control mice (Figure 3C and 3D), and the distribution of the terminals of the nociceptive and thermoreceptive primary afferents in the superficial dorsal horn were normal in the SNS-Slack$^{-/-}$ mice (Figure 3E), suggesting that the lack of Slack did not affect the morphology or general structure of sensory neurons.

After AITC injection into a hindpaw, the SNS-Slack$^{-/-}$ mice demonstrated increased licking and biting behavior as compared to control mice (Figure 3F, left). The cumulative time spent on paw licking and biting during the 30-minute time period was significantly different between SNS-Slack$^{-/-}$ and control mice (Figure 3F, right). However, the extent of mechanical hypersensitivity evoked by the intraplantar injection of AITC was similar at 24 hours after AITC injection (Figure 3G). By contrast, the levels of TRPA1 mRNA

in DRGs from SNS-Slack$^{-/-}$ and control mice were similar (Figure 3H). Taken together, our data demonstrated that Slack in sensory neurons controls TRPA1-mediated pain.

3.1.3 TRPA1-dependent calcium transients in sensory neurons are unaltered in Slack$^{-/-}$ mice

TRPA1 is a nonselective cation channel and its activation elevates the intracellular Ca^{2+} concentration in DRG neurons [149, 150]. To test whether the increased AITC-induced pain behavior in Slack$^{-/-}$ and SNS- Slack$^{-/-}$ mice might be associated with increased Ca^{2+} signals, we compared the TRPA1-dependent changes in the intracellular Ca^{2+} in isolated DRG neurons from naïve Slack$^{-/-}$ and WT littermate controls via Fura-2 Ca^{2+} imaging. After application of 200 μM AITC, we observed that the peak responses in DRG neurons of Slack$^{-/-}$ mice were like those in WT mice (Figure 4A). Similarly, we did not find significant different changes in the total number of neurons that responded to 200 μM AITC in Slack$^{-/-}$ and WT mice (Figure 4B). As shown in Figure 4C, the representative traces for the Ca^{2+} influx following incubation with 200 μM AITC showed similar increases in WT and Slack$^{-/-}$ DRG neurons. Viable neurons were identified by eliciting depolarization with 75 mM KCl for 20 seconds. Similar effects were observed when using a lower concentration of AITC (50 μM): the averaged peak amplitudes (Figure 4D), the percentage of responsive neurons (Figure 4E) and representative traces for Ca^{2+} influx (Figure 4F) showed a comparable change after stimulation of 50 μM AITC. We conclude, therefore, that the TRPA1-dependent Ca^{2+} influx in DRG neurons is not modulated by Slack.

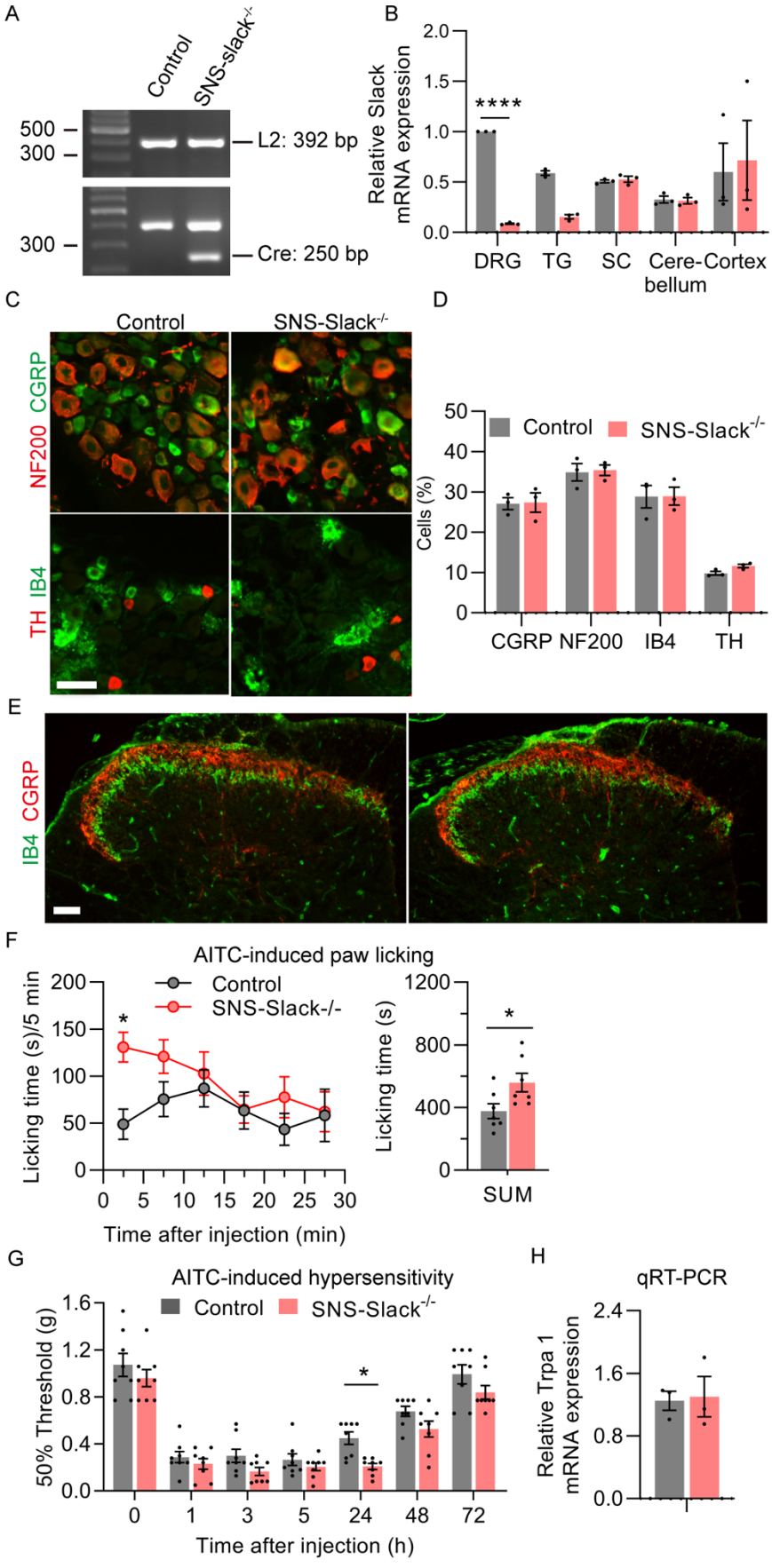
A
Control
SNS-slack-/-
500
300
L2: 392 bp
300
Cre: 250 bp
B
Relative Slack mRNA expression
2.0
1.5
1.0
0.5
0.0
****
DRG
TG
SC
Cere-bellum
Cortex
C
Control
SNS-Slack-/-
NF200 CGRP
TH IB4
D
Control
SNS-Slack-/-
Cells (%)
50
40
30
20
10
0
CGRP
NF200
IB4
TH
E
IB4 CGRP
F
AITC-induced paw licking
Control
SNS-Slack-/-
Licking time (s)/5 min
200
150
100
50
0
*
0
5
10
15
20
25
30
Time after injection (min)
Licking time (s)
1200
800
400
0
*
SUM
G
AITC-induced hypersensitivity
Control
SNS-Slack-/-
50% Threshold (g)
1.6
1.2
0.8
0.4
0.0
*
0
1
3
5
24
48
72
Time after injection (h)
H
qRT-PCR
Relative Trpa 1 mRNA expression
2.4
1.6
0.8
0.0

Figure 3. SNS-Slack$^{-/-}$ mice display significantly increased AITC-evoked pain behavior. (A) Representative example of a genotyping PCR using genomic DNA from mouse ear biopsies as templates (Genotype of control: Slack$^{L2/L2}$, Cre^{-}; Genotype of SNS-Slack$^{-/-}$: Slack$^{L2/L2}$, Cre^{+}) (B) Quantitative RT-PCR in lumbar DRGs, lumbar spinal cord, cerebellum and prefrontal cortex reveals Slack mRNA is selectively reduced in DRGs of SNS-Slack$^{-/-}$ mice ($p = 0.0002$; n = 3 mice per group). (C) Double staining of lumbar DRGs of SNS-Slack$^{-/-}$ and control mice using standard cell markers (neurofilament 200, NF200; calcitonin gene-related peptide, CGRP; tyrosine hydroxylase, TH; isolectin B4, IB4) (Scale bar: 100 µm). (D) Overall frequencies of DRG neurons immunoreactive for CGRP, NF200, TH, or binding IB4 are similar in SNS-Slack$^{-/-}$ and control mice (7-12 sections and 3290-4489 neurons were counted, n = 3 mice per group). (E) Double staining of lumbar spinal cord of SNS-Slack$^{-/-}$ and control mice using markers of sensory neuron populations (CGRP, IB4) indicates that the macroscopic morphology of spinal cord is unaltered in SNS-Slack$^{-/-}$ mice (Scale bar: 100 µm.). (F) Time course of paw licking and biting induced by AITC injection into a hindpaw in control and SNS-Slack$^{-/-}$ littermates. Licking and biting behaviors were significantly increased in SNS-Slack$^{-/-}$ mice at the period of time 0-5 minutes (G, left; $p = 0.0075$; n = 8-9 mice per group), and in the sum of licking and biting time over 30 minutes (G, right; $p = 0.0223$; n = 8-9 mice per group). (G) AITC-induced mechanical hypersensitivity is increased in SNS-Slack$^{-/-}$ mice 24 hours after AITC injection but unaltered during 1-5 h and 48-72 h after AITC injection ($p = 0.0082$; n = 8 mice per group). (H) Quantitative RT-PCR shows similar TRPA1 mRNA expression in lumbar DRGs from control and SNS-Slack$^{-/-}$ mice ($p = 0.8638$; n = 3 mice per group). Two-way ANOVA and unpaired t test. * $p < 0.05$. Data are presented as mean ± SEM.

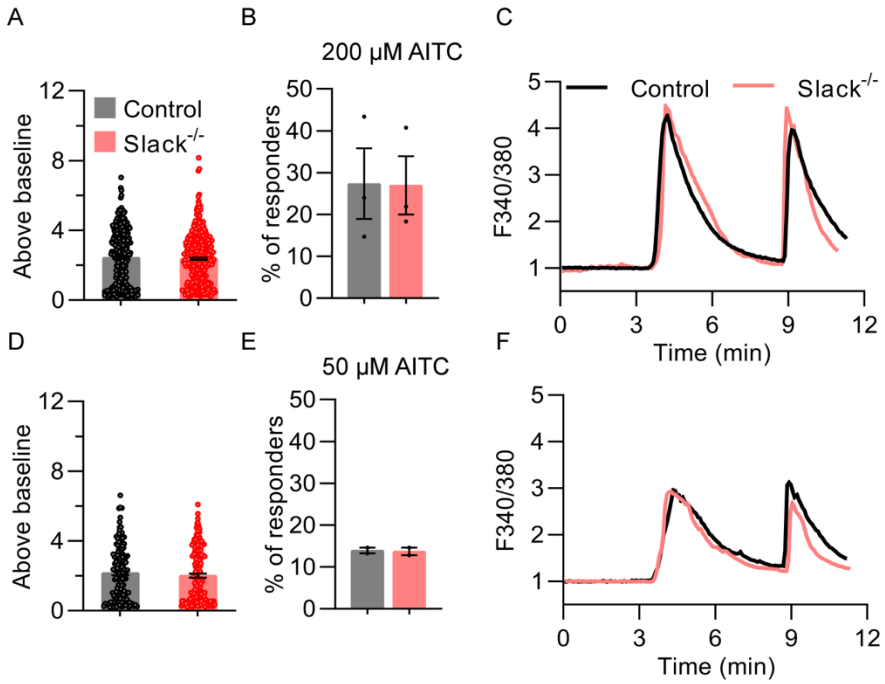

Figure 4. AITC-mediated calcium influx is normal in sensory neurons of Slack$^{-/-}$ mice. Experiments were performed in lumbar DRG neurons (n = 1119-2003 neurons were counted in 3 mice per genotype). (A) Quantification of the magnitude of the calcium response to stimulation with 200 µM AITC (p = 0.5264; 452 responsive neurons from Slack$^{-/-}$ mice and 474 reactive neurons from control mice, n = 3 mice per group). (B) Quantification of the percentage of responsive neurons to 200 µM AITC (p > 0.9999; n = 3 mice per group). (C) Representative Fura-2-ratiometirc calcium traces in DRG neurons of WT and Slack$^{-/-}$ mice evoked by 200 µM AITC and 75 mM KCl. (D) Quantification of the magnitude of the calcium response to stimulation with 50 µM AITC (p = 0.4772; 160 responded neurons from Slack$^{-/-}$ mice and 159 reacting neurons from control mice, n = 3 mice per group). (E) Quantification of the percentage of responsive neurons to 50 µM AITC (p = 0.6667; n = 3 mice per group). (F) Representative Fura-2-ratiometirc calcium traces in DRG neurons of WT and Slack$^{-/-}$ mice evoked by 50 µM AITC and 75 mM KCl. These data show that AITC-evoked calcium responses are normal in DRG neurons from Slack$^{-/-}$ mice compared to WT mice. Unpaired t test. Data are presented as mean ± SEM.

3.1.4 TRPA1 activation modulates Slack-mediated potassium currents in sensory neurons and transfected HEK cells

To assess whether the activation of TRPA1 by AITC influences the Slack-dependent potassium currents in sensory neurons, we measured the outward potassium currents (I_K) in the dissociated sensory neurons of WT and Slack$^{-/-}$ mice by whole-cell patch-clamp. As described previously, only IB4-positive (IB4$^+$) sensory neurons were selected for recording [134]. The I_K currents were recorded at potentials ranging from -120 to +120 mV in intervals of 20 mV. Recordings were performed before and after pipetting AITC (final concentration 200 µM). In the WT DRG neurons, the magnitude of the I_K current

decreased with time (from 30 seconds to 3 minutes) after the stimulation with AITC (Figure 5A). Based on these preliminary data, in this thesis, recordings in Slack$^{-/-}$ and WT mice were analyzed by comparing the baseline recording with that obtained 60 seconds following the addition of AITC. However, it is noteworthy that the I_K current is composed not merely of Slack-mediated currents, but may also involve TRPA1-dependent channels or other sources. Under the conditions of the physiological extracellular buffer, the amplitude of I_K in sensory neurons of WT mice was significantly reduced after stimulation with AITC, with a linear I-V relationship at positive potentials from +80 to +120 mV (Figure 5B, black). By contrast, under same conditions, the I_K amplitude in sensory neurons of Slack$^{-/-}$ mice was not significantly altered following the addition of AITC (Figure 5B, red). These data suggest that TRPA1 activation reduces the Slack-mediated I_K in IB4$^+$ sensory neurons of WT mice, but not the Slack-independent I_K.

TRPA1 can be activated not only by various stimuli and a range of pungent chemicals, but also by highly depolarizing voltages (≥ 100 mV) [151-153]. In order to discern whether the depolarization-dependent activation of TRPA1 participated in the reduction of I_K in our experimental setting, we took advantage of the TRPA1 antagonist A-967079 [123, 154]. Additional whole-cell recordings were made at baseline and at 3 minutes following the addition of A-967079 (final concentration 10 μM) into the bath solution. As shown in Figure 5C, the outward I_K current in sensory neurons of both WT and Slack$^{-/-}$ mice was significantly reduced at +120 mV following the inhibition of TRPA1 by A-967079, suggesting that a proportion of I_K was TRPA1-mediated in our experimental setting. Furthermore, in a control experiment with a Na^+-free extracellular buffer, we observed that the activation of TRPA1 by AITC did not affect I_K in the sensory neurons from either WT or Slack$^{-/-}$ mice (Figure 5D), suggesting that Na^+-dependent activation of Slack is required in this experimental setting.

In order to characterize further the interaction between Slack and TRPA1, we used a HEK-293 cell line which stably expresses human Slack (herein referred to as HEK-Slack cells) and transiently transfected GFP-tagged human TRPA1 into these cells. This strategy led to the expression of TRPA1 in about 35% of the transfected cells (as indicated by green fluorescence under microscopy; the resulting TRPA1-positive cells were referred to as HEK-Slack-TRPA1 cells). A series of whole-cell patch-clamp recording experiments were conducted using a Ca^{2+}-free extracellular buffer in order to avoid Ca^{2+}-

mediated inhibition of Slack activity [135, 155]. We first confirmed that AITC (200 μM) did not directly affect the Slack-mediated I_K in HEK-Slack cells in either the physiological (Figure 6A) or the Ca^{2+}-free extracellular buffer (Figure 6B). However, AITC evoked an increase in I_K in HEK-Slack-TRPA1 cells in physiological extracellular buffer at positive potentials (100 mV and 120 mV) (Figure 6C). In the condition of Ca^{2+}-free extracellular buffer, I_K was significantly increased in the presence of AITC as compared to baseline at positive potentials (≥ 40 mV) in HEK-Slack-TRPA1 cells (Figure 6D). Notably, when the physiological extracellular buffer was replaced with Ca^{2+}-free extracellular buffer, AITC induced a greater increase of I_K. Furthermore, application of the TRPA1 antagonist A-967079 reduced I_K in HEK-Slack-TRPA1 cells (Figure 6E). Altogether, these results further support our finding that TRPA1 may functionally interact with Slack.

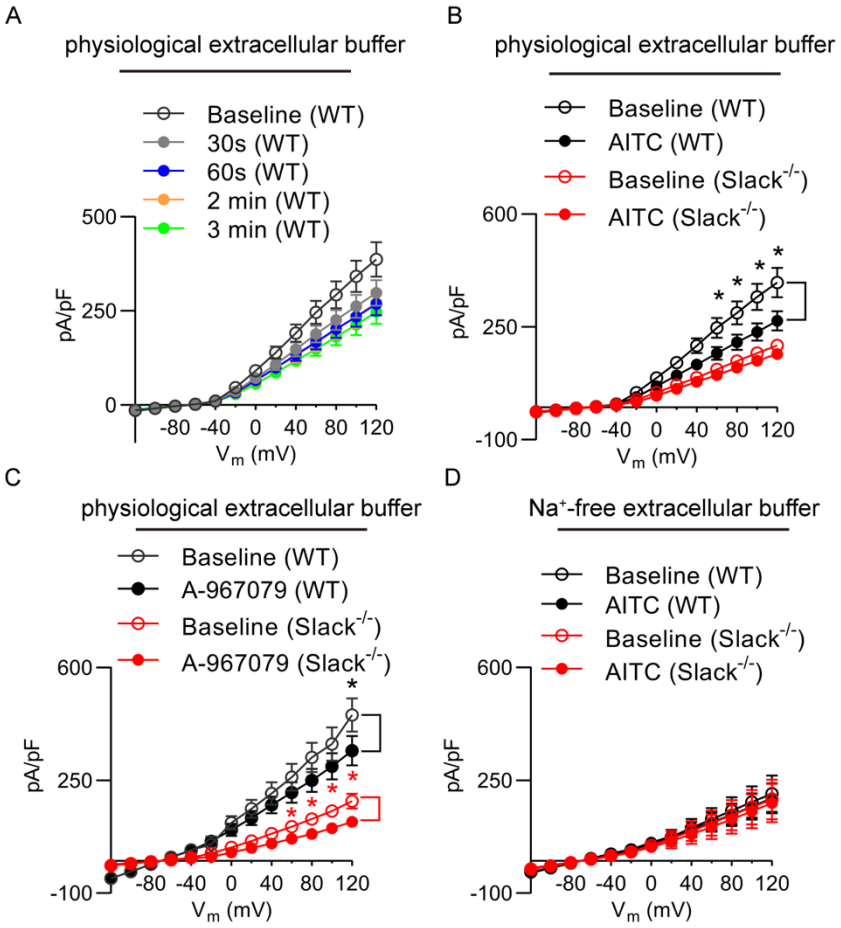

Figure 5. AITC-mediated modulation of potassium currents in sensory neurons from WT and Slack$^{-/-}$ mice. (A) Time course of IV relations of outward potassium currents (I_K) after AITC stimulation obtained in whole cell patch-clamp recordings in IB4$^+$ sensory neurons from WT mice in physiological extracellular buffer (n = 14-18 cells per time point). (B) IV relations of

outward potassium currents (I_K) obtained in whole cell patch-clamp recordings in $IB4^+$ sensory neurons from 4 WT (black color; 60 mV, p = 0.0475; 80 mV, p = 0.0135; 100 mV, p = 0.0016; 120 mV, p = 0.0003; n = 18 cells) and 4 $Slack^{-/-}$ mice (red color; n = 13 cells) before and after 200 µM AITC application in physiological extracellular buffer. Note that in this experimental setting (which includes 2 mM Ca^{2+} and 140 mM Na^+ in the external solution) TRPA1 activation leads to a significant reduction of I_K in sensory neurons from WT but not $Slack^{-/-}$ mice. (C) IV relations of I_K obtained in whole cell patch-clamp recordings in $IB4^+$ sensory neurons from 3 WT (black color; p = 0.0003; n = 13 cells) and 3 $Slack^{-/-}$ mice (red color; 60mV, p = 0.0295; 80 mV, p = 0.0031; 100 mV, p = 0.0004; 120 mV, p < 0.0001; n = 12 cells) before and after 10 µM A-967079 in physiological extracellular buffer. Note that in this experimental setting (which includes 2 mM Ca^{2+} and 140 mM Na^+ in the external solution) TRPA1 inhibition leads to a significant reduction of I_K in sensory neurons from both WT and $Slack^{-/-}$ mice. (D) IV relations of I_K obtained in whole cell patch-clamp recordings in $IB4^+$ sensory neurons from 3 WT (black color; n = 9 cells) and 3 $Slack^{-/-}$ mice (red color; n = 8 cells) before and after 200 µM AITC in Na^+-free extracellular buffer. Note that in this experimental setting (which includes 2 mM Ca^{2+}, but without Na^+ in the external solution) TRPA1 activation leads to no changes of I_K in sensory neurons from both WT and $Slack^{-/-}$ mice. Two-way analysis of variance (ANOVA), effect of different potentials with Sidak´s multiple comparisons test, * p < 0.05. Data are presented as mean ± SEM.

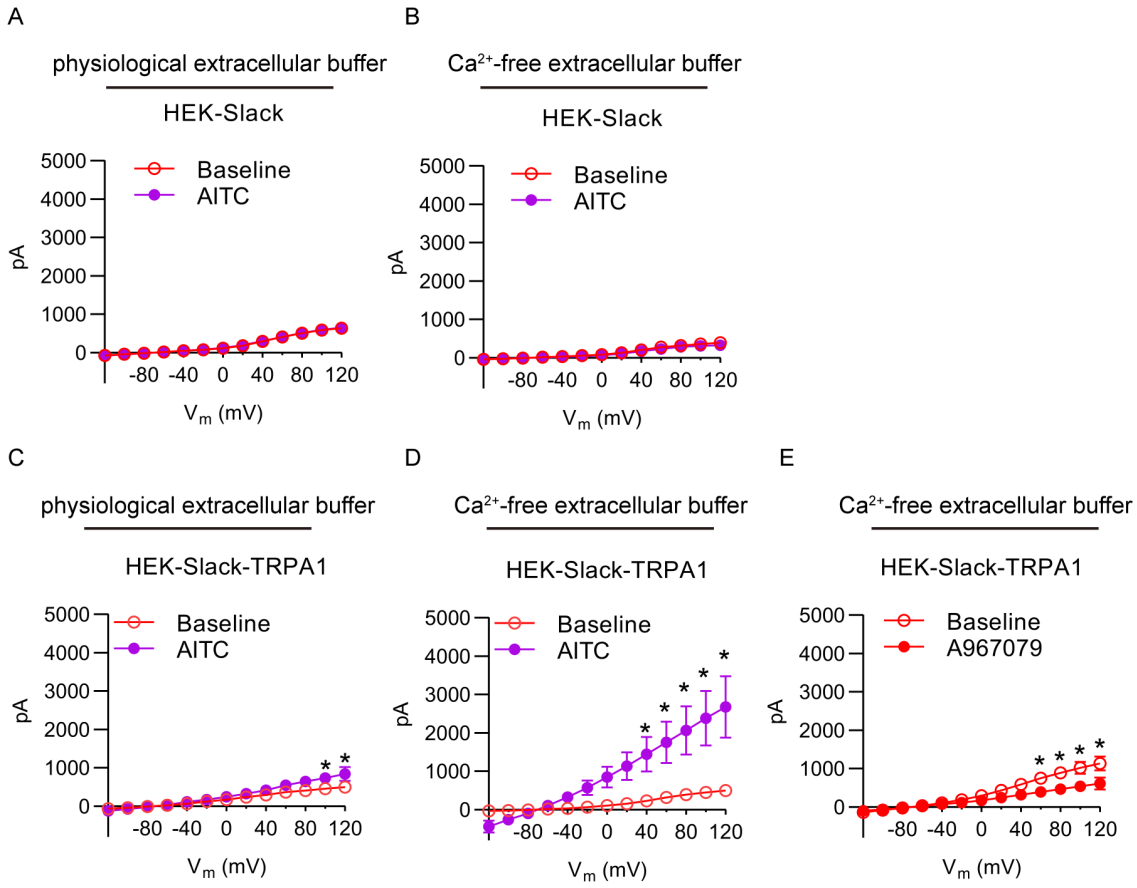

Figure 6. AITC-mediated modulation of potassium currents in transfected HEK-293 cells. (A) IV relations of I_K in HEK-Slack cells in physiological extracellular buffer (A; n = 11 cells). (B) IV relations of I_K in HEK-Slack cells in Ca^{2+}-free extracellular buffer (A; n = 11 cells). (C) IV relations of I_K in HEK-Slack-TRPA1 cells before and after 200 µM AITC application (100 mV, p = 0.0158; 120 mV, p = 0.0012; n = 10 cells) in physiological extracellular buffer. (D) IV relations of I_K in HEK-Slack-TRPA1 cells before and after 200 µM AITC application in Ca^{2+}-free extracellular buffer (40 mV, p = 0.004; 60 mV, p = 0.008; 80 mV, p = 0.0011; 100 mV, p < 0.0001; 120 mV, p < 0.0001; n = 14 cells). (E) IV relations of outward potassium currents (I_K) in HEK-Slack-TRPA1 cells before and after 10 µM A-967079 application in Ca^{2+}-free extracellular buffer (60 mV, p = 0.0388; 80 mV, p = 0.0088; 100 mV, p = 0.0018; 120 mV, p = 0.0005; n = 9 cells). Two-way analysis of variance (ANOVA), effect of different potentials with Sidak´s multiple comparisons test, * p < 0.05. Data are presented as mean ± SEM.

3.2 Slack potassium channels in spinal dorsal horn neurons control neuropathic pain behavior

3.2.1 Slack mRNA is expressed in both inhibitory and excitatory interneurons of the spinal cord.

Spinal dorsal horn interneurons can be divided into inhibitory interneurons and excitatory interneurons according to their neurotransmitter contents. Inhibitory interneurons, which use GABA and/or glycine as their principal transmitter, are marked by the vesicular GABA transporter (VGAT) [31, 156, 157], while the excitatory interneurons release glutamate and express the vesicular glutamate transporter 2 (VGLUT2) [158, 159]. In addition, $VGLUT2^+$ projection neurons are expressed in the spinal dorsal horn. To characterize the Slack expression in neuronal populations of the spinal dorsal horn, we performed fluorescent ISH and found that Slack was widely distributed in the whole spinal cord but mainly centralized in the dorsal horn (Figure 7A and 7B). To estimate the distribution of Slack in inhibitory and excitatory neurons of the superficial dorsal horn, we performed double-labeling ISH of Slack mRNA with VGAT mRNA and VGLUT2 mRNA. We found that Slack is not only expressed in a subset of inhibitory neurons ($VGAT^+$, Figure 7C) but also in a subset of excitatory neurons ($VGLUT2^+$, Figure 7D). The wide colocalization of Slack with Slick in the brain suggests that these two K_{Na} channels are likely to be heteromers in these regions [62]. This result is supported by a previous study using single-cell RNA sequencing (http://linnarssonlab.org/dorsalhorn/). Therefore, we further examined the cellular distribution of Slack and Slick in the spinal cord. As shown in Figure 7E, some Slack mRNA-positive neurons co-express Slick mRNA in the spinal dorsal horn. Taken together, our results showed that Slack is highly expressed in both spinal dorsal horn inhibitory and excitatory neurons of the spinal dorsal horn.

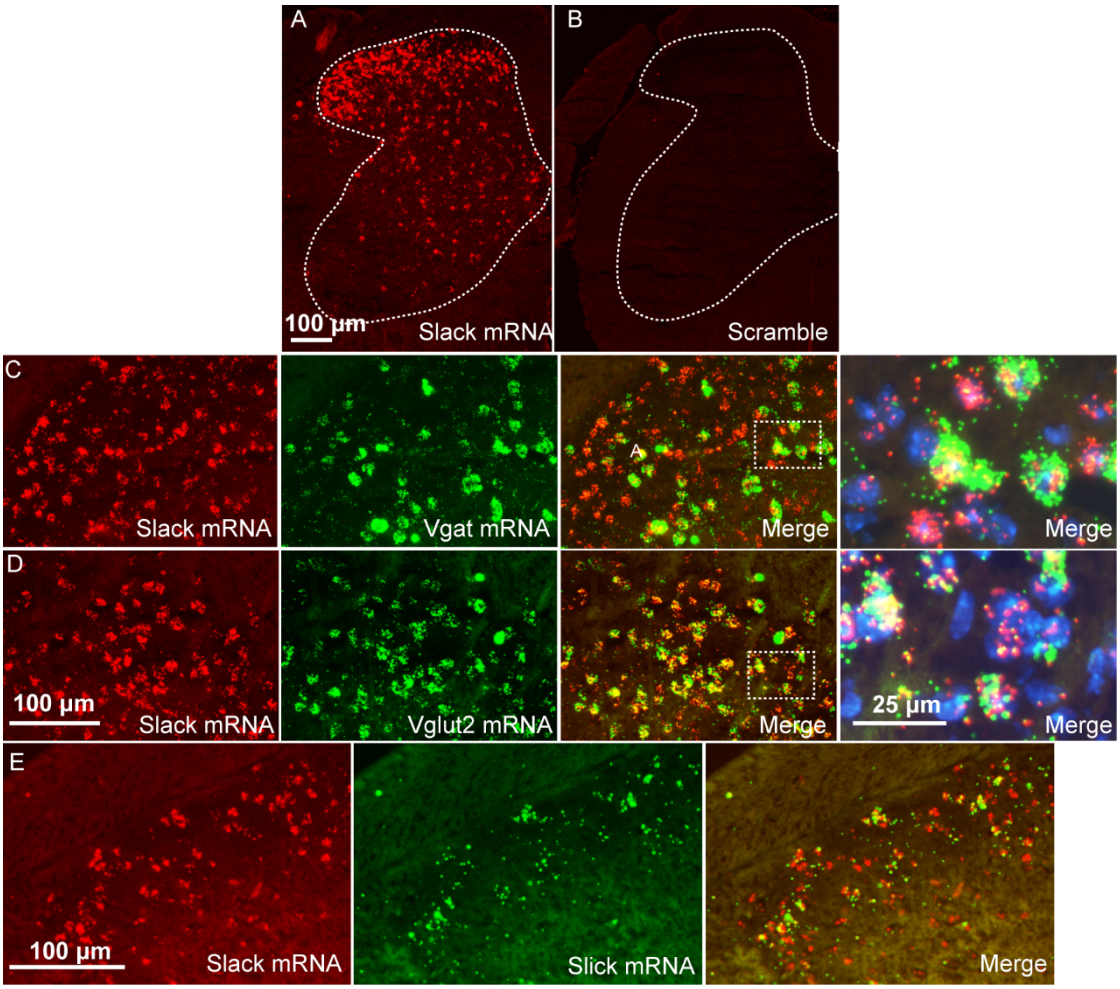

Figure 7. Expression of Slack in inhibitory and excitatory interneurons. (A-B) Distribution of Slack mRNA in the spinal dorsal horn assessed by fluorescent in situ hybridization. (C) Double in situ hybridization of Slack mRNA with VGAT mRNA, a marker of inhibitory neurons. (D) Double in situ hybridization of Slack mRNA with VGLUT2 mRNA, a marker of excitatory neurons. (E) Double in situ hybridization of Slack mRNA with slick mRNA. In all in situ hybridization pictures, type 1 probes are presented in red and type 6 probes are shown pseudocolored in green.

3.2.2 Generation of spinal dorsal horn neuron-specific Slack mutants (Lbx1-Slack$^{-/-}$)

A recent single cell RNA-sequencing (sc-RNAseq) study revealed that Slack is highly expressed in afferent populations of neurons in the spinal dorsal horn [82], suggesting that Slack may contribute to pain processing in spinal circuits. To analyze the functional role of Slack expressed in spinal dorsal horn neurons, we crossbred Slack$^{fl/fl}$ mice with Lbx1^{Cre} mice via Cre/loxP-mediated recombination to generate Lbx1-Slack$^{-/-}$ mice which lack Slack specifically in dorsal horn neurons. As reported previously, Lbx1 plays

a critical role in the development of sensory pathways in the dorsal horn that relay pain and touch [136]. The genotypes of the offspring were determined by PCR. A representative example of a genotyping PCR using genomic DNA from the mouse ear biopsy as a template is shown in Figure 8A. The conditional knockout Lbx1-Slack$^{-/-}$ was defined as a homozygous floxed Slack band with a Cre band (Figure 8A). In contrast, the littermate control mice only exhibited a homozygous floxed Slack band (Figure 8A). To confirm the selective ablation of Slack in the spinal dorsal horn of Lbx1-Slack$^{-/-}$ mice, we examined the Slack mRNA expression in DRGs, spinal cord, cerebellum and cortex by quantitative RT-PCR. These experiments showed an approximately 40% reduction of Slack mRNA in the spinal cord of Lbx1-Slack$^{-/-}$ mice compared to control mice (Figure 8B). In contrast, Slack mRNA expression was similar in both genotypes in DRGs, cerebellum and cortex (Figure 8B), thus indicating the specific ablation of Slack in the spinal cord dorsal horn. Further qRT-PCR experiments revealed that mRNA expression of related potassium channels (Slick and Slo1) (Figure 8C) and of inhibitory interneuron markers like Calbindin, Galanin, Parvalbumin, nNOS and Neuropeptide Y (NPY) (Figure 8D) was similar in the spinal cord of Lbx1-Slack$^{-/-}$ and control mice, suggesting that there is no compensatory regulation due to the Slack knockout. In addition, western blot analyses confirmed that Slack protein was significantly reduced in the spinal cord of Lbx1-Slack$^{-/-}$ mice compared to control mice (Figure 8E and 8F). Altogether, the Lbx1-Slack$^{-/-}$ mouse line yielded the specific conditional gene deletion in the dorsal horn neurons of the spinal cord while leaving Slack mRNA expression in the DRGs or brain intact; this observation is supported by other groups that have used Lbx1^{Cre} mice for generating deficient mice specifically in spinal dorsal horn neurons [160-162].

Some anatomical defects, such as the aberrant innervation by central terminals of DRG neurons or the loss of spinal cord neurons, have been observed in mouse mutants with spinal cord gene deletions [163-165]. It could be possible that such changes potentially influence the pain behavior in Lbx1-Slack$^{-/-}$ mice. We therefore performed IHC staining of lumbar DRG sections using several neuron markers (CGRP, NF200, IB4 and TH) to determine whether the ablation of Slack in dorsal horn neurons affects the gross morphology of the DRG neurons. We found that the general structural properties of the somata of sensory neurons and the overall frequencies of the markers for nociceptors were not impaired (Figure 9A). In addition, the spinal termination of the primary nociceptive afferents (IB4^{+} and CGRP^{+} neurons; Figure 9B) were similar

between the Lbx1-Slack$^{-/-}$ and control mice. Moreover, the distribution of inhibitory interneurons expressing GAD67 [166] and excitatory interneurons positive for PKC-γ [167] in the superficial dorsal horn appeared to be normal in Lbx1-Slack$^{-/-}$ mice (Figure 9C and 9D). Furthermore, Lbx1-Slack$^{-/-}$ mice and the controls were born at the expected Mendelian ratios and showed no gross anatomical defects (data not shown), and the body weights from both genotypes showed no obvious differences (Figure 9E). Overall, the deletion of Slack in the spinal dorsal horn did not affect the macroscopic morphology of sensory neurons and the spinal cord dorsal horn.

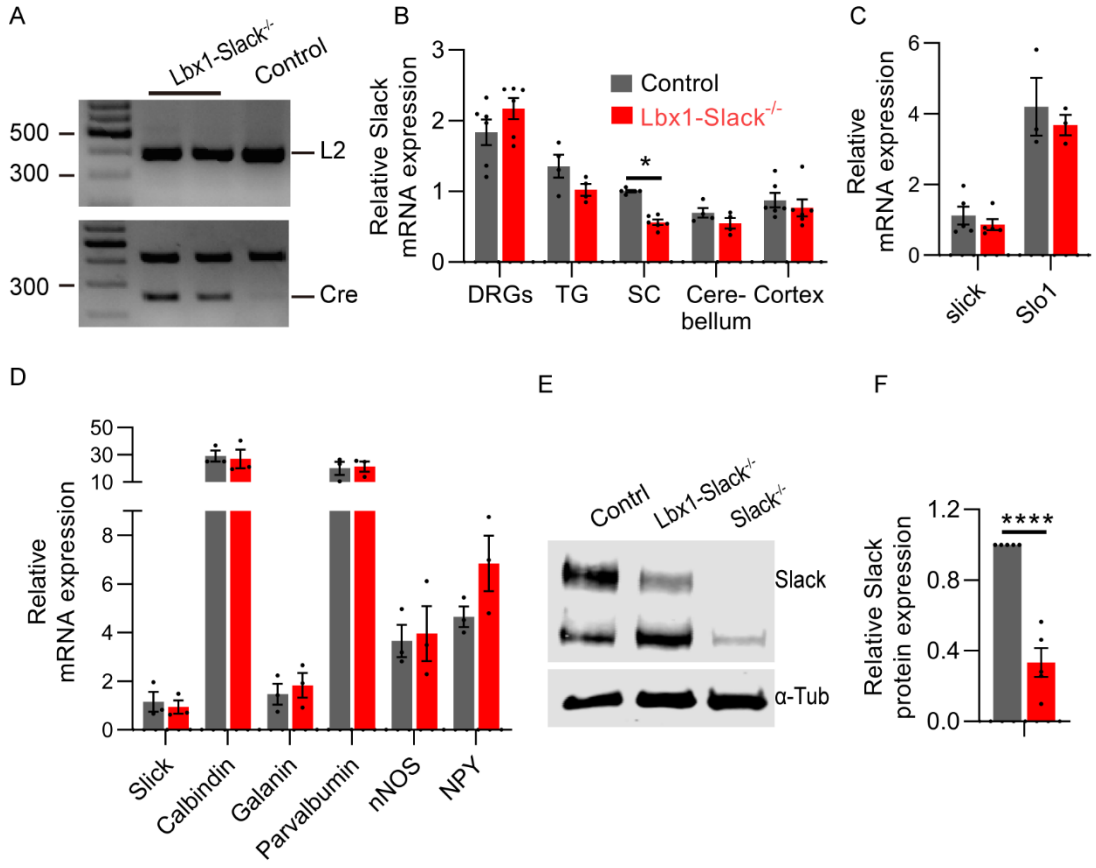

Figure 8. Generation of Lbx1-Slack$^{-/-}$ mice. (A) Genotyping of Lbx1-Slack$^{-/-}$ and control mice. L2: 392 bp, Cre: 250 bp. (B) Quantitative RT-PCR analyses show Slack mRNA expression in spinal cord (SC) is significantly reduced in Lbx1-Slack$^{-/-}$ mice as compared to control mice, while it is unaltered in DRGs, TG, cerebellum and cortex (two-tailed student's unpaired t test; n = 5 mice per group; *, p = 0.032). (C) Slick or Slo1 mRNA expression in spinal cord is not compensatory regulated in Lbx1-Slack$^{-/-}$ mice (two-tailed student's unpaired t test; n = 3 mice per group). (D) qRT-PCR analyses show no compensatory regulation of mRNA expression of inhibitory interneuron makers (two-tailed student's unpaired t test; n = 3 mice per group). (E)

Western blot analyses of Slack (140 kDa) in the spinal cord indicate that Slack protein expression is reduced in Lbx1-Slack$^{-/-}$ mice. (F) Quantitative results show a significantly reduction of Slack protein in Lbx1-Slack$^{-/-}$ mice (two-tailed student's unpaired t test; n = 3 mice per group; ****, $p < 0.0001$). Data are presented as mean ± SEM.

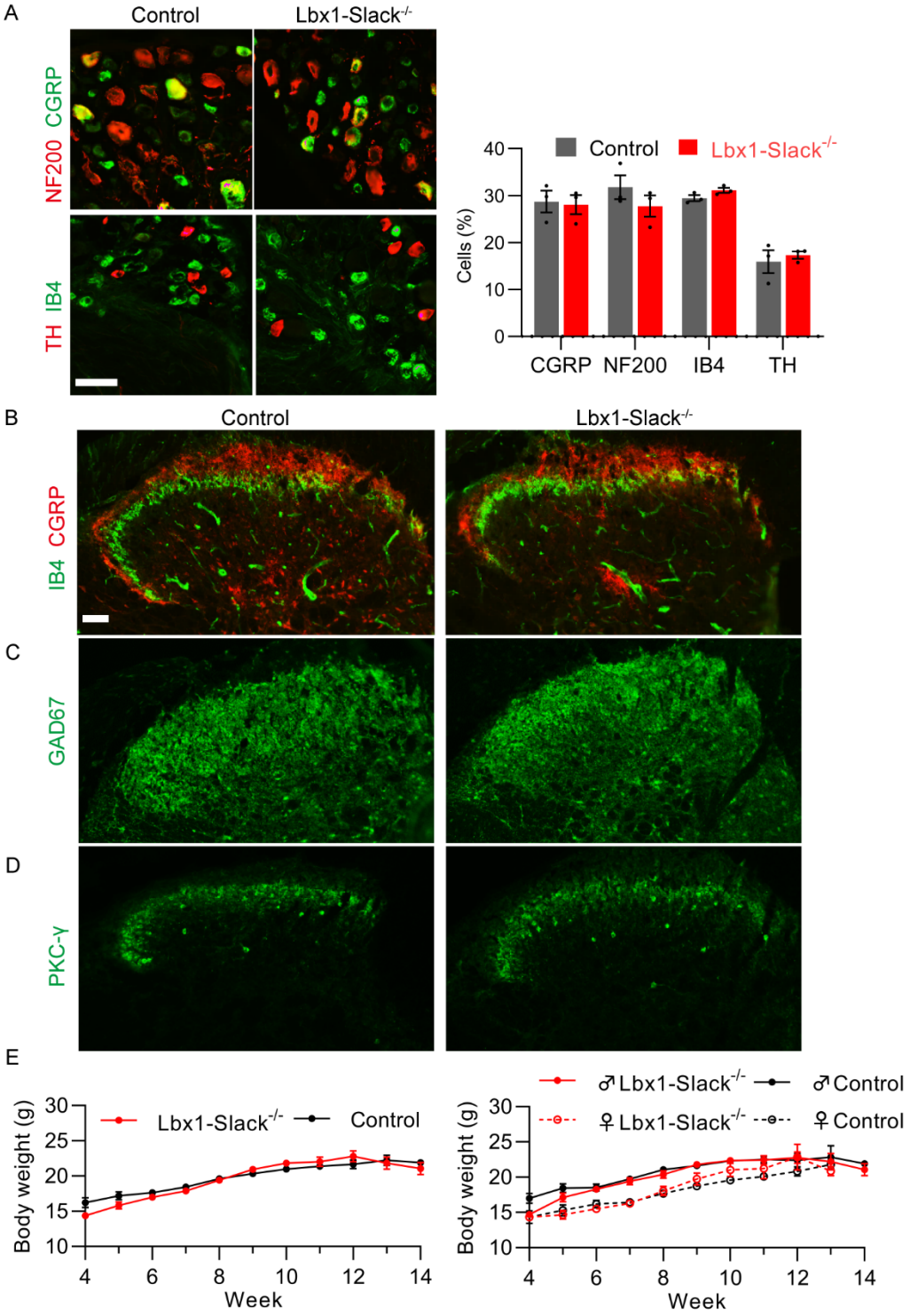

Figure 9. General features of Lbx1-Slack$^{-/-}$ mice (A) Double staining on Lumbar DRGs of Lbx1-Slack$^{-/-}$ and control mice. Percentages of DRG neurons immunoreactivity for CGRP-, NF200-, or IB4- binding are similar in Lbx1-Slack$^{-/-}$ and control mice (3300-4300 neuron cells were counted, n = 3 mice per group). (B) Double staining on spinal cord dorsal horn of Lbx1-Slack$^{-/-}$ and control mice. The termination of primary nociceptive afferents in the dorsal horn of the spinal cord is similar between Lbx1-Slack$^{-/-}$ and control mice, as indicated by CGRP immunoreactivity and IB4-binding. (C) The distribution of GAD67+ inhibitory interneurons in the spinal dorsal horn of Lbx1-Slack$^{-/-}$ and control mice is comparable. (D) Lbx1-Slack$^{-/-}$ mice show similar expression pattern of PKC-γ^{+} excitatory interneurons with control littermates. (E) Body weight of 4-14 weeks old Lbx1-Slack$^{-/-}$ and control mice (n = 8-12 mice per group). Scale bars: 50 µm. DRG: dorsal root ganglion, NF200: neurofilament 200, CGRP: Calcitonin gene-related peptide, TH: tyrosine hydroxylase, IB4: isolectin B4. Data are presented as mean ± SEM.

3.2.3 Basal characterization of Lbx1-Slack$^{-/-}$ mice

To determine further the Slack expression pattern in the spinal cord of Lbx1-Slack$^{-/-}$ mice, we performed immunostaining experiments. The immunostaining of Slack in spinal cord slices from Lbx1-Slack$^{-/-}$ mice revealed that a great amount of Slack was ablated in the spinal dorsal horn (Figure 10A) compared to control mice (Figure 10B), but that it was not completely absent when compared to Slack$^{-/-}$ mice (Figure 10C). In addition, double staining immunohistochemistry with lamina-specific markers showed that the most prominent Slack immunoreactivity in the dorsal horn of Lbx1-Slack$^{-/-}$ mice was mainly intermingled with IB4^{+} terminals (Figure 10D and 10E); which mark primary afferents that terminate in the dorsal lamina II inner layer [168]. A study by Peirs et al. (2015) described a large population of excitatory interneurons in lamina III that transiently expressed VGLUT3 and demonstrated that these were required for mechanical hypersensitivity in both neuropathic and inflammatory pain [38, 169]. We found that Slack showed no overlap with the VGLUT3^{+} neurons (Figure 10F and 10G). Other interneurons may contain protein kinase C; one isoform, PKC-γ, is mainly distributed within a band of excitatory interneurons of the ventral portion of the lamina II inner layer (vIIi) and in the most dorsal area of lamina III (dIII) [30, 170]. Various studies have shown that PKC-γ^{+}

interneurons are necessary for the development of mechanical allodynia [171-173] and the transmission of neuropathic pain [37, 174]. We observed that Slack in the dorsal horn of Lbx1-Slack$^{-/-}$ mice did not overlap with the PKC-γ^{+} interneurons (Figure 10H and 10I). Together, these data show that the vast majority of Slack^{+} neurons were ablated in the dorsal horn of Lbx1-Slack$^{-/-}$ mice. The band-shaped Slack immunoreactivity in lamina II of Lbx1-Slack$^{-/-}$ mice binds IB4 and therefore represent the central terminals of Slack-positive DRG neurons entering the spinal dorsal horn. These Slack-positive afferents in the dorsal horn of the Lbx1-Slack$^{-/-}$ mice are mainly localized to the dorsal border of VGLUT3^{+} and PKC-γ^{+} neurons. Altogether, these data suggested an efficient, conditional ablation of Slack in the spinal dorsal horn of Lbx1-Slack$^{-/-}$ mice.

3.2.4 Acute nociceptive pain behavior in Lbx1-Slack$^{-/-}$ mice

In order to determine the functional role of Slack in pain processing in the dorsal horn of the spinal cord, we compared the nociceptive behavior of Lbx1-Slack$^{-/-}$ mice with that of littermate control mice in various standardized behavioral assays. We first checked the motor coordination of the mice by using an accelerating Rotarod test; coordination was measured with an increasing rod speed from 4–40 rpm over 300 seconds. Our data showed that the motor function was intact in Lbx1-Slack$^{-/-}$ mice (Figure 11A). In addition, similar latency times were observed in both genotypes after applying thermal stimuli in the hot plate (Figure 11B), cold plate (Figure 11C) and cold plantar tests (Figure 11D). Furthermore, there were no significant differences in the mechanical thresholds after applying the light and intense noxious mechanical stimuli when using the dynamic plantar (Figure 11E) and von Frey test, respectively (Figure 11F). These data indicate that Slack in the dorsal horn neurons is not involved in the processing of acute nociceptive pain.

Subsequently, we analyzed the nociceptive behavior after intraplantar AITC injection into one hindpaw. Interestingly, we found no significant differences in paw licking and biting between control and Lbx1-Slack$^{-/-}$ mice (Figure 11G and 11H). Our results thus demonstrated that Slack in spinal dorsal horn neurons is most probably not involved in TRPA1-dependent pain processing.

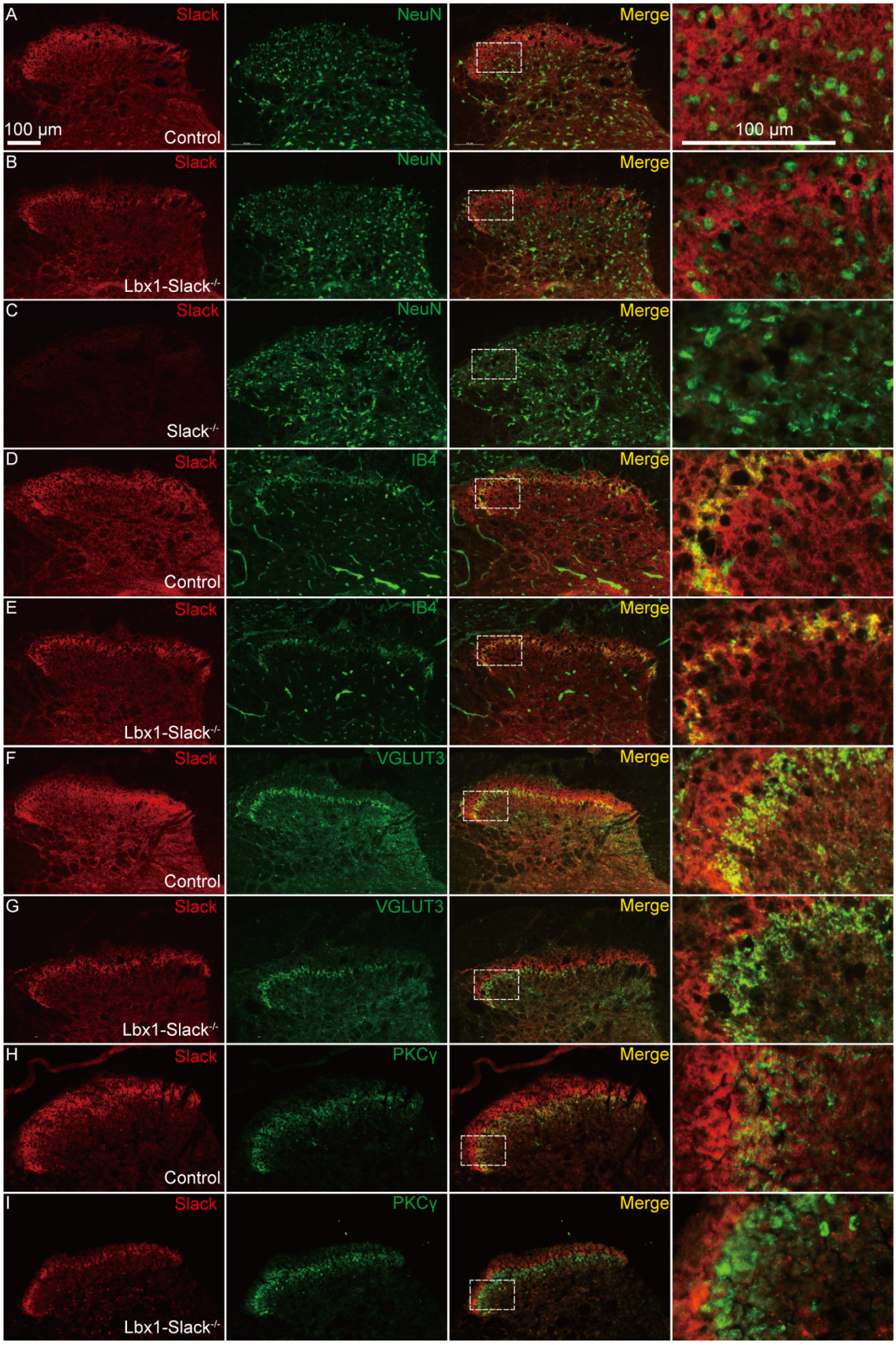
A
Slack
NeuN
Merge
100 μm
Control
100 μm
B
Slack
NeuN
Merge
Lbx1-Slack-/-
C
Slack
NeuN
Merge
Slack-/-
D
Slack
IB4
Merge
Control
E
Slack
IB4
Merge
Lbx1-Slack-/-
F
Slack
VGLUT3
Merge
Control
G
Slack
VGLUT3
Merge
Lbx1-Slack-/-
H
Slack
PKCγ
Merge
Control
I
Slack
PKCγ
Merge
Lbx1-Slack-/-

Figure 10. Slack immunoreactivity in the spinal dorsal horn of Lbx1-Slack$^{-/-}$ and control mice. (A-C) Double staining of Slack (red) and the neuronal somata maker NeuN (green) in control (A), Lbx1-Slack$^{-/-}$ (B) and Slack$^{-/-}$ (C) mice. (D-E) Double staining of Slack (red) and IB4 (green) in control (D) and Lbx1-Slack$^{-/-}$ (E) mice. Note that the most prominent Slack immunoreactivity in Lbx1-Slack$^{-/-}$ mice is mainly colocalized with IB4, which marks central terminals of primary afferents. (F-G) Double staining of Slack (red) and VGLUT3 (green) in control (F) and Lbx1-Slack$^{-/-}$ (G) mice. Slack immunoreactivity is mainly localized to the dorsal side of VGLUT3 immunoreactivity in Lbx1-Slack$^{-/-}$ mice. (H-I) Double staining of Slack (red) and PKC-γ (green) in control (H) and Lbx1-Slack$^{-/-}$ (I) mice. Slack immunoreactivity is mainly localized to the dorsal side of PKC-γ immunoreactivity in Lbx1-Slack$^{-/-}$ mice.

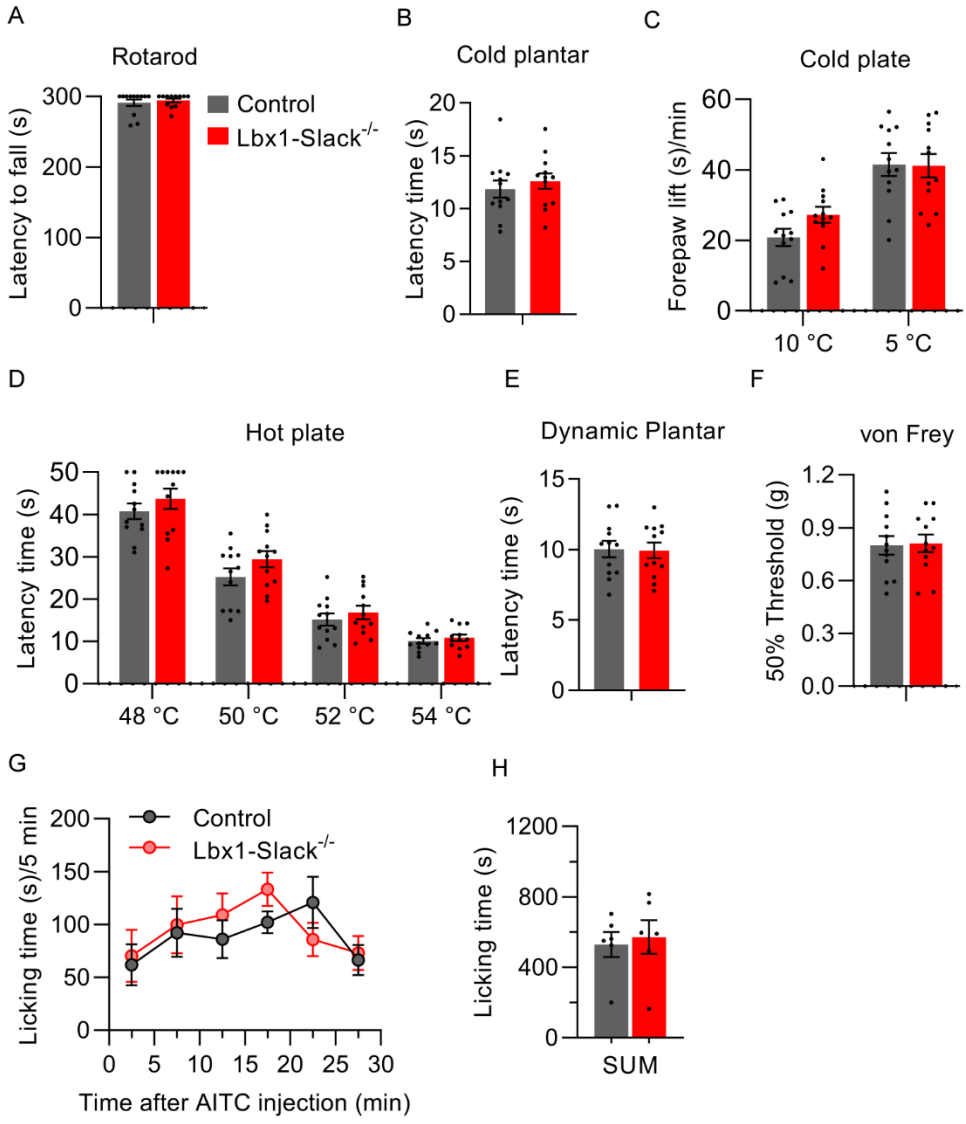

Figure 11. Acute nociceptive pain behavior is normal in Lbx1-Slack$^{-/-}$ mice. (A) Motor function assessed by on an accelerating Rotarod is similar between Lbx1-Slack$^{-/-}$ and control mice (n = 12 mice per group). (B, C) Cold pain sensitivity investigated by cold plantar test (B, n = 12 mice per group) and on a 4 °C cold plate (C, n = 12 mice per group) is similar between Lbx1-Slack$^{-/-}$ and control mice. (D) Thermal pain thresholds assessed in a hot plate test (n = 12 mice per group) are similar between Lbx1-Slack$^{-/-}$ and control mice. (E, F) Mechanical pain sensitivity measured using dynamic plantar test and von Frey up and down method (n = 12 mice per group) show no difference between Lbx1-Slack$^{-/-}$ and control mice. (G and H) AITC-induced pain behavior. (G) Time course of paw licking and biting induced by intraplantar AITC injection is similar in control and Lbx1-Slack$^{-/-}$ littermates. (H) The sum of licking and biting time over 30 minutes is comparable between groups (p = 0.7319; n = 6 mice per group). Data are presented as mean ± SEM and analyzed with two-tailed student's unpaired t test.

3.2.5 Neuropathic pain is increased in Lbx1-Slack$^{-/-}$ mice while inflammatory pain behavior is normal

A previous study revealed that Slack is involved in nerve injury-induced neuropathic pain processing [134]. To investigate the function of Slack in the spinal dorsal horn in neuropathic pain, we employed the spared nerve injury (SNI) model with Lbx1-Slack$^{-/-}$ mice. Subsequently, to assess whether Slack in the spinal dorsal horn is involved in chronic inflammatory pain, we injected CFA into the plantar space of a hindpaw. Notably, similar to our previous results obtained with global Slack$^{-/-}$ mice [134], the SNI-induced mechanical hypersensitivity was significantly increased in Lbx1-Slack$^{-/-}$ mice compared to control littermates (Figure 12A). Unlike the SNI-induced hypersensitivity, CFA-induced mechanical hyperalgesia was similar between Lbx1-Slack$^{-/-}$ and control mice (Figure 12B). Taken together, these data implicate an important role of Slack in the spinal dorsal horn in SNI-induced neuropathic pain processing.

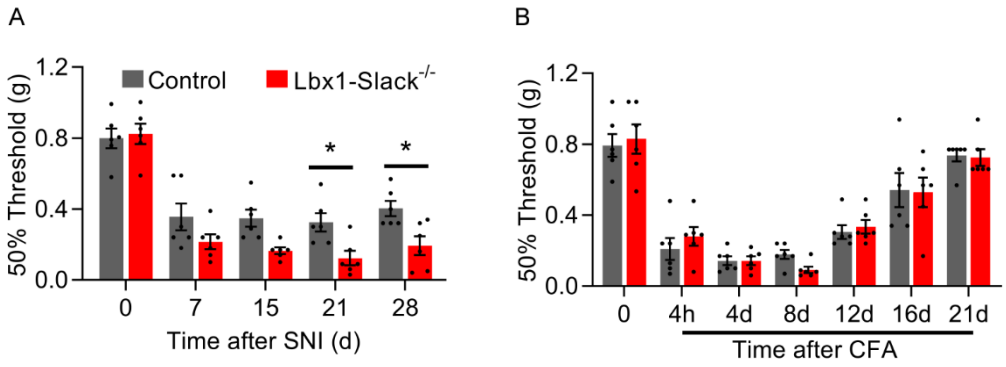

Figure 12. Behavior of Lbx1-Slack$^{-/-}$ mice in models of persistent pain. (A) Mechanical threshold of Lbx1-Slack$^{-/-}$ and control mice in the spinal nerve injury (SNI) model of neuropathic pain. Time course of paw withdrawal threshold (von Frey up and down method) after mechanical stimulation (n = 6 mice per group). (B) Paw withdrawal threshold of Lbx1-Slack$^{-/-}$ and control mice in CFA model of inflammatory pain (n = 6 mice per group). Two-way ANOVA with Sidak's multiple comparisons test, * $p < 0.05$; Data are presented as mean ± SEM.

3.2.6 Systemic and intrathecal administration of loxapine ameliorates SNI-induced neuropathic pain behavior

A recent study revealed that the first generation antipsychotic drug loxapine activates Slack channels [175]. Other studies have revealed that loxapine alleviates nerve injury-induced neuropathic pain [134, 176]. To further characterize the effect of pharmacological Slack activation in neuropathic pain, we assessed the pain behavior after delivery of loxapine by different administration routes in mice with SNI-induced neuropathic pain. To test the systemic effect of loxapine, we intraperitoneally (i.p.) administered loxapine (0.175 mg/kg, loxapine succinate salt; Sigma Aldrich, Steinheim, Germany) in WT and Lbx1-Slack$^{-/-}$ mice. After SNI, these mice successfully developed SNI-induced mechanical hypersensitivity (Figure 13A). At 1 and 2 hours following the loxapine administration, WT mice showed significantly increased withdrawal thresholds (Figure 13A). Lbx1-Slack$^{-/-}$ mice also showed slightly attenuation of mechanical hypersensitivity after administration of loxapine which was however not significant (Figure 13A). We next injected loxapine intrathecally (0.035 mg/kg). Interestingly, WT mice demonstrated increased withdrawal thresholds at 2 and 3 hours after the loxapine administration, whereas the withdrawal thresholds were unaltered in Lbx1-Slack$^{-/-}$ mice

(Figure 13B). Finally, we tested the effects of loxapine after intraplantar administration (0.035 mg/kg) on the ipsilateral hindpaw (injured). No distinguishable alterations of the withdrawal thresholds were found when compared to the conditions before treatment of loxapine in both WT and Lbx1-Slack$^{-/-}$ mice (Figure 13C). In conclusion, Slack expressed in the spinal dorsal horn plays an inhibitory function in SNI-induced neuropathic pain while loxapine, as a Slack activator, can relieve neuropathic pain.

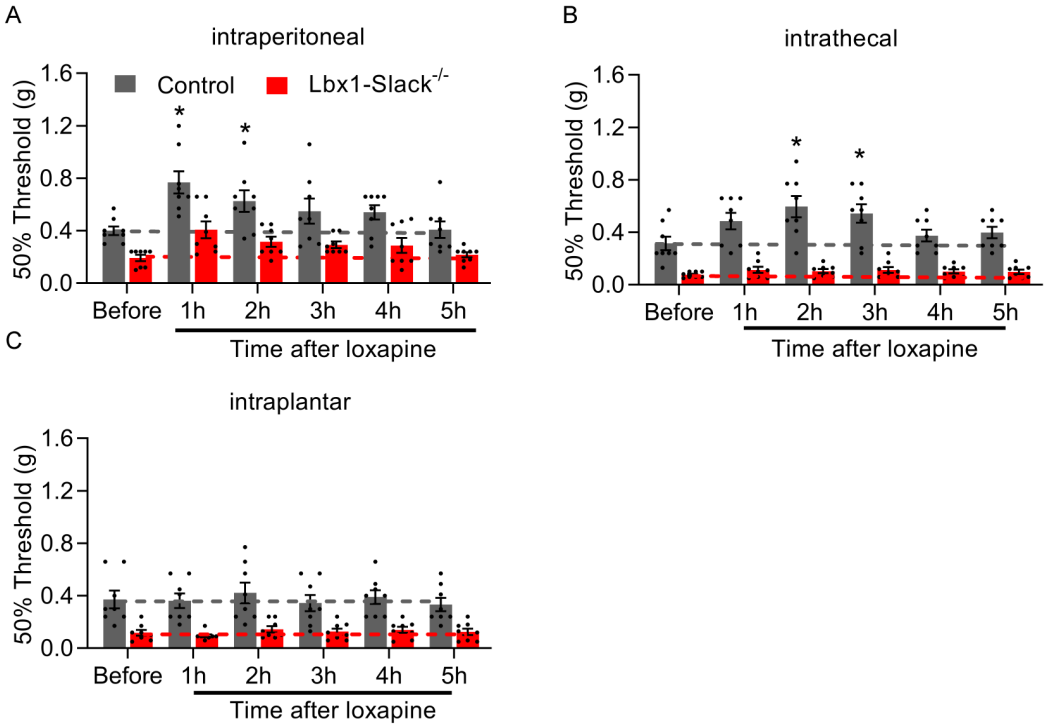

Figure 13. Systemic and intrathecal treatment with loxapine inhibits neuropathic pain. (A) The effect of systemic administration of loxapine in mice at day 14 after SNI (n = 8 mice per group; *, p = 0.0468, 0.0472). (B) Intrathecal injection of loxapine at day 28 after SNI (n = 8 mice per group; *, p = 0.0165, 0.0299). (C) Intraplantar injection of loxapine at day 35 after SNI (n = 8 mice per group). Two-way ANOVA, Sidak's multiple comparisons test, * $p < 0.05$; data are presented as mean ± SEM.

4. Discussion

4.1 Functions of Slack in sensory neurons in TRPA1-mediated nociception

By using Slack$^{-/-}$, SNS-Slack$^{-/-}$ and Lbx1-Slack$^{-/-}$ mouse strains, we have provided evidence that Slack expressed in sensory neurons controls TRPA1-triggered pain. The high degree of colocalization of Slack with TRPA1, but not TRPV1, in sensory neurons is in accordance with a specific functional coupling of TRPA1 and Slack. Our electrophysiological experiments further suggest that Slack-mediated potassium currents can be modulated by TRPA1 activation.

TRPA1 is activated by a variety of noxious stimuli and its activation is required for noxious cold sensation [132], noxious heat sensation [177], formalin-induced pain [178], acute itch [130] and neuropathic pain [179], while it additionally acts as an immunological co-activator [180, 181]. Previous reports using *in situ* hybridization and quantitative PCR have demonstrated that inflammation and nerve injury increases TRPA1 expression in DRGs [182, 183]. However, the detailed TRPA1 expression pattern still remains controversial. For example, one earlier study using *in situ* hybridization showed that TRPA1 was virtually exclusively detected in TRPV1^{+} sensory neurons of adult mice, while the double-labeling suggested that 30% of the TRPV1^{+} neurons expressed TRPA1 [184]. Using immunohistochemistry another study demonstrated similar results reporting that TRPA1 is expressed in the TRPV1^{+} neurons and that it could be further detected as being partially co-expressed with CGRP, a marker of peptidergic C-fiber neurons [185]. However, other studies have found more TRPA1 present in the IB4-binding, non-peptidergic sensory neurons [103, 104, 186], of which only a minority express CGRP or TRPV1 [187]. These discrepancies between the studies may have resulted from limitations of the *in situ* hybridization and immunohistochemistry techniques [104]. Our observation that the majority of Slack^{+} sensory neurons (70%) co-expressed TRPA1, but that only 14% were positive for TRPV1, provides indirect evidence for an only partial overlap of TRPA1 and TRPV1 in the sensory neurons. This finding is consistent with recent scRNA-seq studies [25, 133]. Hence, the distribution pattern of Slack, TRPA1 and TRPV1 in sensory neurons that we report in our study further supports the finding that Slack modulates TRPA1-induced, but not TRPV1-induced, pain processing.

Based on our findings that TRPA1-mediated nociceptive behavior is increased in Slack$^{-/-}$ and SNS-Slack$^{-/-}$ mice, the question arises of how TRPA1 functionally interacts with Slack in sensory neurons. In general, Slack is activated by elevations in intracellular Na^+, driven by voltage-dependent Na^+ channels, N-Methyl-D-aspartic acid receptors or other nonselective cation channels [188], and is responsible for a delayed outward Na^+-activated K^+ current [189]. On the other hand, its activity is inhibited by intracellular divalent cations that modify channel gating by an allosteric mechanism [135, 155, 190]. Furthermore, Slack activity is regulated by a variety of signaling pathways, including phosphorylation of the C-terminal domain by protein kinase C [191, 192], transmembrane protein TMEM16C [193], G protein-coupled receptors [194], and the fragile X mental retardation protein [195-197]. Although highly speculative, it is possible that a TRPA1-driven influx of Na^+ might lead to Slack activation and subsequent K^+ efflux that limits the nociceptor activity in vivo. However, in our patch-clamp recordings in sensory neurons we observed a reduced Slack-mediated I_K following TRPA1 activation. The observation that AITC reduced the I_K in the sensory neurons of WT mice in a physiological extracellular buffer was unexpected. As based on the exaggerated AITC-evoked pain behavior in the Slack$^{-/-}$ and SNS-Slack$^{-/-}$ mice, we hypothesized that the Slack-mediated I_K would be increased after TRPA1 activation in the sensory neurons. Given the fact that (i) TRPA1 activation may induce substantial Ca^{2+} influx and this Ca^{2+} permeation restricts monovalent cation flux (such as Na^+) through TRPA1 [150, 198, 199], and (ii) Slack is not only activated by intracellular Na^+ but is inhibited by intracellular Ca^{2+} [135, 155], we reasoned that the observed reduction of I_K in the presence of AITC might be driven by Ca^{2+} influx in our patch-clamp setting, which contained 2 mM Ca^{2+} in the external solution. Unfortunately, recordings of sensory neurons in a Ca^{2+}-free external solution are not feasible, because Ca^{2+} has a dramatic effect on the metabolism of cell, and, therefore, sufficient amounts of Ca^{2+} in the external solution are required [200]. Nevertheless, our data show that the activity of Slack channels in sensory neurons can be modulated in a TRPA1-dependent manner. In the dilated state, the permeability sequence through TRPA1 has been calculated to be $Ca^{2+} > Ba^{2+} > Mg^{2+} > NH_4^+ > Li^+ > Na^+ > K^+ > Rb^+$, suggesting that the binding of calcium in the pore may effectively hinter monovalent cation permeation [150, 199]. Therefore, we speculate that in the experimental setting of the patch-clamp analyses of sensory neurons with 2 mM Ca^{2+} in the external solution, the Slack activity is inhibited. The increased I_K after TRPA1

activation in the HEK-Slack-TRPA1 cells in a Ca^{2+}-free setting further supports our hypothesis. However, we cannot exclude the possibility that Slack activity is modulated by other mechanisms upon TRPA1 activation. Further studies are required to determine exactly how TRPA1 activation affects the Slack I_K currents in sensory neurons.

Previous studies in our lab and by others have found that Slack significantly contributes to neuropathic pain [134, 135, 201] and acute itch [80]. However, a previous study revealed that 0.5% formalin-induced paw-licking behavior and zymosan-induced hypersensitivity were indistinguishable between $Slack^{-/-}$ and WT mice [134]. In the formalin model (0.5–5%), the rodents exhibit two temporally distinct phases of pain responses: the first robust phase is associated with paw lifting, licking and flinching during the first 10 minutes which is followed by transiently reduced responses and a subsequent second phase lasting 30–60 minutes [202-204]. The first phase has been attributed to the direct activation of the primary afferent sensory neurons, and the second phase has been attributed to their inflammatory and/or spinal sensitization [202, 203, 205]. Several investigations have shown that TRPA1 is required for the generation of formalin-induced pain behaviors in rodents [202, 206, 207]. These observations which apparently oppose our findings may reflect the complex mechanisms underlying nociception in vivo. It is also noteworthy that TRPA1-deficient mice have been shown to display significant attenuation of the formalin-evoked behavior although this is not ablated in either phase of the formalin test [202]. This was supported by another investigation of single-fiber recordings from an isolated $TRPA1^{-/-}$ mouse skin-nerve preparation where TRPA1 was the predominant but not the only driving force in the formalin test [208]. Although speculative, the difference may be due to the fact that AITC is a more specific TRPA1 agonist than formalin which may exert "unspecific" TRPA1-independent effects [209-211]. Similar to keratinocytes, the inhibition of the sarco/endoplasmic reticulum calcium-ATPase by formaldehyde may account for the TRPA1-independent release of cytosolic calcium which then leads to ATP release and the activation of sensory nerve endings via P_2X_4 receptor-channels [212, 213]. Thus, our hypothesis is that AITC may be more "specific" when investigating the function of Slack in TRPA1-induced pain sensation. It should be noted that in our AITC behavior experiments, 2% and 0.05% DMSO were used as vehicles in the experiments with $Slack^{-/-}$ and SNS-$Slack^{-/-}$ mice, respectively. Previous reports which used a higher concentration of DMSO (20–25%) for intraplantar injection did not find a vehicle effect [214, 215]. Hence, we do not expect that the pain

behavior in our experiments was affected by the different concentrations of DMSO. It is also noteworthy that the alteration in the AITC-induced mechanical hypersensitivity was more pronounced in Slack$^{-/-}$ mice (significantly different from the WT mice 3 hours to 48 hours after the AITC injection) than in SNS-Slack$^{-/-}$ mice (significantly different from the control mice only at 24 hours after the AITC injection). By contrast, AITC-induced nociceptive behavior in Lbx1-Slack$^{-/-}$ mice was similar to control mice. Therefore, it seems plausible that Slack channels expressed in $Na_V1.8$-negative sensory neurons (in which Slack is not knocked out in the SNS-Slack$^{-/-}$ mice) or in the central nervous system may also contribute to TRPA1-mediated pain processing.

4.2 Functions of Slack in spinal dorsal horn neurons in neuropathic pain processing

Considerable progress has been made in understanding the role of primary afferent neurons in nociceptive processing, thus leading to the development of new therapies that successfully target nociceptors. Our previous studies have evaluated the important role of Slack expressed in sensory neurons on modulating neuropathic pain processing [134] and have further identified P_2X_3/Slack signaling as a mechanism contributing to hypersensitivity following peripheral nerve injury [135]. However, the function of Slack channels in the spinal cord remains challenging to address. Here, by using Lbx1-Slack$^{-/-}$ mice, we provide further evidence that Slack in the spinal dorsal horn plays an important role in neuropathic pain processing.

Previous studies in our lab and by other groups have demonstrated that Slack channels are widely expressed in the central and peripheral nervous systems, especially in the IB4-positive, non-peptidergic sensory neurons [25, 134, 135, 193]. However, the distribution of Slack in the spinal cord has not been well documented. By generating Lbx1-Slack$^{-/-}$ mice, we characterized the functional roles of Slack in both excitatory and inhibitory neurons of the dorsal horn of the spinal cord. It is noteworthy that the extent of the ablation of Slack was not comparable between the mRNA and protein level. This is in line with the notion that mRNA is not a uniformly good predictor of protein levels: the expression of mRNA can vary 20-fold among comparably expressed proteins, while protein expression can vary 30-fold among comparably expressed mRNAs [216, 217].

Subsequent to our previous *in vivo* assays that the ablation of Slack, either globally or selectively in sensory neurons, leads to increased hypersensitivity in the SNI model [134], the behavioral analysis described in this thesis have demonstrated that Slack expressed in

spinal dorsal horn neurons plays an inhibitory function in processing of SNI-induced neuropathic pain. This is further confirmed by the finding that intrathecal administration of loxapine ameliorated the SNI-induced hyperalgesia only in the control mice but not in the Lbx1-Slack$^{-/-}$ mice.

SNI leads not only to increased spontaneous firing of sensory neurons or alterations in their conduction and neurotransmitter properties in peripheral nerve system, but also to central sensitization, a state of hyperexcitability that established in the central nervous system [3]. One of these mechanisms for central sensitization is called “disinhibition”, which was first proposed by Melzack and Wall in their gate control theory of pain [218]. This theory suggests that nociceptive sensory information is under pre- and postsynaptic inhibitory control of GABAergic or glycinergic interneurons in the spinal cord and that loss of balance between the excitatory and inhibitory neurotransmission in the dorsal horn would result in allodynia [218]. It is also noteworthy that spinal inhibitory interneurons not only modulate the activity of their target cells postsynaptically, but also contribute to the regulation of afferent terminals presynaptically [219]. For example, $GABA_A$ receptors located in primary afferent terminals can modulate the afferent input from DRG neurons into nociceptive-specific projection neurons (presynaptic inhibition) by inhibition of transmitter release, whereas postsynaptic $GABA_A$ receptors in the spinal cord interneurons directly reduce their excitability and thus control the output (postsynaptic inhibition) [220]. A study by Chen et al. reported a brain-derived neurotrophic factor (BDNF)-dependent shift in the reverse potential accompanied with a reduction of presynaptic GABA conductance on primary afferent terminals following nerve injury, thus suggesting that presynaptic inhibition mediated by the depolarizing effects of GABA is attenuated following nerve injury [220]. A study by Evely et al. [221] reported that Slack plays a role in regulating synaptic transmission at the level of the superficial dorsal horn (lamina II). Specifically, in the absence of Slack, intrinsic properties and synaptic drive were altered to favor an overall enhanced excitatory tone, meanwhile, presynaptic release from primary afferents was also increased [221]. As a recent study found that Slack is widely expressed in GABAergic and glutamatergic neurons in spinal dorsal horn [82], thus from this point Slack may be involved in the SNI-induced hyperexcitability in the spinal circuits in an inhibitory manner. However, further investigations are needed to clarify whether this inhibitory mechanism is driven presynapticlly or postsynapticlly. In addition, in our study, we have not observed an increased CFA-induced hypersensitivity

in the Lbx1-Slack$^{-/-}$ mice. Peirs et al. identified a distinct population of excitatory interneurons in the deeper laminae of the spinal cord that transient express VGLUT3 and are required for mechanical pain and allodynia [5]. In their study, they also observed c-Fos expression in PKC-γ^{+} excitatory neurons in the SNI model of neuropathic pain, but not in the carrageenan model of inflammatory pain, suggesting that the involvement of these neurons in the two models of mechanical hypersensitivity (neuropathic and inflammatory) may differ [5]. One possible explanation for these distinct functions is that the PKC-γ^{+} neurons overlapping with Lbx1 mediate mechanical pain but not inflammatory pain [34]. In our study, we found that Slack is absent from PKC-γ^{+} and VGLUT3^{+} neurons in the spinal dorsal horn of the Lbx1-Slack$^{-/-}$ mice. We presume that Slack in Lbx1^{+} dorsal horn neurons inhibits the SNI-induced mechanical hypersensitivity but not the CFA-induced inflammatory hypersensitivity, via the interaction with the PKC-γ^{+} and/or VGLUT3^{+} neurons. The precise functions of Slack in these neuronal populations in spinal dorsal horn will require further investigation.

Overall, we have identified that Slack in spinal dorsal horn neurons plays an important role in regulating peripheral nerve injury-induced neuropathic pain. These findings expand our previous finding that Slack in sensory neurons controls neuropathic pain, and will further help guide efforts to design new treatment strategies.

5. References

1. Raja, S.N., et al., The revised International Association for the Study of Pain definition of pain: concepts, challenges, and compromises. PAIN, 2020. **161**(9).
2. Baron, R., A. Binder, and G. Wasner, Neuropathic pain diagnosis, pathophysiological mechanisms, and treatment. The Lancet, 2010. **9**: p. 807.
3. Basbaum, A.I., et al., Cellular and molecular mechanisms of pain. Cell, 2009. **139**(2): p. 267-84.
4. Varrassi, G., et al., Pharmacological treatment of chronic pain – the need for CHANGE. Current Medical Research and Opinion, 2010. **26**(5): p. 1231-1245.
5. Peirs, C., et al., Dorsal Horn Circuits for Persistent Mechanical Pain. Neuron, 2015. **87**(4): p. 797-812.
6. Treede, R.-D., et al., Chronic pain as a symptom or a disease: the IASP Classification of Chronic Pain for the International Classification of Diseases (ICD-11). Pain, 2019. **160**(1): p. 19-27.
7. Zimmer, Z., et al., A global study of pain prevalence across 52 countries: examining the role of country-level contextual factors. PAIN, 9000.
8. Doth, A.H., et al., The burden of neuropathic pain: a systematic review and meta-analysis of health utilities. Pain, 2010. **149**(2): p. 338-344.
9. Attal, N., et al., The specific disease burden of neuropathic pain: results of a French nationwide survey. Pain, 2011. **152**(12): p. 2836-2843.
10. Finnerup, N.B., Nonnarcotic Methods of Pain Management. N Engl J Med, 2019. **380**(25): p. 2440-2448.
11. Alles, S.R.A. and P.A. Smith, Etiology and Pharmacology of Neuropathic Pain. Pharmacol Rev, 2018. **70**(2): p. 315-347.
12. Attal, N., D. Bouhassira, and R. Baron, Diagnosis and assessment of neuropathic pain through questionnaires. The Lancet Neurology, 2018. **17**(5): p. 456-466.
13. Wood, J.N., E.C. Emery, and P. Ernfors, Dorsal Root Ganglion Neuron Types and Their Functional Specialization, in The Oxford Handbook of the Neurobiology of Pain. 2020. p. 127-155.
14. Peirs, C. and R.P. Seal, Neural circuits for pain: Recent advances and current views. Science, 2016. **354**(6312).
15. Djouhri, L. and S.N. Lawson, Abeta-fiber nociceptive primary afferent neurons: a review of incidence and properties in relation to other afferent A-fiber neurons in mammals. Brain Res Brain Res Rev, 2004. **46**(2): p. 131-45.

16. Meyer, R.A., Peripheral mechanisms of cutaneous nociception. Wall and Melzack's Textbook of Pain, 2006: p. 3-34.
17. McCarthy, P. and S. Lawson, Cell type and conduction velocity of rat primary sensory neurons with calcitonin gene-related peptide-like immunoreactivity. J Neuroscience, 1990. **34**(3): p. 623-632.
18. Lawson, S., P. McCarthy, and E. Prabhakar, Electrophysiological properties of neurones with CGRP-like immunoreactivity in rat dorsal root ganglia. Journal of Comparative Neurology, 1996. **365**(3): p. 355-366.
19. Silverman, J.D. and L. Kruger, Acid phosphatase as a selective marker for a class of small sensory ganglion cells in several mammals: spinal cord distribution, histochemical properties, and relation to fluoride-resistant acid phosphatase (FRAP) of rodents. J Somatosensory research, 1988. **5**(3): p. 219-246.
20. Silverman, J.D. and L. Kruger, Lectin and neuropeptide labeling of separate populations of dorsal root ganglion neurons and associated “nociceptor” thin axons in rat testis and cornea whole-mount preparations. J Somatosensory research, 1988. **5**(3): p. 259-267.
21. Nagy, J.I. and S.P. Hunt, Fluoride-resistant acid phosphatase-containing neurones in dorsal root ganglia are separate from those containing substance P or somatostatin. Neuroscience, 1982. **7**(1): p. 89-97.
22. Wiesenfeld-Hallin, Z., et al., Immunoreactive calcitonin gene-related peptide and substance P coexist in sensory neurons to the spinal cord and interact in spinal behavioral responses of the rat. Neuroscience Letters, 1984. **52**(1): p. 199-204.
23. Hökfelt, T., et al., Substance P: Localization in the Central Nervous System and in Some Primary Sensory Neurons. Science, 1975. **190**(4217): p. 889-890.
24. Hökfelt, T., et al., Immunohistochemical evidence for separate populations of somatostatin-containing and substance P-containing primary afferent neurons in the rat. Neuroscience, 1976. **1**(2): p. 131-IN24.
25. Usoskin, D., et al., Unbiased classification of sensory neuron types by large-scale single-cell RNA sequencing. Nat Neurosci, 2015. **18**(1): p. 145-53.
26. Zholudeva, L.V., et al., Spinal Interneurons as Gatekeepers to Neuroplasticity after Injury or Disease. The Journal of Neuroscience : the Official Journal of the Society For Neuroscience, 2021. **41**(5): p. 845-854.
27. Wang, L.-H., W.-Q. Ding, and Y.-G. Sun, Spinal ascending pathways for somatosensory information processing. Trends In Neurosciences, 2022.
28. Zholudeva, L.V., et al., The Neuroplastic and Therapeutic Potential of Spinal Interneurons in the Injured Spinal Cord. Trends In Neurosciences, 2018. **41**(9): p. 625-639.

29. Polgar, E., et al., Functional differences between neurochemically defined populations of inhibitory interneurons in the rat spinal dorsal horn. Pain, 2013. **154**(12): p. 2606-2615.
30. Todd, A.J., Identifying functional populations among the interneurons in laminae I-III of the spinal dorsal horn. Mol Pain, 2017. **13**: p. 1744806917693003.
31. Hughes, D.I. and A.J. Todd, Central Nervous System Targets: Inhibitory Interneurons in the Spinal Cord. Neurotherapeutics, 2020. **17**(3): p. 874-885.
32. Bell, A.M., et al., Expression of green fluorescent protein defines a specific population of lamina II excitatory interneurons in the GRP::eGFP mouse. Sci Rep, 2020. **10**(1): p. 13176.
33. Gutierrez-Mecinas, M., et al., A quantitative study of neurochemically defined excitatory interneuron populations in laminae I-III of the mouse spinal cord. Mol Pain, 2016. **12**.
34. Duan, B., et al., Identification of spinal circuits transmitting and gating mechanical pain. Cell, 2014. **159**(6): p. 1417-1432.
35. Nelson, T.S., et al., Facilitation of neuropathic pain by the NPY Y1 receptor-expressing subpopulation of excitatory interneurons in the dorsal horn. Scientific Reports, 2019. **9**(1): p. 7248.
36. Alba-Delgado, C., et al., 5-HT Receptor-Induced Morphological Reorganization of PKCγ-Expressing Interneurons Gates Inflammatory Mechanical Allodynia in Rat. The Journal of Neuroscience : the Official Journal of the Society For Neuroscience, 2018. **38**(49): p. 10489-10504.
37. Petitjean, H., et al., Dorsal Horn Parvalbumin Neurons Are Gate-Keepers of Touch-Evoked Pain after Nerve Injury. Cell Reports, 2015. **13**(6): p. 1246-1257.
38. Peirs, C., et al., Dorsal Horn Circuits for Persistent Mechanical Pain. Neuron, 2015. **87**(4): p. 797-812.
39. Scholz, J. and C.J. Woolf, Can we conquer pain? Nature Neuroscience, 2002. **5**(11): p. 1062-1067.
40. Basbaum, A.I. and T.M. Jessell, The Perception of Pain. Principles of neuroscience, ed. E.R. Kandel and J.H. Schwartz. 2000, New York: Appleton and Lange.
41. Dubin, A.E. and A. Patapoutian, Nociceptors: the sensors of the pain pathway. J Clin Invest, 2010. **120**(11): p. 3760-72.
42. Gold, M.S. and G.F. Gebhart, Nociceptor sensitization in pain pathogenesis. Nat Med, 2010. **16**(11): p. 1248-57.
43. Kuner, R., Central mechanisms of pathological pain. Nat Med, 2010. **16**(11): p. 1258-66.
44. Vasko, M.R., Inflammatory Pain, in Encyclopedia of Neuroscience, M.D. Binder, N. Hirokawa, and U. Windhorst, Editors. 2009, Springer Berlin Heidelberg: Berlin, Heidelberg. p. 1952-1955.

45. Ellis, A. and D.L. Bennett, Neuroinflammation and the generation of neuropathic pain. Br J Anaesth, 2013. **111**(1): p. 26-37.
46. Linley, J.E., et al., Understanding inflammatory pain: ion channels contributing to acute and chronic nociception. Pflugers Arch, 2010. **459**(5): p. 657-69.
47. McMahon, S.B., F. La Russa, and D.L. Bennett, Crosstalk between the nociceptive and immune systems in host defence and disease. Nat Rev Neurosci, 2015. **16**(7): p. 389-402.
48. Chavan, S.S., V.A. Pavlov, and K.J. Tracey, Mechanisms and Therapeutic Relevance of Neuro-immune Communication. Immunity, 2017. **46**(6): p. 927-942.
49. H, M. and B. N, Classification of chronic pain: Descriptions of chronic pain syndromes and definitions of pain terms. Pain, 1986. **Suppl 3**: p. 226-226.
50. Colloca, L., et al., Neuropathic pain. Nat Rev Dis Primers, 2017. **3**: p. 17002.
51. Kosek, E., et al., Do we need a third mechanistic descriptor for chronic pain states? Pain, 2016. **157**(7): p. 1382-1386.
52. Fitzcharles, M.-A., et al., Nociplastic pain: towards an understanding of prevalent pain conditions. Lancet (London, England), 2021. **397**(10289): p. 2098-2110.
53. WHO. International Classifcation of Diseases 11th revision: the global standard for diagnostic health information. 2019; Available from: https://icd.who.int/en (accessed May 11, 2020).
54. Nicholas, M., et al., The IASP classification of chronic pain for ICD-11: chronic primary pain. Pain, 2019. **160**(1): p. 28-37.
55. Waxman, S.G. and G.W. Zamponi, Regulating excitability of peripheral afferents: emerging ion channel targets. Nature Neuroscience, 2014. **17**(2): p. 153-163.
56. Waxman, S.G., et al., Sodium channels and pain. Proceedings of the National Academy of Sciences, 1999. **96**(14): p. 7635-7639.
57. Bourinet, E., et al., Calcium-Permeable Ion Channels in Pain Signaling. Physiological Reviews, 2014. **94**(1): p. 81-140.
58. Tsantoulas, C. and S.B. McMahon, Opening paths to novel analgesics: the role of potassium channels in chronic pain. Trends Neurosci, 2014. **37**(3): p. 146-58.
59. Ocaña, M., et al., Potassium channels and pain: present realities and future opportunities. European Journal of Pharmacology, 2004. **500**(1): p. 203-219.
60. Maljevic, S. and H. Lerche, Potassium channels: a review of broadening therapeutic possibilities for neurological diseases. Journal of Neurology, 2013. **260**(9): p. 2201-2211.
61. COETZEE, W.A., et al., Molecular Diversity of K+ Channels. Annals of the New York Academy of Sciences, 1999. **868**(1): p. 233-255.

62. Kaczmarek, L.K., et al., International Union of Basic and Clinical Pharmacology. C. Nomenclature and Properties of Calcium-Activated and Sodium-Activated Potassium Channels. Pharmacological Reviews, 2017. **69**(1).
63. Waxman, S.G. and G.W. Zamponi, Regulating excitability of peripheral afferents: emerging ion channel targets. Nat Neurosci, 2014. **17**(2): p. 153-63.
64. Plant, L.D., A Role for K2P Channels in the Operation of Somatosensory Nociceptors. Frontiers In Molecular Neuroscience, 2012. **5**: p. 21.
65. D'Ambrosio, R., D.S. Gordon, and H.R. Winn, Differential role of KIR channel and Na(+)/K(+)-pump in the regulation of extracellular K(+) in rat hippocampus. Journal of Neurophysiology, 2002. **87**(1).
66. Wang, N., et al., Potassium channel K 4.1 regulates oligodendrocyte differentiation via intracellular pH regulation. Glia, 2022.
67. Janigro, D., et al., Reduction of K+ Uptake in Glia Prevents Long-Term Depression Maintenance and Causes Epileptiform Activity. The Journal of Neuroscience, 1997. **17**(8): p. 2813-2824.
68. Bhattacharjee, A. and L.K. Kaczmarek, For K+ channels, Na+ is the new Ca2+. Trends in Neurosciences, 2005. **28**(8): p. 422-428.
69. Haimann, C., et al., Potassium current activated by intracellular sodium in quail trigeminal ganglion neurons. The Journal of general physiology, 1990. **95**(5): p. 961-979.
70. Dryer, S.E., Na+-activated K+ channels: a new family of large-conductance ion channels. Trends in Neurosciences, 1994. **17**(4): p. 155-160.
71. Mercer, A.R. and J.G. Hildebrand, Developmental Changes in the Density of Ionic Currents in Antennal-Lobe Neurons of the Sphinx Moth, Manduca sexta. Journal of Neurophysiology, 2002. **87**(6): p. 2664-2675.
72. Safronov, B.V. and W. Vogel, Properties and functions of Na(+)-activated K+ channels in the soma of rat motoneurones. The Journal of Physiology, 1996. **497**(3): p. 727-734.
73. Dale, N., A large, sustained Na(+)- and voltage-dependent K+ current in spinal neurons of the frog embryo. The Journal of Physiology, 1993. **462**(1): p. 349-372.
74. Egan, T., et al., Properties and rundown of sodium-activated potassium channels in rat olfactory bulb neurons. The Journal of Neuroscience, 1992. **12**(5): p. 1964-1976.
75. Dryer, S.E., Na(+)-activated K+ channels and voltage-evoked ionic currents in brain stem and parasympathetic neurones of the chick. The Journal of Physiology, 1991. **435**(1): p. 513-532.
76. Schwindt, P.C., W.J. Spain, and W.E. Crill, Long-lasting reduction of excitability by a sodium-dependent potassium current in cat neocortical neurons. Journal of Neurophysiology, 1989. **61**(2): p. 233-244.

77. Martin, H.C., et al., Clinical whole-genome sequencing in severe early-onset epilepsy reveals new genes and improves molecular diagnosis. Human Molecular Genetics, 2014. **23**(12): p. 3200-3211.
78. Heron, S.E., et al., Missense mutations in the sodium-gated potassium channel gene KCNT1 cause severe autosomal dominant nocturnal frontal lobe epilepsy. Nature Genetics, 2012. **44**(11): p. 1188-1190.
79. Barcia, G., et al., De novo gain-of-function KCNT1 channel mutations cause malignant migrating partial seizures of infancy. Nature Genetics, 2012. **44**(11): p. 1255-1259.
80. Martinez-Espinosa, P.L., et al., Knockout of Slo2.2 enhances itch, abolishes KNa current, and increases action potential firing frequency in DRG neurons. Elife, 2015. **4**.
81. Flauaus, C., et al., Slick Potassium Channels Control Pain and Itch in Distinct Populations of Sensory and Spinal Neurons in Mice. Anesthesiology, 2022. **136**(5): p. 802-822.
82. Häring, M., et al., Neuronal atlas of the dorsal horn defines its architecture and links sensory input to transcriptional cell types. Nature neuroscience, 2018. **21**(6): p. 869-880.
83. Hardie, R.C., A brief history of trp: commentary and personal perspective. Pflugers Archiv : European journal of physiology, 2011. **461**(5): p. 493-498.
84. Diver, M.M., et al., Sensory TRP Channels in Three Dimensions. Annu Rev Biochem, 2022.
85. Cao, E., Structural mechanisms of transient receptor potential ion channels. Journal of General Physiology, 2020. **152**(3): p. e201811998.
86. Earley, S. and J.E. Brayden, Transient receptor potential channels in the vasculature. Physiological reviews, 2015. **95**(2): p. 645-690.
87. Nilius, B. and V. Flockerzi, Mammalian transient receptor potential (TRP) cation channels. Vol. 2. 2014: Springer.
88. Talavera, K., et al., Mammalian Transient Receptor Potential TRPA1 Channels: From Structure to Disease. Physiol Rev, 2020. **100**(2): p. 725-803.
89. Julius, D., TRP Channels and Pain. Annual Review of Cell and Developmental Biology, 2013. **29**(1): p. 355-384.
90. Vennekens, R., J. Vriens, and B. Nilius, Herbal compounds and toxins modulating TRP channels. J Current neuropharmacology, 2008. **6**(1): p. 79-96.
91. Cuypers, E., et al., Jellyfish and other cnidarian envenomations cause pain by affecting TRPV1 channels. FEBS Letters, 2006. **580**(24): p. 5728-5732.
92. Kitaguchi, T. and K.J. Swartz, An Inhibitor of TRPV1 Channels Isolated from Funnel Web Spider Venom. Biochemistry, 2005. **44**(47): p. 15544-15549.
93. Rosenbaum, T., S.L. Morales-Lázaro, and L.D. Islas, TRP channels: a journey towards a molecular understanding of pain. Nature Reviews Neuroscience, 2022.

94. Liao, M., et al., Structure of the TRPV1 ion channel determined by electron cryo-microscopy. Nature, 2013. **504**(7478): p. 107-112.
95. Ramsey, I.S., M. Delling, and D.E. Clapham, AN INTRODUCTION TO TRP CHANNELS. Annual Review of Physiology, 2006. **68**(1): p. 619-647.
96. McKemy, D.D., W.M. Neuhausser, and D. Julius, Identification of a cold receptor reveals a general role for TRP channels in thermosensation. Nature, 2002. **416**(6876): p. 52-58.
97. Bandell, M., et al., Noxious cold ion channel TRPA1 is activated by pungent compounds and bradykinin. Neuron, 2004. **41**(6): p. 849-857.
98. Wang, Y.Y., et al., A TRPA1-dependent mechanism for the pungent sensation of weak acids. The Journal of general physiology, 2011. **137**(6): p. 493-505.
99. Vilceanu, D. and C.L. Stucky, TRPA1 mediates mechanical currents in the plasma membrane of mouse sensory neurons. PloS one, 2010. **5**(8): p. e12177.
100. Brierley, S.M., et al., TRPA1 contributes to specific mechanically activated currents and sensory neuron mechanical hypersensitivity. The Journal of physiology, 2011. **589**(Pt 14): p. 3575-3593.
101. Dai, Y., et al., Sensitization of TRPA1 by PAR2 contributes to the sensation of inflammatory pain. The Journal of Clinical Investigation, 2007. **117**(7): p. 1979-1987.
102. Story, G.M., et al., ANKTM1, a TRP-like channel expressed in nociceptive neurons, is activated by cold temperatures. Cell, 2003. **112**(6): p. 819-829.
103. Caspani, O., et al., The contribution of TRPM8 and TRPA1 channels to cold allodynia and neuropathic pain. PLoS One, 2009. **4**(10): p. e7383.
104. Barabas, M.E., E.A. Kossyreva, and C.L. Stucky, TRPA1 is functionally expressed primarily by IB4-binding, non-peptidergic mouse and rat sensory neurons. PLoS One, 2012. **7**(10): p. e47988.
105. Eid, S.R., et al., HC-030031, a TRPA1 Selective Antagonist, Attenuates Inflammatory- and Neuropathy-Induced Mechanical Hypersensitivity. Molecular Pain, 2008. **4**: p. 1744-8069-4-48.
106. Wei, H., et al., Spinal transient receptor potential ankyrin 1 channel contributes to central pain hypersensitivity in various pathophysiological conditions in the rat. PAIN, 2011. **152**(3).
107. Wei, H., et al., Attenuation of Mechanical Hypersensitivity by an Antagonist of the TRPA1 Ion Channel in Diabetic Animals. Anesthesiology, 2009. **111**(1): p. 147-154.
108. Wei, H., et al., Roles of cutaneous versus spinal TRPA1 channels in mechanical hypersensitivity in the diabetic or mustard oil-treated non-diabetic rat. Neuropharmacology, 2010. **58**(3): p. 578-584.

109. Koivisto, A., et al., Inhibiting TRPA1 ion channel reduces loss of cutaneous nerve fiber function in diabetic animals: Sustained activation of the TRPA1 channel contributes to the pathogenesis of peripheral diabetic neuropathy. Pharmacological Research, 2012. **65**(1): p. 149-158.
110. Jordt, S.-E., et al., Mustard oils and cannabinoids excite sensory nerve fibres through the TRP channel ANKTM1. Nature, 2004. **427**(6971): p. 260-265.
111. Bahia, P.K., et al., The exceptionally high reactivity of Cys 621 is critical for electrophilic activation of the sensory nerve ion channel TRPA1. The Journal of General Physiology, 2016. **147**(6): p. 451-465.
112. Macpherson, L.J., et al., Noxious compounds activate TRPA1 ion channels through covalent modification of cysteines. Nature, 2007. **445**(7127): p. 541-545.
113. Hinman, A., et al., TRP channel activation by reversible covalent modification. Proceedings of the National Academy of Sciences of the United States of America, 2006. **103**(51): p. 19564-19568.
114. Trevisan, G., et al., TRPA1 mediates trigeminal neuropathic pain in mice downstream of monocytes/macrophages and oxidative stress. Brain : a Journal of Neurology, 2016. **139**(Pt 5): p. 1361-1377.
115. De Logu, F., et al., Schwann cell TRPA1 mediates neuroinflammation that sustains macrophage-dependent neuropathic pain in mice. Nature Communications, 2017. **8**(1): p. 1887.
116. Trevisan, G., et al., TRPA1 receptor stimulation by hydrogen peroxide is critical to trigger hyperalgesia and inflammation in a model of acute gout. Free Radical Biology and Medicine, 2014. **72**: p. 200-209.
117. Okada, Y., et al., TRPA1 is required for TGF-β signaling and its loss blocks inflammatory fibrosis in mouse corneal stroma. Laboratory Investigation, 2014. **94**(9): p. 1030-1041.
118. de David Antoniazzi, C.T., et al., Topical treatment with a transient receptor potential ankyrin 1 (TRPA1) antagonist reduced nociception and inflammation in a thermal lesion model in rats. European Journal of Pharmaceutical Sciences : Official Journal of the European Federation For Pharmaceutical Sciences, 2018. **125**: p. 28-38.
119. Zimova, L., et al., Intracellular cavity of sensor domain controls allosteric gating of TRPA1 channel. Science Signaling, 2018. **11**(514).
120. Sura, L., et al., C-terminal acidic cluster is involved in Ca2+-induced regulation of human transient receptor potential ankyrin 1 channel. The Journal of Biological Chemistry, 2012. **287**(22): p. 18067-18077.
121. Zurborg, S., et al., Direct activation of the ion channel TRPA1 by Ca2+. Nature Neuroscience, 2007. **10**(3): p. 277-279.

122. Wang, Y.Y., et al., The nociceptor ion channel TRPA1 is potentiated and inactivated by permeating calcium ions. The Journal of Biological Chemistry, 2008. **283**(47): p. 32691-32703.
123. Zhao, J., et al., Irritant-evoked activation and calcium modulation of the TRPA1 receptor. Nature, 2020. **585**(7823): p. 141-145.
124. Ferreira, L.G. and R.X. Faria, TRPing on the pore phenomenon: what do we know about transient receptor potential ion channel-related pore dilation up to now? J Bioenerg Biomembr, 2016. **48**(1): p. 1-12.
125. Mammalian transient receptor potential (TRP) cation channels. 2014, New York: Springer. pages cm.
126. Staruschenko, A., N.A. Jeske, and A.N. Akopian, Contribution of TRPV1-TRPA1 interaction to the single channel properties of the TRPA1 channel. J Biol Chem, 2010. **285**(20): p. 15167-15177.
127. Nishizawa, Y., et al., Possible involvement of transient receptor potential ankyrin 1 in Ca(2+) signaling via T-type Ca(2+) channel in mouse sensory neurons. J Neurosci Res, 2018. **96**(5): p. 901-910.
128. Memon, T., et al., TRPA1 expression levels and excitability brake by KV channels influence cold sensitivity of TRPA1-expressing neurons. Neuroscience, 2017. **353**: p. 76-86.
129. Lehto, S.G., et al., Selective antagonism of TRPA1 produces limited efficacy in models of inflammatory- and neuropathic-induced mechanical hypersensitivity in rats. Mol Pain, 2016. **12**.
130. Han, Q., et al., miRNA-711 Binds and Activates TRPA1 Extracellularly to Evoke Acute and Chronic Pruritus. Neuron, 2018. **99**(3): p. 449-463 e6.
131. Reese, R.M., et al., Behavioral characterization of a CRISPR-generated TRPA1 knockout rat in models of pain, itch, and asthma. Sci Rep, 2020. **10**(1): p. 979.
132. Kwan, K.Y., et al., TRPA1 contributes to cold, mechanical, and chemical nociception but is not essential for hair-cell transduction. Neuron, 2006. **50**(2): p. 277-89.
133. Zeisel, A., et al., Molecular Architecture of the Mouse Nervous System. Cell, 2018. **174**(4): p. 999-1014 e22.
134. Lu, R., et al., Slack channels expressed in sensory neurons control neuropathic pain in mice. J Neurosci, 2015. **35**(3): p. 1125-35.
135. Lu, R., et al., Functional Coupling of Slack Channels and P2X3 Receptors Contributes to Neuropathic Pain Processing. Int J Mol Sci, 2021. **22**(1).
136. Gross, M.K., M. Dottori, and M. Goulding, Lbx1 specifies somatosensory association interneurons in the dorsal spinal cord. Neuron, 2002. **34**(4): p. 535-49.

137. Müller, T., et al., The homeodomain factor lbx1 distinguishes two major programs of neuronal differentiation in the dorsal spinal cord. Neuron, 2002. **34**(4): p. 551-62.
138. Jakkamsetti, V., et al., Quantification of early learning and movement sub-structure predictive of motor performance. Scientific Reports, 2021. **11**(1): p. 14405.
139. Lu, R., et al., K3.1 channels modulate the processing of noxious chemical stimuli in mice. Neuropharmacology, 2017. **125**: p. 386-395.
140. Lu, R., et al., BKCa channels expressed in sensory neurons modulate inflammatory pain in mice. Pain, 2014. **155**(3): p. 556-65.
141. Christensen, S.L., et al., Von Frey testing revisited: Provision of an online algorithm for improved accuracy of 50% thresholds. Eur J Pain, 2020. **24**(4): p. 783-790.
142. Brenner, D.S., J.P. Golden, and R.W.t. Gereau, A novel behavioral assay for measuring cold sensation in mice. PLoS One, 2012. **7**(6): p. e39765.
143. Ferreira, J., et al., Evidence for the participation of kinins in Freund's adjuvant-induced inflammatory and nociceptive responses in kinin B1 and B2 receptor knockout mice. Neuropharmacology, 2001. **41**(8): p. 1006-1012.
144. Bourquin, A.-F., et al., Assessment and analysis of mechanical allodynia-like behavior induced by spared nerve injury (SNI) in the mouse. Pain, 2006. **122**(1-2): p. 14.e1-14.14.
145. Decosterd, I. and C.J. Woolf, Spared nerve injury: an animal model of persistent peripheral neuropathic pain. Pain, 2000. **87**(2): p. 149-158.
146. Schmidtko, A., et al., Cysteine-rich protein 2, a novel downstream effector of cGMP/cGMP-dependent protein kinase I-mediated persistent inflammatory pain. The Journal of neuroscience : the official journal of the Society for Neuroscience, 2008. **28**(6): p. 1320-1330.
147. Gouin, O., et al., TRPV1 and TRPA1 in cutaneous neurogenic and chronic inflammation: pro-inflammatory response induced by their activation and their sensitization. Protein Cell, 2017. **8**(9): p. 644-661.
148. Usoskin, D., et al., Unbiased classification of sensory neuron types by large-scale single-cell RNA sequencing. Nature neuroscience, 2015. **18**(1): p. 145-153.
149. Sisignano, M., et al., 5,6-EET is released upon neuronal activity and induces mechanical pain hypersensitivity via TRPA1 on central afferent terminals. J Neurosci, 2012. **32**(18): p. 6364-72.
150. Nilius, B., G. Appendino, and G. Owsianik, The transient receptor potential channel TRPA1: from gene to pathophysiology. Pflugers Arch, 2012. **464**(5): p. 425-58.
151. Macpherson, L.J., et al., Noxious compounds activate TRPA1 ion channels through covalent modification of cysteines. Nature, 2007. **445**(7127): p. 541-545.

152. Samad, A., et al., The C-terminal basic residues contribute to the chemical-and voltage-dependent activation of TRPA1. J Biochemical Journal, 2011. **433**(1): p. 197-204.
153. Hinman, A., et al., TRP channel activation by reversible covalent modification. Proc Natl Acad Sci U S A, 2006. **103**(51): p. 19564-19568.
154. Paulsen, C.E., et al., Structure of the TRPA1 ion channel suggests regulatory mechanisms. Nature, 2015. **520**(7548): p. 511-517.
155. Budelli, G., et al., SLO2 Channels Are Inhibited by All Divalent Cations That Activate SLO1 K+ Channels. J Biol Chem, 2016. **291**(14): p. 7347-56.
156. Maxwell, D.J., et al., Morphology of inhibitory and excitatory interneurons in superficial laminae of the rat dorsal horn. The Journal of physiology, 2007. **584**(2): p. 521-533.
157. Chaudhry, F.A., et al., The vesicular GABA transporter, VGAT, localizes to synaptic vesicles in sets of glycinergic as well as GABAergic neurons. The Journal of Neuroscience, 1998. **18**(23): p. 9733-9750.
158. Yasaka, T., et al., Populations of inhibitory and excitatory interneurons in lamina II of the adult rat spinal dorsal horn revealed by a combined electrophysiological and anatomical approach. PAIN®, 2010. **151**(2): p. 475-488.
159. Todd, A., et al., The expression of vesicular glutamate transporters VGLUT1 and VGLUT2 in neurochemically defined axonal populations in the rat spinal cord with emphasis on the dorsal horn. European Journal of Neuroscience, 2003. **17**(1): p. 13-27.
160. Sieber, M.A., et al., Lbx1 acts as a selector gene in the fate determination of somatosensory and viscerosensory relay neurons in the hindbrain. The Journal of neuroscience : the official journal of the Society for Neuroscience, 2007. **27**(18): p. 4902-4909.
161. Huang, T., et al., Identifying the pathways required for coping behaviours associated with sustained pain. Nature, 2019. **565**(7737): p. 86-90.
162. Cheng, L., et al., Identification of spinal circuits involved in touch-evoked dynamic mechanical pain. Nat Neurosci, 2017. **20**(6): p. 804-814.
163. Xu, Y., et al., Ontogeny of Excitatory Spinal Neurons Processing Distinct Somatic Sensory Modalities. The Journal of Neuroscience, 2013. **33**(37): p. 14738.
164. Wang, X., et al., Excitatory Superficial Dorsal Horn Interneurons Are Functionally Heterogeneous and Required for the Full Behavioral Expression of Pain and Itch. Neuron, 2013. **78**(2): p. 312-324.
165. Ross, S.E., et al., Loss of Inhibitory Interneurons in the Dorsal Spinal Cord and Elevated Itch in Bhlhb5 Mutant Mice. Neuron, 2010. **65**(6): p. 886-898.

166. Schmidtko, A., et al., cGMP produced by NO-sensitive guanylyl cyclase essentially contributes to inflammatory and neuropathic pain by using targets different from cGMP-dependent protein kinase I. J Neurosci, 2008. **28**(34): p. 8568-76.
167. Petitjean, H., et al., Dorsal Horn Parvalbumin Neurons Are Gate-Keepers of Touch-Evoked Pain after Nerve Injury. Cell Rep, 2015. **13**(6): p. 1246-1257.
168. Madisen, L., et al., A robust and high-throughput Cre reporting and characterization system for the whole mouse brain. Nature neuroscience, 2010. **13**(1): p. 133-140.
169. Gutierrez-Mecinas, M., et al., Expression of cholecystokinin by neurons in mouse spinal dorsal horn. J Comp Neurol, 2019. **527**(11): p. 1857-1871.
170. Abraira, V.E. and D.D. Ginty, The sensory neurons of touch. Neuron, 2013. **79**(4): p. 618-639.
171. Miraucourt, L.S., R. Dallel, and D.L. Voisin, Glycine inhibitory dysfunction turns touch into pain through PKCgamma interneurons. PloS one, 2007. **2**(11): p. e1116.
172. Polgár, E., et al., The types of neuron which contain protein kinase C gamma in rat spinal cord. Brain research, 1999. **833**(1): p. 71-80.
173. Malmberg, A.B., et al., Preserved acute pain and reduced neuropathic pain in mice lacking PKCgamma. Science (New York, N.Y.), 1997. **278**(5336): p. 279-283.
174. Lu, Y., et al., A feed-forward spinal cord glycinergic neural circuit gates mechanical allodynia. The Journal of clinical investigation, 2013. **123**(9): p. 4050-4062.
175. Biton, B., et al., The antipsychotic drug loxapine is an opener of the sodium-activated potassium channel slack (Slo2.2). The Journal of pharmacology and experimental therapeutics, 2012. **340**(3): p. 706-715.
176. Schmiedl, S., et al., Loxapine for Treatment of Patients With Refractory, Chemotherapy-Induced Neuropathic Pain: A Prematurely Terminated Pilot Study Showing Efficacy But Limited Tolerability. Frontiers In Pharmacology, 2019. **10**: p. 838.
177. Vandewauw, I., et al., A TRP channel trio mediates acute noxious heat sensing. Nature, 2018. **555**(7698): p. 662-666.
178. McNamara, C.R., et al., TRPA1 mediates formalin-induced pain. Proc Natl Acad Sci U S A, 2007. **104**(33): p. 13525-30.
179. Eid, S.R., et al., HC-030031, a TRPA1 selective antagonist, attenuates inflammatory- and neuropathy-induced mechanical hypersensitivity. Mol Pain, 2008. **4**: p. 48.
180. Shin, S.M., et al., Satellite glial cells in sensory ganglia express functional transient receptor potential ankyrin 1 that is sensitized in neuropathic and inflammatory pain. Mol Pain, 2020. **16**: p. 1744806920925425.

181. Cevikbas, F., et al., A sensory neuron-expressed IL-31 receptor mediates T helper cell-dependent itch: Involvement of TRPV1 and TRPA1. J Allergy Clin Immunol, 2014. **133**(2): p. 448-60.
182. Obata, K., et al., TRPA1 induced in sensory neurons contributes to cold hyperalgesia after inflammation and nerve injury. J Clin Invest, 2005. **115**(9): p. 2393-401.
183. da Costa, D.S.M., et al., The involvement of the transient receptor potential A1 (TRPA1) in the maintenance of mechanical and cold hyperalgesia in persistent inflammation. Pain, 2010. **148**(3): p. 431-437.
184. Story, G.M., et al., ANKTM1, a TRP-like channel expressed in nociceptive neurons, is activated by cold temperatures. Cell, 2003. **112**(6): p. 819-29.
185. Bautista, D.M., et al., Pungent products from garlic activate the sensory ion channel TRPA1. Proc Natl Acad Sci U S A, 2005. **102**(34): p. 12248-52.
186. Kim, Y.S., et al., Expression of transient receptor potential ankyrin 1 (TRPA1) in the rat trigeminal sensory afferents and spinal dorsal horn. J Comp Neurol, 2010. **518**(5): p. 687-98.
187. Cavanaugh, D.J., et al., Restriction of transient receptor potential vanilloid-1 to the peptidergic subset of primary afferent neurons follows its developmental downregulation in nonpeptidergic neurons. J Neurosci, 2011. **31**(28): p. 10119-27.
188. Ehinger, R., et al., Slack K(+) channels attenuate NMDA-induced excitotoxic brain damage and neuronal cell death. FASEB J, 2021. **35**(5): p. e21568.
189. Budelli, G., et al., Na+-activated K+ channels express a large delayed outward current in neurons during normal physiology. Nat Neurosci, 2009. **12**(6): p. 745-50.
190. Joiner, W.J., et al., Formation of intermediate-conductance calcium-activated potassium channels by interaction of Slack and Slo subunits. Nat Neurosci, 1998. **1**(6): p. 462-9.
191. Santi, C.M., et al., Opposite regulation of Slick and Slack K+ channels by neuromodulators. J Neurosci, 2006. **26**(19): p. 5059-68.
192. Barcia, G., et al., De novo gain-of-function KCNT1 channel mutations cause malignant migrating partial seizures of infancy. Nat Genet, 2012. **44**(11): p. 1255-9.
193. Huang, F., et al., TMEM16C facilitates Na(+)-activated K+ currents in rat sensory neurons and regulates pain processing. Nat Neurosci, 2013. **16**(9): p. 1284-90.
194. Fleming, M.R. and L.K. Kaczmarek, Use of optical biosensors to detect modulation of Slack potassium channels by G protein-coupled receptors. J Recept Signal Transduct Res, 2009. **29**(3-4): p. 173-81.
195. Kaczmarek, L.K., et al., International Union of Basic and Clinical Pharmacology. C. Nomenclature and Properties of Calcium-Activated and Sodium-Activated Potassium Channels. Pharmacol Rev, 2017. **69**(1): p. 1-11.

196. Kaczmarek, L.K., Slack, Slick and Sodium-Activated Potassium Channels. ISRN Neurosci, 2013. **2013**(2013).
197. Zhang, Y., et al., Regulation of neuronal excitability by interaction of fragile X mental retardation protein with slack potassium channels. J Neurosci, 2012. **32**(44): p. 15318-27.
198. Meents, J.E., C.I. Ciotu, and M.J.M. Fischer, TRPA1: a molecular view. J Neurophysiol, 2019. **121**(2): p. 427-443.
199. Bobkov, Y.V., E.A. Corey, and B.W. Ache, The pore properties of human nociceptor channel TRPA1 evaluated in single channel recordings. Biochim Biophys Acta, 2011. **1808**(4): p. 1120-8.
200. Patton, C., S. Thompson, and D. Epel, Some precautions in using chelators to buffer metals in biological solutions. Cell Calcium, 2004. **35**(5): p. 427-31.
201. Schmiedl, S., et al., Loxapine for Treatment of Patients With Refractory, Chemotherapy-Induced Neuropathic Pain: A Prematurely Terminated Pilot Study Showing Efficacy But Limited Tolerability. Front Pharmacol, 2019. **10**: p. 838.
202. McNamara, C.R., et al., TRPA1 mediates formalin-induced pain. Proceedings of the National Academy of Sciences of the United States of America, 2007. **104**(33): p. 13525-13530.
203. Tjølsen, A., et al., The formalin test: an evaluation of the method. Pain, 1992. **51**(1): p. 5-17.
204. Detweiler, D.J., D.S. Rohde, and A.I. Basbaum, The development of opioid tolerance in the formalin test in the rat. PAIN®, 1995. **63**(2): p. 251-254.
205. Fischer, M., et al., The interphase of the formalin test. Pain, 2014. **155**(3): p. 511-521.
206. Martínez-Rojas, V.A., et al., Peripheral and spinal TRPA1 channels contribute to formalin-induced long-lasting mechanical hypersensitivity. Journal of Pain Research, 2018. **11**: p. 51-60.
207. Wei, H., et al., Spinal transient receptor potential ankyrin 1 channel contributes to central pain hypersensitivity in various pathophysiological conditions in the rat. Pain, 2011. **152**(3): p. 582-591.
208. Hoffmann, T., et al., The formalin test does not probe inflammatory pain but excitotoxicity in rodent skin. Physiological Reports, 2022. **10**(6): p. e15194.
209. Jordt, S.E., et al., Mustard oils and cannabinoids excite sensory nerve fibres through the TRP channel ANKTM1. Nature, 2004. **427**(6971): p. 260-5.
210. Paulsen, C.E., et al., Structure of the TRPA1 ion channel suggests regulatory mechanisms. Nature, 2015. **525**(7570): p. 552.

211. Bráz, J.M. and A.I. Basbaum, Differential ATF3 expression in dorsal root ganglion neurons reveals the profile of primary afferents engaged by diverse noxious chemical stimuli. Pain, 2010. **150**(2): p. 290-301.
212. Sadler, K.E., F. Moehring, and C.L. Stucky, Keratinocytes contribute to normal cold and heat sensation. ELife, 2020. **9**.
213. Fischer, M.J.M., et al., Formalin evokes calcium transients from the endoplasmatic reticulum. PloS One, 2015. **10**(4): p. e0123762.
214. Zhuang, Z.Y., et al., Phosphatidylinositol 3-kinase activates ERK in primary sensory neurons and mediates inflammatory heat hyperalgesia through TRPV1 sensitization. J Neurosci, 2004. **24**(38): p. 8300-9.
215. Braz, J.M. and A.I. Basbaum, Differential ATF3 expression in dorsal root ganglion neurons reveals the profile of primary afferents engaged by diverse noxious chemical stimuli. Pain, 2010. **150**(2): p. 290-301.
216. Wellington, C.L., et al., ABCA1 mRNA and Protein Distribution Patterns Predict Multiple Different Roles and Levels of Regulation. Laboratory Investigation, 2002. **82**(3): p. 273-283.
217. Gygi Steven, P., et al., Correlation between Protein and mRNA Abundance in Yeast. Molecular and Cellular Biology, 1999. **19**(3): p. 1720-1730.
218. Melzack, R. and P.D. Wall, Pain mechanisms: a new theory. Science (New York, N.Y.), 1965. **150**(3699): p. 971-979.
219. Finnerup, N.B., R. Kuner, and T.S. Jensen, Neuropathic Pain: From Mechanisms to Treatment. Physiol Rev, 2021. **101**(1): p. 259-301.
220. Chen, J.T.-c., et al., Presynaptic GABAergic inhibition regulated by BDNF contributes to neuropathic pain induction. Nature Communications, 2014. **5**(1): p. 5331.
221. Evely, K.M., et al., Slack KNa Channels Influence Dorsal Horn Synapses and Nociceptive Behavior. Mol Pain, 2017. **13**: p. 1744806917714342.

6. Abbreviations index

Abbreviation	Explanation
AITC	Allyl isothiocyanate
BDNF	Brain-derived neurotrophic factor
BSA	Bovine Serum Albumin
CFA	Complete Freund's Adjuvant
CGRP	Calcitonin Gene-Related Peptide
CNS	Central nervous system
DEPC	Diethyl pyrocarbonate
DMEM	Dulbecco's Modified Eagle Medium
DRG	Dorsal Root Ganglia
dNTP	Deoxyribonucleoside Triphosphate
EDTA	Ethylenediaminetetraacetic Acid
FCS	Fetal Calf Serum
GABA	Gamma-Aminobutyric Acid
GAD 67	Glutamic acid decarboxylase 67
GDNF	Glial-derived neurotrophic factor
HBSS	Hank's Balanced Salt Solution
HEPES	2-[4-(2-Hydroxyethyl) piperazin-1-yl]ethane-1-sulfonic acid
HIV	Human immunodeficiency virus
IASP	International Association for the Study of Pain
IB4	Isolectin B4
ICD	International Classification of Diseases
IHC	Immunohistochemistry
ISH	In Situ Hybridization
LSN	Lateral spinal nucleus
MEM	Minimal Essential Medium
Mrgpr	Mas-related G protein-coupled receptors
NF200	Neurofilament 200
NP	Non-peptidergic

NGF	Nerve growth factor
NTC	No Template Control
PBS	Phosphate Buffered Saline
PBS-T	Phosphate Buffered Saline with 0.1 % Tween 20
PBST	Phosphate Buffered Saline with 0.1% Triton X-100
PEP	Peptidergic
PFA	Paraformaldehyde
PKC-γ	Protein Kinase C γ
RT^-	Reverse Rranscriptase minus
SDS	Sodium Dodecyl Sulfate
SDS-PAGE	Sodium Dodecyl Sulfate Poly-Acrylamide Gel Electrophoresis
Slack	Sequence like a calcium-activated K channel
Slick	Sequence like an intermediate conductance K channel
SNI	Spared Nerve Injury
SNL	Spinal nerve ligation
SpINs	Spinal interneurons
TH	Tyrosine Hydroxylase
TRP	Transient Receptor Potential
TRPA1	TRP ankyrin type 1
VGLUT	Vesicular Glutamate Transporter
VGAT	Vesicular GABA Transporter
WT	Wild Type

7. Key Materials

7.1 Instruments

Apparatus	Supplier
Borosilicate glass	Science Products, Hofheim, Germany
CFX96 Touch Real-Time System	Bio-Rad, Hercules, USA
Cryotome Cryostat NX50	Thermo Fisher, Waltham, USA
DG4	Sutter Instruments, Novato, USA
Digital camera (ORCA-05G)	Hamamatsu, Tokyo, Japan
Dynamic Plantar Aesthesiometer	Ugo Basile, Gemonio, Italy
EPC 9 amplifier	HEKA, Reutlingen, Germany
Fitmaster software	HEKA, Reutlingen, Germany
Flaming/Brown Micropipette Puller	Sutter Instruments, Novato, USA
Fura-2 Filter	Nikon, Düsseldorf, Germany
HD camera HC-V380	Panasonic, Kadoma Osaka, Japan
Microliter Syringes	Hamilton, Franklin, USA
Microscope camera Nikon DS-Qi2	Nikon, Düsseldorf, Germany
Microscope DMI4000 B	Leica, Wetzlar, Germany
Microscope DM LS	Leica, Wetzlar, Germany
Microscope Nikon Eclipse Ni-U	Nikon, Düsseldorf, Germany
Mini-Protean 3	Bio-Rad, Hercules, USA
Motorized microscope stage	Märzhäuser Wetzlar, Wetzlar, Germany
Mouse Rota-Rod 47600	Ugo Basile, Gemonio, Italy
NanoDrop 2000	Thermo Fisher, Waltham, USA
Patchmaster software	HEKA, Reutlingen, Germany
PCR cycler T100 Thermal Cycler	Bio-Rad, Hercules, USA
PowerPac200	Bio-Rad, Hercules, USA
Trans-Blot Turbo System	Bio-Rad, Hercules, USA
ValveLink8.2 Perfusion Controller	Automate Scientific, Berkeley, USA
von Frey filaments	Ugo Basile, Gemonio, Italy

7.2 Chemicals

Chemical	Supplier
Agarose	Sigma-Aldrich, Seelze, Germany
Albumin, IgG-free	Carl Roth, Karlsruhe, Germany
Boric acid	Sigma-Aldrich, Steinheim, Germany
Calcium chloride	Sigma-Aldrich, Steinheim, Germany
Calcium chloride dihydrate	Merck, Darmstadt, Germany
Capsaicin	Sigma-Aldrich, Steinheim, Germany
Chloroform	Merck, Darmstadt, Germany
Choline chloride	Merck, Darmstadt, Germany
Chloroquine diphosphate	Sigma-Aldrich, Steinheim, Germany
Clofilium	Merck, Darmstadt, Germany
DEPC	Carl Roth, Karlsruhe, Germany
DAPI	Thermo Fisher, Waltham, USA
Dimethyl sulfoxide (DMSO)	Carl Roth, Karlsruhe, Germany
DMSO, sterile	Sigma-Aldrich, Steinheim, Germany
Disodium hydrogen phosphate	Sigma-Aldrich, Steinheim, Germany
Disodium hydrogen phosphate	Sigma-Aldrich, Steinheim, Germany
EDTA	Sigma-Aldrich, Steinheim, Germany
Ethanol 70%	Carl Roth, Karlsruhe, Germany
Ethanol absolute	Merck, Darmstadt, Germany
Formaldehyde	Sigma-Aldrich, Steinheim, Germany
Glucose anhydrous	Carl Roth, Karlsruhe, Germany
Glucose monohydrate	Merck, Darmstadt, Germany
Gycerol	AppliChem, Darmstadt, Germany
HEPES	Merck, Darmstadt, Germany
Hydrochloric acid (37%)	Carl Roth, Karlsruhe, Germany
Hydrochloric acid 1 M	Merck KGaA Darmstadt, Germany
Isopropanol 100%	Carl Roth, Karlsruhe, Germany
Isoflurane	Abbot, Wiesbaden, Germany
Loxapine succinate salt	Sigma-Aldrich, Steinheim, Germany
Magnesium chloride	AppliChem, Darmstadt, Germany

Magnesium sulfate heptahydrate	Merck, Darmstadt, Germany
NaCl 0.9%	Braun, Melsungen, Germany
Oligonucleotide	Biomers.net GmbH Ulm, Germany
Paraformaldehyde	Sigma-Aldrich, Steinheim, Germany
Potassium chloride	Merck, Darmstadt, Germany
Potassium hydroxide	Merck, Darmstadt, Germany
SDS pellets (sodium dodecyl sulfate)	Carl Roth, Karlsruhe, Germany
Sodium chloride	Carl Roth, Karlsruhe, Germany
Sodium dihydrogen phosphate	Sigma-Aldrich, Steinheim, Germany
Sodium dihydroxide	Sigma-Aldrich, Steinheim, Germany
Sodium Hydroxide 1 M	Thermo Fisher, Waltham, USA
Sucrose	Carl Roth, Karlsruhe, Germany
Sudan black B	Sigma-Aldrich, Steinheim, Germany
TRIS-Base	Carl Roth, Karlsruhe, Germany
TRIS hydrochloride	Carl Roth, Karlsruhe, Germany
TritonX-100	Carl Roth, Karlsruhe, Germany
Tween-20	Sigma-Aldrich, Steinheim, Germany
Zymosan A	Sigma-Aldrich, Steinheim, Germany

7.3 Reagents

Reagent	Supplier
BSA	Sigma-Aldrich, Darmstadt, Germany
DAPI	Invitrogen, Eugene, USA
Fetal Bovine Serum (FBS)	Life Science, Steinheim, Germany
Flouromount G	Southern Biotech, Birmingham, USA
GAPDH Taqman gene expression assay	Applied Biosystems, San Mateo, USA
Goat serum	Thermo Fisher, Waltham, USA
Intercept Blocking Buffer	LI-COR Biosciences, Lincoln, USA
Prestained Protein Ladders	Bio-Rad, Hercules, USA
Protease Inhibitor Cocktail Tablets	Roche, Mannheim, Germany
QutantiGene ViewRNA	Thermo Fisher, Waltham, USA
RNase free water	Qiagen, Hilden, Germany

Roti-Liquid Barrier Mix	Carl Roth, Karlsruhe, Germany
Roti-Load (4 x)	Carl Roth, Karlsruhe, Germany
Roti Quant	Carl Roth, Karlsruhe, Germany
Roti-Safe	Carl Roth, Karlsruhe, Germany
Tissue-Tek O.C.T.	Sakura, Staufen, Germany
Trans-Blot Turbo 5x Transfer buffer	Bio-Rad, Hercules, USA
TRIzol reagent	Thermo Fisher, Waltham, USA
TRPV1 Taqman gene expression assay	Applied Biosystems, San Mateo, USA
100 bp GeneRuler	Thermo Fisher, Waltham, USA

7.4 Commercial Kits

Kit	Supplier
cDNA synthesis kit	Thermo Fisher, Waltham, USA
DNA Polymerase Master Mix RED	Ampliqon, Odense, Denmark
dNTPs	Qiagen, Hilden, Germany
First Strand cDNA Synthesis Kit	Thermo Fisher, Waltham, USA
Proteinase K	Carl Roth, Karlsruhe, Germany
Micro RNA Kit	AJ Innuscreen, Berlin, Germany
QIAZOL Lysis-Reagent	Qiagen, Hilden, Germany
RNAse-Free DNAse I Set	Qiagen GmbH Hilden, Germany
RNeasy Mini Kit	Qiagen, Hilden, Germany
SYBR Green SuperMix	Bio-Rad, Hercules, USA
Taqman gene expression assays	Applied Biosystems, San Mateo, USA
TRIzol reagent	Thermo Fisher, Waltham, USA
ViewRNA Tissue Kit Affymetrix	Thermo Fisher, Waltham, USA

7.5 Cells and Cell culture Medium

Medium	Supplier
B27	Life Technologies, Grand Island, USA
Collagenase IV	Sigma-Aldrich, Mannheim, Germany

Dispase II	Sigma-Aldrich, Mannheim, Germany
FCS	Sigma-Aldrich, Steinheim, Germany
Fura-2-AM-ester	Biotium, Fremont, USA
Geneticin	Life Technologies, Paisley, UK
Gentamicin	Carl Roth, Karlsruhe, Germany
HBSS	Life Technologies, Paisley, UK
L-Glutamine	Life Technologies, Paisley, UK
Minimum Essential Medium Eagle	Life Technologies, Paisley, UK
Neurobasal medium	Life Technologies, Paisley, UK
pcDNA3.1^{+} vector plasmid	Invitrogen, Carlsbad, USA
Penicillin-Streptomycin	Life Technologies, Paisley, UK
pIRSES2-EGFP	Carl Roth, Karlsruhe, Germany
Poly-D-Lysine	Life Technologies, Frederick, USA
Roti-Fect	Carl Roth, Karlsruhe, Germany
0.05% Trypsin/EDTA	Life Technologies, Paisley, UK

7.5 Consumables

Consumable	Supplier
Cryomold embedding bowls	Sakura, Staufen, Germany
Cryogenic tubes	Sigma-Aldrich, Steinheim, Germany
Cover glasses 24 x 60 mm	Waldemar Knittel, Braunschweig, Germany
CELLSTAR® 96 well plates	Greiner Bio-One, Frickenhausen, Germany
Hard-Shell 96-Well PCR Plate	Bio-Rad California, USA
Microseal PCR Plate Sealing Film	Bio-Rad California, USA
Nitrocellulose membrane	Amersham Biosciences, Freiburg, Germany

7.6 Primary Antibodies

Antibody	Catalog	Source

AF488 conjugated IB4 Griffonia simplicifolia	I21411	Invitrogen
CGRP, Rabbit	PC205L	Calbiochem Merck
GAD 67, Rabbit	AB9706	Chemicon
NeuN, Mouse	MAB377	Millipore
NeuN, Guinea Pig	266004	Synaptic Systems
NeuN, Rabbit	24307T	Cell Signaling
NF200, Rabbit	N4142	Sigma
NF200, Mouse	N0142	Sigma
Peripherin, Mouse	MAB1527	Chemicon
PKC-γ, Mouse	sc-166385	Santa Cruz
PKC-γ, Guinea Pig	AB_2571826	Frontier institute
Slack, Mouse	75-051	Neuromab Davis
Slick, Mouse	75-055	Neuromab Davis
Substance P, Rat	556312	BD Biosciences
TRPV1, Rabbit	ACC-030	Alomone
VGLUT3, Rabbit	135 203	Synaptic Systems
VGLUT2, Rabbit	135 403	Synaptic Systems
Tyrosine Hydrolase, Rabbit,	AB152	Millipore
TUB βIII AF488, Mouse	TUBB3	BioLegend

7.7 Secondary antibodies

Antibody	Specie	Catalog	Source
Anti-Mouse AF350	goat	A21049	Invitrogen
Anti-Mouse AF488	goat	A21121	Life Technologies
Anti-Mouse AF555	goat	A21127	Invitrogen
Anti-Mouse Cy3	sheep	C2181	Sigma
Anti-Rabbit AF488	goat	A11008	Invitrogen
Anti-Rabbit AF555	donkey	A31572	Life Technologies
Anti-Rabbit Cy5	goat	ab6564	Abcam
Anti-Guinea pig AF488	goat	A11073	Invitrogen

7.8 Primers

Primer	fwd	rev
Calbindin	*AGCTGACTGCATCCCAGTTC*	*CGCCAGCATGCCAGAACC*
Galanin	*AAGAGAGGTTGGACCCTGAAC*	*GCACATCAACACTTCCTGGTCT*
GAPDH	*CAATGTGTCCGTCGTGGATCT*	*GTCCTCAGTGTAGCCCAAGAT*
Grp	*CCGGTGTCGACAGGCGCAG*	*TCAGCCGCATACAGGGACGG*
Grpr	*AGTGGGGGTGTCTGTCTTCACACT*	*TCAGGGCATGGGATGCCTGGAT*
MrgprD	*TGGCATCCCAACAAACAC*	*CACATCCACCCAGTAGAGTAAG*
Npr1	*TGGAGACACAGTCAACACAGC*	*CGAAGACAAGTGGATCCTGAG*
NPY	*GATACTACTCCGCTCTGCGA*	*TCCCATCACCACATGGAAGG*
nNOS	*ACC CAA CGT CAT TTC TGT CC*	*AAG GTG GTC TCC AGG TGT GT*
Parvalbumin	*CGGCAAGATTGGGGTTGAAG*	*ATCCGAGGGCCATAGAGGAT*
Slack	*CTGCTGTGCCTGGTCTTCA*	*AAGGAGGTCAGCAGGTTCAA*
Slick	*GAAAGCACCATGAGTGCAGA*	*GTTTTGAAAGCGCGAGAGAG*
Sstr2	*GGCGTGGTACACAGGTTTC*	*GAAGACAGCCACTACGATGG*
Sstr2a	*ATTTGAGTCTGGCTTGTCCGAA*	*AGCACACATACACACAGGACTT*
TRPA1	*GGAAATACCCCACTGCATTGT*	*CAGCTATGTGAAGGGGTGACA*
Slack	*AGGGGCTGAGAGGGGTCTCG*	*TGGGTAGGGCTGCCACAAGC; GCCACAATCTGTTCCTTGGCAC*
CB1	*GCTGTCTCTGGTCCTCTTAAA*	*GGTGTCACCTCTGAAACCAGA*
Cre	*GAAAGCCATGTCCAATTTACTGACCG TA*	*GCGCGCCTGAAGATATAGAAG*

7.9 Solution and buffers

Ringer solution for Calcium-Imaging:

Material	Quantity for 1l	Concentration
NaCl	8.47 g	145 mM
CaCl2 · 2 H2O	0.18 g	1.25 mM
MgCl2 · 7 H2O	0.20 g	1 mM
KCl	0.37 g	5 mM
Glucose	1.80 g	10 mM
HEPES	2.38 g	10 mM

→ Adjust pH to 7.3-7.4 with NaOH.

Extracellular solution for Patch-Clamp

Material	Quantity for 1l	Concentration
NaCl	8.18 g	140 mM
CaCl2 · 2 H2O	0.29 g	2 mM
MgCl2	0.19 g	2 mM
KCl	0.37 g	5 mM
HEPES	2.38 g	10 mM

→ Adjust pH to 7.3-7.4 with NaOH.

Ca^{2+} free extracellular solution for patch clamp:

Material	Quantity for 1l	Concentration
NaCl	8.18 g	140 mM
MgCl2	0.38 g	4 mM
KCl	0.37 g	5 mM
HEPES	2.38 g	10 mM

→ Adjust pH to 7.3-7.4 with NaOH.

Intracellular solution for Patch-Clamp

Material	Quantity for 1l	Concentration
KCl	10.44 g	140 mM
EGTA	1.90 g	5 mM
MgCl2	0.19 g	2 mM
HEPES	2.38 g	10 mM

→ Adjust pH to 7.3 with KOH.

1 M $MgCl_2$ buffer

Material	Quantity for 50 ml	Concentration
$MgCl_2$	4.76 g	1 M
H_2O	50 ml	

→ autoclave

1 M Tris-HCl (pH 8 or 7.4)

Material	Quantity for 100 ml	Concentration
Tris	12.12 g	1 M
H_2O	to 100 ml	

→ Adjust pH to 8 with HCl or adjust to pH 7.4 with HCl

Membrane preparation lysis buffer for western blot (pH 8)

Material	Quantity for 200 ml	Concentration
1 M Tris-HCl (pH 8)	20 ml	100 mM
1 M $MgCl_2$	200 µl	1 mM
H_2O	to 200 ml	

→ Store in 4 °C

Sucrose buffer for western blot (pH 7.4)

Material	Quantity for 200 ml	Concentration
Sucrose	17.12 g	250 mM
1 M Tris-HCl (pH 7.4)	2 ml	10 mM
H_2O	to 200 ml	

→ Store in 4 °C

Lysis buffer for genotyping

Material	Quantity for 1l	Concentration
TRIS HCl (pH 8,5)	15.76 g	100 mM
EDTA	1.46 g	5 mM
SDS	2 g	0.2 %
NaCl	11.69 g	200 mM

SDS-PAGE running buffer

Material	Quantity for 1l	Concentration
TRIS base	3.03 g	25 mM
Glycin	14.4 g	0.19 M
SDS	1 g	0.1 %

IB4 dilution buffer

Material	Quantity for 1 l	Concentration
$CaCl_2$	0.011 g	0.1 mM
$MgCl_2$	0.01 g	0.1 mM
$MnCl_2$	0.013 g	0.1 mM
Triton	2 ml	0.2 %

PBS

Material	Quantity for 1l	Concentration
NaCl	10 g	0.17 M
KCl	0.25 g	3.4 mM
Na_2HPO_4	1.77 g	11.1 mM
KH_2PO_4	0.25 g	1.84 mM

TBE

Material	Quantity for 1l	Concentration
TRIS-Base	10.8 g	0.09 M
Boric acid	5.5 g	0.09 M
EDTA (0,5 M, pH 8,0)	4 ml	2 mM

8. Summary

Slack (sequence like a Ca^{2+}-activated K^+ channel; also termed Slo2.2, Kcnt1, or $K_{Na}1.1$) is a Na^+-activated K^+ channel that is highly expressed in the peripheral and central nervous system. Previous studies have shown that Slack is enriched in the isolectin B4-binding, non-peptidergic subpopulation of C-fiber sensory neurons and that Slack controls the sensory input in neuropathic pain. Recent single-cell RNA-sequencing studies suggested that Slack is highly co-expressed with transient receptor potential (TRP) ankyrin 1 (TRPA1) in sensory neurons. By using in situ hybridization and immunostaining we confirmed that Slack is highly co-localized with TRPA1 in sensory neurons, but only to a minor extent with TRP vanilloid 1. Mice lacking Slack globally or conditionally in sensory neurons (SNS-Slack$^{-/-}$), but not mice lacking Slack conditionally in neurons of the spinal dorsal horn (Lbx1-Slack$^{-/-}$), displayed increased pain behavior after intraplantar injection of the TRPA1 activator allyl isothiocyanate. Patch-clamp recordings with cultured primary neurons and in a HEK-293 cell line transfected with TRPA1 and Slack revealed that Slack-dependent K^+ currents are modulated in a TRPA1-dependent manner. Taken together, these findings highlight Slack as a modulator of TRPA1-mediated activation of sensory neurons.

Furthermore, we investigated the contribution of Slack in the spinal dorsal horn to pain processing. Lbx1-Slack$^{-/-}$ mice demonstrated normal basal pain sensitivity and Complete Freund's Adjuvant-induced inflammatory pain. Interestingly, we observed a significantly increased spared nerve injury (SNI)-induced neuropathic pain hypersensitivity in Lbx1-Slack$^{-/-}$ mutants compared to control littermates. Moreover, we tested the effects of pharmacological Slack activation in the SNI model. Systemic and intrathecal, but not intraplantar administration of the Slack opener loxapine significantly alleviated SNI-induced hypersensitivity in control mice, but only slightly in Lbx1-Slack$^{-/-}$ mice, further supporting the inhibitory function of Slack in spinal dorsal horn neurons in neuropathic pain processing.

Altogether, our data suggest that Slack in sensory neurons controls TRPA1-induced pain, whereas Slack in spinal dorsal horn neurons inhibits peripheral nerve injury induced neuropathic pain. These data provide further insights into the molecular mechanisms of pain sensation.

9. Deutsche Zusammenfassung

Slack (englisch “sequence like a Ca^{2+}-activated K^+ channels”, auch als Slo2.2, Kcnt1, oder $K_{Na}1.1$ bezeichnet) ist ein natriumabhängiger Kaliumkanal, der im peripheren und zentralen Nervensystem exprimiert wird. Frühere Studien konnten zeigen, dass Slack in Isolektin B4- bindenden sensorischen Neuronen lokalisiert ist. Diese Neurone werden der nicht-peptidergen Subpopulation der C-Fasern zugeordnet, einer Gruppe, die verschiedene eintreffende sensorische Informationen verarbeitet. In vorangegangenen Einzelzell-RNA Sequenzierungsexperimenten wurde herausgefunden, dass Slack mit dem Ionenkanal TRPA1 (transient receptor potential ankyrin 1) co-kolokalisiert ist. In dieser Arbeit konnte mit in-situ Hybridisierung und immunhistochemischen Methoden bestätigt werden, dass Slack hauptsächlich in TRPA1-positiven Neuronen, jedoch nur in geringem Ausmaß in TRPV1 (transient receptor potential vanilloid 1) -positiven Neuronen exprimiert wird. Mäuse, bei denen Slack global oder gewebespezifisch in sensorischen Neuronen deletiert ist, zeigten nach intraplantarer Gabe des TRPA1-Aktivators Allylisothiocyanat ein stärkeres Schmerzverhalten als die entsprechenden Kontrolltiere. In Mäusen, bei denen Slack gewebespezifisch in Neuronen des Dorsalhorns (Lbx1-Slack$^{-/-}$) deletiert ist, konnte nach Applikation von Allylisothiocyanat kein Verhaltensunterschied im Vergleich zu Kontrolltieren festgestellt werden. Elektrophysiologische Untersuchungen an sensorischen Neuronen und an HEK 293 Zellen, die mit Slack und TRPA1 transfiziert wurden, enthüllten, dass Slack-abhängige Kaliumströme TRPA1-abhängig moduliert werden. Zusammenfassend konnte gezeigt werden, dass Slack die TRPA1-abhängige Aktivierung von sensorischen Neuronen beeinflussen kann.

Des Weiteren wurde der Einfluss von Slack im Dorsalhorn des Rückenmarks auf die Schmerzverarbeitung untersucht. Lbx1-Slack$^{-/-}$ Mäuse zeigten ein normales Schmerzverhalten, sowohl in Modellen der akuten Nozizeption als auch in einem Modell für entzündliche Schmerzen. Interessanterweise zeigten die Lbx1-Slack$^{-/-}$ Mäuse jedoch im “spared nerve injury” (SNI) Modell für neuropathische Schmerzen eine stärkere Schmerzreaktion als Kontrolltiere. Darüber hinaus wurde nach systemischer und intrathekaler Applikation des Slack-Aktivators Loxapin die Schmerzreaktion reduziert, jedoch nicht nach intraplantarer Injektion. Dies weist auf eine schmerzhemmende Funktion von Slack im Dorsalhorn bei neuropathischen Schmerzen hin.

Insgesamt zeigen die erhobenen Daten, dass Slack im sensorischen System die TRPA1-abhängige Schmerzreaktion moduliert, während Slack im Dorsalhorn periphere neuropathische Schmerzen moduliert. Diese Daten gewähren tiefere Einblicke in die molekularen Mechanismen der Schmerzverarbeitung.

10. Own Publications

1. Zhou F, Metzner K, Engel P, Balzulat A, Sisignano M, Ruth P, et al. Slack Potassium Channels Modulate TRPA1-Mediated Nociception in Sensory Neurons. Cells. 2022;11(10):1693.

2. Flauaus C, Engel P, Zhou F, Petersen J, Ruth P, Lukowski R, et al. Slick Potassium Channels Control Pain and Itch in Distinct Populations of Sensory and Spinal Neurons in Mice. Anesthesiology. 2022;136(5):802-22.

3. Lu R, Metzner K, Zhou F, Flauaus C, Balzulat A, Engel P, et al. Functional Coupling of Slack Channels and P2X3 Receptors Contributes to Neuropathic Pain Processing. Int J Mol Sci. 2021;22(1).

4. Shi Y, Yi C, Li X, Wang J, Zhou F, Chen X. Overexpression of Mitofusin2 decreased the reactive astrocytes proliferation in vitro induced by oxygen-glucose deprivation/reoxygenation. Neurosci Lett. 2017;639:68-73.

5. Zhou F, Yi C, Wang J, Li H, Shi Y, Bai X. Pelvic fracture complicated with retroperitoneal hematoma lead to abdominal compartment syndrome: a report of two cases. Journal of Clinical Emergency 2016;7:503-5.